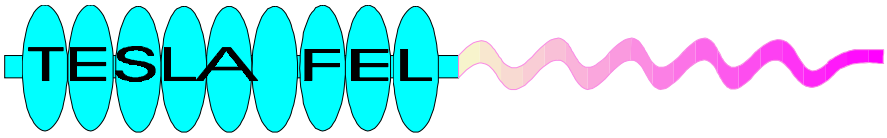

Contributions to the FEL2002 Conference, September 9-13, 2002 in Argonne, USA

October 2002, TESLA-FEL 2002-06

Contents

[1]V. Ayvazyan, N. Baboi, I. Bohnet, R. Brinkmann, M.Castellano, P. Castro, L. Catani, S. Choroba, A. Cianchi, M. Dohlus, H.T. Edwards, B. Faatz, A.A. Fateev, J. Feldhaus, K. Flöttmann, A. Gamp, T. Garvey, H. Genz, Ch. Gerth, V. Gretchko, B. Grigoryan, U. Hahn, C. Hessler, K. Honkavaara, M. Hüning, M. Jablonka, T. Kamps, M. Körfer, M. Krassilnikov, J. Krzywinski, P. Kulinski, C. Lackas, M. Liepe, A. Liero, T. Limberg, H. Loos, M. Luong, C. Magne, J. Menzel, P. Michelato, M. Minty, U.-C. Müller, D. Nölle, A. Novokhatski, C. Pagani, F. Peters, J. Petrowicz, J. Pflüger, P. Piot, L. Plucinski, K. Rehlich, I. Reyzl, A. Richter, J. Rossbach, E. Saldin, W. Sandner, H. Schlarb, G. Schmidt, P. Schmüser, J.R. Schneider, E. Schneidmiller, H.-J. Schreiber, S. Schreiber, D. Sertore, S. Setzer, S. Simrock, R. Sobierajski, B. Sonntag, B. Steeg, F. Stephan, N. Sturm, K.P. Sytchev, K. Tiedtke, M. Tonutti, R. Treusch, D. Trines, D. Türke, V. Verzilov, R. Wanzenberg, T. Weiland, H. Weise, M. Wendt, T. Wilhein, I. Will, K. Wittenburg, S. Wolff, M. Yurkov, K. Zapfe

RF Commissioning of the Photo Injector Test Facility at DESY Zeuthen

K. Abrahamyan[a], J. Bähr[a], I. Bohnet[a⋆], S. Choroba[b], K. Flöttmann[b], H.-J. Grabosch[a], M. v. Hartrott[c], R. Ischebeck[b], O. Krebs[b], Z. Li[a], D. Lipka[a], A. Oppelt[a], V. Peplov[a], B. Petrosyan[a], M. Pohl[a], J. Rossbach[b], S. Simrock[b], F. Stephan[a], T. Thon[a], R. Wenndorff[a], M. Winde[a]

[a]DESY, Platanenallee 6, 15738 Zeuthen, Germany

[b]DESY, Notkestr.85, 22603 Hamburg, Germany

[c]BESSY, Albert-Einstein-Str. 15, 12489 Berlin, Germany

The photo injector test facility at DESY Zeuthen (PITZ) was built to develop, operate and optimize photo injectors for future free electron lasers and linear colliders. First photo electrons were produced in January 2002. An extensive conditioning work on the rf gun has been done in order to achieve high gradients for different pulse lengths and repetition rates. To increase the efficiency and safety aspects of the rf commissioning an Automatic Conditioning Program (ACP) was developed. In addition, a Data Aquisition system (DAQ) which enables a deeper analysis of the commissioning work was realized. The conditioning procedures, the specific diagnostic elements and the achieved results are described. Furthermore, dark current measurements under different conditions are presented.

1. Introduction

The laser driven rf gun at DESY Zeuthen consists of a 1.5 cell L-band copper cavity with coaxial rf coupler, and a Cs_2Te cathode, and two solenoids for space charge compensation. The diagnostic section contains several diagnostic elements as Faraday cups, beam position monitors, and YAG screens to measure the beam parameters (see Fig. 1). An extensive rf commissioning based on a 5 MW klystron was done to allow a stable production of short electron bunches with a low transverse emittance and a small energy spread [1].

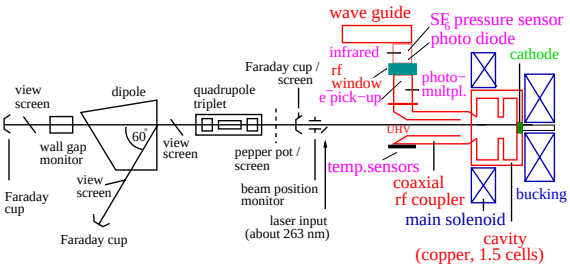

Figure 1. Sketch of the photo injector test facility.

⋆ Presenting author: ilja.bohnet@desy.de

2. Data aquisition and conditioning

A Data Aquisition system (DAQ) has been established to enable a deeper analysis of the behaviour of the facility and all its parts as well as the correlation between different components. This program was developed in the framework of ROOT [2], which supplies an object-oriented data base as well as multiple analysis tools. DOOCS servers are used to get access to the elements of the facility [3]. Especially rf conditioning is the crucial procedure in which different effects like field emission and sparks can produce destructions. To prevent this, a gun interlock consisting of e.g. vacuum pressure, temperature and photo-optic sensors is installed. An Automatic Conditioning Program (ACP) has been developed to increase the efficiency and the safety of the conditioning work. The ACP controls the rf power and reacts appropriately on interlock signals. ACP is based on a C++ program running a graphical user interface as a collection of Labview virtual instruments. It offers a comfortable control of the conditioning process in connection with an online-analysis. The ADC signals of fast gun

interlock detectors as well as the rf signals are dumped with a sampling rate of 1-9 MHz into a ring buffer. This buffer is stopped just after an interlock event happened which allows to read out the data stored during the last rf pulse trains. Acoustic sensors with a sampling rate of 1 MHz and a high position resolution are in development to localize the emission of rf breakdowns.

3. rf commissioning and dark current

The rf commissioning was started with a low average power corresponding to short rf pulse lengths ($50-100\,\mu$s) and a repetition rate of 1 Hz. The resonance frequency of the cavity was tuned with the cooling water system. The current of the solenoids were swept within a small range starting from zero which was extended step by step up to the full range of 0–400 A of the main.

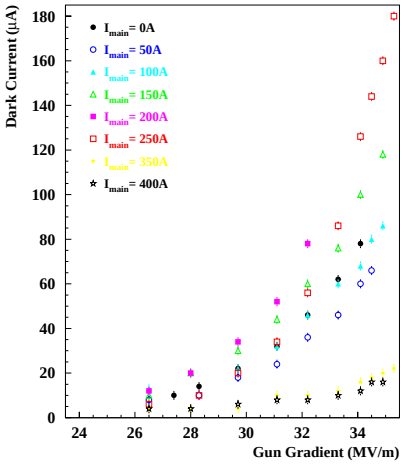

Figure 2. Dark current for 100 μs long rf pulses.

In the beginning the gradient on the cathode was limited to about 20 MV/m whereas at the end the gradient was swept within 20 to 37 MV/m. The vacuum pressure was reduced within this time by almost three orders of magnitude. The dark current emission from the cavity has been measured as a function of the gradient at the cathode position for different currents of the main solenoid. The current of the bucking was chosen accordingly to zero the magnetic field at the cathode. Fig. 2 shows the measurement results for the Cs_2Te cathode for different solenoid currents. A maximum dark current of about 180 μA was observed for gradients of 35 MV/m. For bigger solenoid currents above 250 A (corresponding to a standard operation with 1 nC charge), the dark current is over-focussed, as expected. The dark current emission was also studied for the Mo cathode. Here, the dark current is reduced by a factor of 2 compared to the Cs_2Te cathode (see Fig. 3).

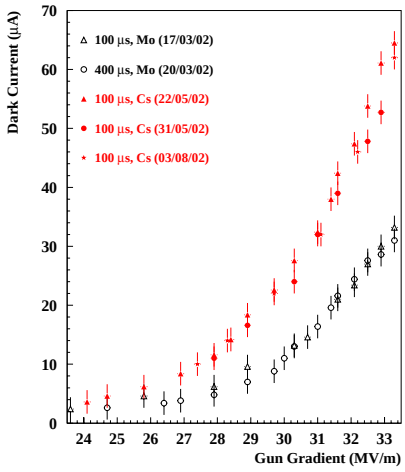

Figure 3. Dark current for the Mo and Cs_2Te cathodes, solenoids are switched off.

4. Conclusions

Using an automatic conditioning program a stable operation for rf pulses up to a length of 400 μs at a repetition rate of 5 Hz including a solenoidal field between 0 and 0.25 T was obtained. A maximum gradient was measured of about 37 MV/m with a repetition rate of 1 Hz and a rf pulse length of 100 μs.

REFERENCES

1. J. Bähr et al., "First Beam Measurements at the Photo Injector Test Facility at DESY Zeuthen", FEL 2002, Argonne.
2. http://root.cern.ch/root/Welcome.html
3. http://tesla.desy.de/doocs/extprograms/daq/index.html

Study of the statistical properties of the radiation from a VUV SASE FEL operating in the femtosecond regime

V. Ayvazyan[a], J.-P. Carneiro[a], P. Castro[a], B. Faatz[a], A.A. Fateev[b], J. Feldhaus[a], Ch. Gerth[a*], V. Gretchko[c], B. Grigoryan[d], U. Hahn[a], K. Honkavaara[a], M. Hüning[e], R. Ischebeck[e], U. Jastrow[a], R. Kammering[a], J. Menzel[e], M. Minty[a], D. Nölle[a], J. Pflüger[a], Ph. Piot[a], L. Plucinski[a], K. Rehlich[a], J. Rossbach[a], E.L. Saldin[a], H. Schlarb[a], E.A. Schneidmiller[a], S. Schreiber[a], R. Sobierajski[a], B. Steeg[a], F. Stulle[a], K.P. Sytchev[b], K. Tiedtke[a], R. Treusch[a], H. Weise[a], M. Wendt[a], M.V. Yurkov[b]

[a]Deutsches Elektronen-Synchrotron (DESY), Notkestraße 85, D-22603 Hamburg, Germany

[b]Joint Institute for Nuclear Research, Dubna, 141980 Moscow Region, Russia

[c]Institute for Nuclear Research of RAS, 117312 Moscow, 60th October Anniversary prospect 7A, Russia

[d]Yerevan Physics Institute, 2 Alikhanyan Brothers str., 375036 Yerevan, Armenia

[e]RWTH Aachen-Physikzentrum, Phys. Inst. IIIa, Sommerfeldstraße 26-28, D-52056 Aachen, Germany

The Free-Electron Laser (FEL) at the TESLA Test Facility at DESY operates in the self-amplified spontaneous emission mode and generates sub-100-fs radiation pulses in the vacuum ultraviolet spectral region. During operation in the saturation regime, radiation pulses with GW peak power are produced. The statistical properties of the FEL radiation have been studied for different amplification regimes as well as behind a narrow-band monochromator and found to be in good agreement with the results of numerical simulations. Information about the spectral and temporal structure of the FEL radiation has been deduced from the statistical properties. The pulse duration of the FEL radiation can be varied by tailoring the electron bunch that drives the FEL.

1. Introduction

Free-Electron Lasers (FEL) based on the principle of Self-Amplified Spontaneous Emission (SASE) [1–4] produce powerful, transversely coherent radiation within a single pass of the electron beam through an undulator. The amplification process in a SASE FEL starts from shot noise in the electron beam and, hence, the SASE FEL radiation itself is of stochastic nature. Theoretical investigations [5] predict that the radiation from a SASE FEL operating in the high-gain linear regime incorporates all features of completely chaotic polarized radiation. Experimental studies of the statistical properties in this regime have been presented in Ref. [6].

In this paper, we present a comprehensive experimental and theoretical study of the statistical properties of the SASE FEL radiation covering the linear and nonlinear regime. The probability densities of the total energy in the radiation pulse as well as a small spectrally resolved fraction measured behind a monochromator are found to be in good agreement with the results from numerical simulations obtained with the code FAST [7]. We can infer information about the spectral and temporal structure of the SASE FEL radiation from the statistical properties.

2. Experimental setup and data recording

The experimental results presented in this paper have been achieved at the TESLA Test Facility (TTF) FEL at the Deutsches Elektronen-Synchrotron DESY. The principal layout of the experimental setup and a detailed description of the TTF FEL is given in Ref. [8].

The energy in the radiation pulse has been monitored with a micro-channel plate (MCP) based detec-

*Corresponding author. Tel.: +49-40-8998-1841; fax: +49-40-8998-4475.
E-mail address: christopher.gerth@desy.de (Ch. Gerth)

tor consisting of a gold wire mesh that scatters a tiny fraction of the FEL radiation onto a MCP (for further details and method of calibration see Ref. [9]). During the data recording, the individual bunch charges and beam offsets at the undulator entrance – the most critical beam parameters influencing the FEL process – have been measured simultaneously. In order to exclude machine jitter contributions from the data analysis, only those pulses have been taken into account for which the bunch charge was within 1% (rms) of the average charge and the orbit deviation was less than 50 μm (rms) of the nominal orbit. After such a data selection, the measured pulse-to-pulse fluctuations of the energy in the radiation pulse are dominated by the statistical properties of the SASE FEL radiation.

The statistical behaviour of the pulse energy for a small spectral bandwidth has been studied using a narrow-band monochromator of an optical feedback system [10]. The monochromator consists of a spherical grating in Littrow mounting with a resolution of about $(\Delta\omega/\omega)_{\rm M} \simeq 10^{-4}$.

The full spectral distribution of the SASE FEL radiation has been measured with a commercial 1-m normal incidence monochromator (0.2 nm resolution) equipped with a fluorescent screen (P46) in the focal exit plane which was imaged with an intensified CCD camera [11]. Both, the short exposure times (down to 5 ns) of the ICCD camera and the imaged dispersive range (about 7 nm) enabled the recording of the full spectral distribution of single FEL pulses (single-shot spectra).

3. SASE FEL amplification process

The upper part of Fig. 1 shows the typical evolution of the average energy in the radiation pulse as a function of the active undulator length. The active length of the undulator has been varied by orbit deflections of the electron beam at the position z which were sufficient to inhibit the SASE process. Apparently, the amplification process passes three stages: start-up from shot noise (lethargy regime), exponential gain (i.e. high-gain linear regime), and saturation (nonlinear regime). The fluctuations of the pulse energy presented in the lower part of Fig. 1 are inherent in the SASE process. For a length $z < 5$ m the rms fluctuation is in the order of 4% and mainly given

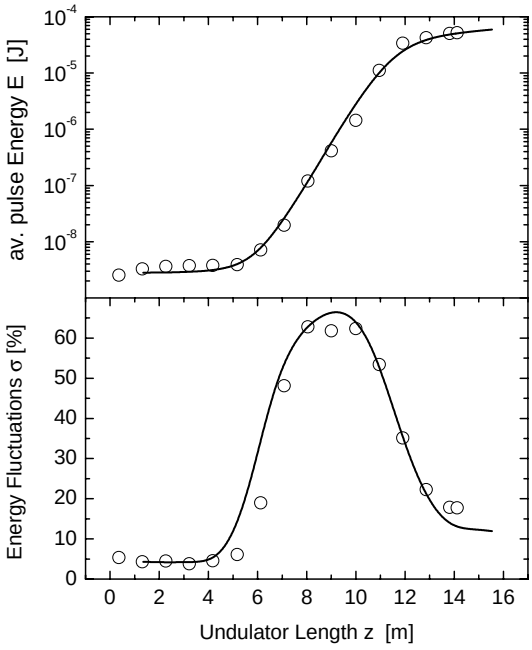

Figure 1. Average energy in the radiation pulse (top) and the rms energy deviation (bottom) versus the active undulator length. The wavelength of the FEL radiation was 98 nm. Circles: experimental results. Solid curves: numerical simulations with the code FAST [7].

by the MCP-based detector. When the FEL radiation exceeds the level of spontaneous emission, the rms energy deviation increases rapidly to more than 60%. The growth of the intensity fluctuations in the high-gain linear regime ($z = 6 - 10$ m) is due to transverse mode selection along with the increase of the longitudinal coherence. A sharp drop of the energy fluctuations is observed when the energy in the radiation pulse approaches the saturation level in the nonlinear regime [12].

4. High-gain linear regime

The fluctuations of the energy in the radiation pulse have been measured in the high-gain linear regime for two different electron beam parameters (Fig. 2). The radiation from SASE FELs operating in the high-gain linear regime possesses all the features of completely

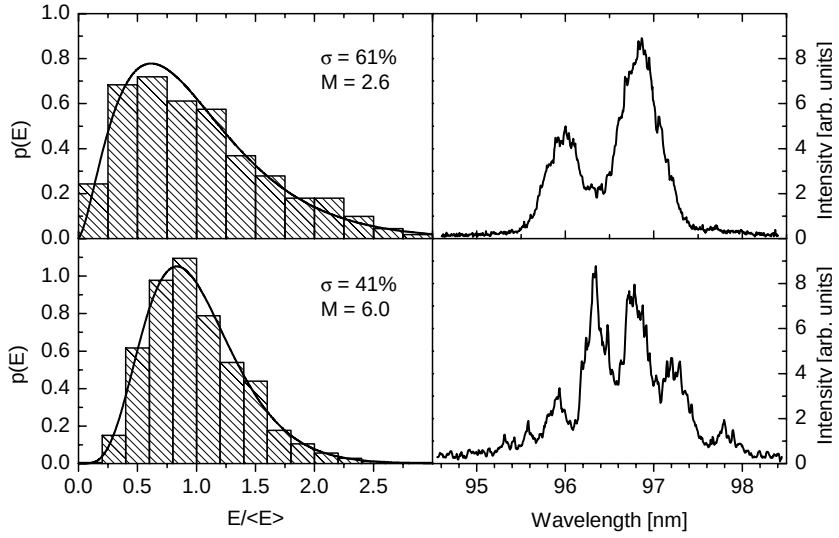

Figure 2. Left: Probability density distributions of the energy in the radiation pulse for different tailoring of the electron bunch. The FEL has been operated in the high-gain linear regime. Solid curves represent gamma distributions. Right: Single-shot spectra for the corresponding modes of operation.

chaotic polarized light [5]. In particular, fluctuations of the energy in the radiation pulse follow a gamma distribution:

$$p(E) = \frac{M^M}{\Gamma(M)} \left(\frac{E}{\langle E\rangle}\right)^{M-1} \frac{1}{\langle E\rangle} \exp\left(-M\frac{E}{\langle E\rangle}\right),$$

where $\Gamma(M)$ is the gamma function, $M = 1/\sigma^2$, and $\sigma^2 = \langle(E - \langle E\rangle)^2\rangle/\langle E\rangle^2$. The parameter M can be interpreted as the average number of "degrees of freedom" or "modes" in a radiation pulse. In the high-gain linear regime the radiation from SASE FELs is almost completely transversely coherent [13], and the value of M is the typical number of spikes in the temporal and spectral distribution of the radiation pulse.

The left part of Fig. 2 shows the probability density distributions of the pulse energy together with the deduced number of modes $M = 2.6$ (top) and $M = 6.0$ (bottom). The measured probability density distributions perfectly match gamma distributions. Single-shot spectra, corresponding to these modes of operation, are presented in the right part of Fig. 2. The number of spikes in the spectra corresponds to the number of modes M derived from the statistical analysis. The typical duration of one spike in the time domain is given by the value of the coherence time t_c. The latter quantity is directly related to the gain length or to the averaged spectral width [14] and has been measured to be $t_c \simeq 20$ fs [15]. Finally, the pulse durations can be calculated by $\tau_{\rm rad} \simeq M \cdot t_c$ and amount to $\tau_{\rm rad} \simeq 50$ fs (top) and $\tau_{\rm rad} \simeq 120$ fs (bottom). Furthermore, the width of the spikes in the spectra is reduced for larger values of M. The spectral width of the spikes is inversely proportional to the pulse duration.

The variation of the number of modes in the radiation pulse and, hence, the pulse duration has been achieved for different bunch compressor settings in combination with the correct matching of the phases of the accelerating modules (see Ref. [8]). Thus, the duration of the radiation pulse at the TTF FEL can be tuned depending on the tailoring of the driving electron bunch.

Another fundamental property of the radiation from SASE FELs operating in the high-gain linear regime is that the radiation energy of a narrow spectral band fluctuates according to the negative exponential distribution:

$$p(E) = \frac{1}{\langle E\rangle} \exp\left(-\frac{E}{\langle E\rangle}\right), \qquad (1)$$

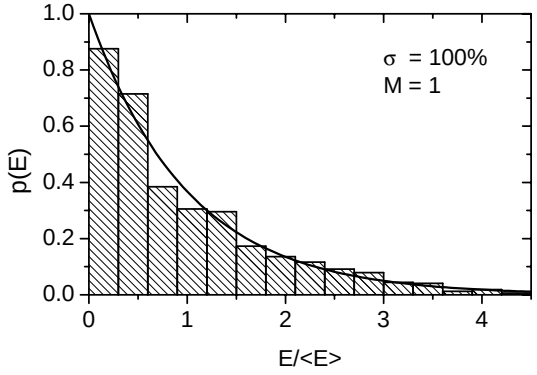

Figure 3. Probability density distributions of the pulse energy behind a narrow-band monochromator. The SASE FEL has been operated in the high-gain linear regime. The active undulator length was 9 m. The solid curve represents the negative exponential distribution.

where $\langle E \rangle$ is the average pulse energy. Measurements of the fluctuations of the radiation energy have been performed behind the narrow-band monochromator of the optical feedback system [10]. The resolution of the monochromator is of the order of a spike in the spectrum. The measured probability density distribution of the energy in the radiation pulse behind the monochromator is shown in Fig. 3. The solid curve represents the negative exponential distribution (Eq. (1)) and is in good agreement with the experimental results. That means, energy fluctuations amount to 100% for the fraction of the radiation behind a monochromator with a resolution in the order of a spike in the spectrum.

5. Nonlinear mode of SASE FEL operation

A detailed quantitative study of the statistical properties in the nonlinear regime has been performed for a pulse duration of about 50 fs ($M = 2.6$). The average energy in the radiation pulse presented in Fig. 1 has been recorded under these conditions. Figure 4 shows the evolution of the probability distribution of the energy fluctuations in the nonlinear regime. Energy fluctuations are presented for active undulator lengths $z = 9$ m, 12 m, and 14.2 m. In the nonlinear regime, the probability distribution no longer matches the gamma distribution and the number of modes M cannot be deduced anymore from the (rms) width σ of the probability distribution. The step from the high-gain linear to the nonlinear regime occurs abruptly within the order of a field gain length ($\approx$ 1.4 m [15]). The evolution of the probability distribution is in good agreement with theoretical predictions and numerical simulations (solid curves).

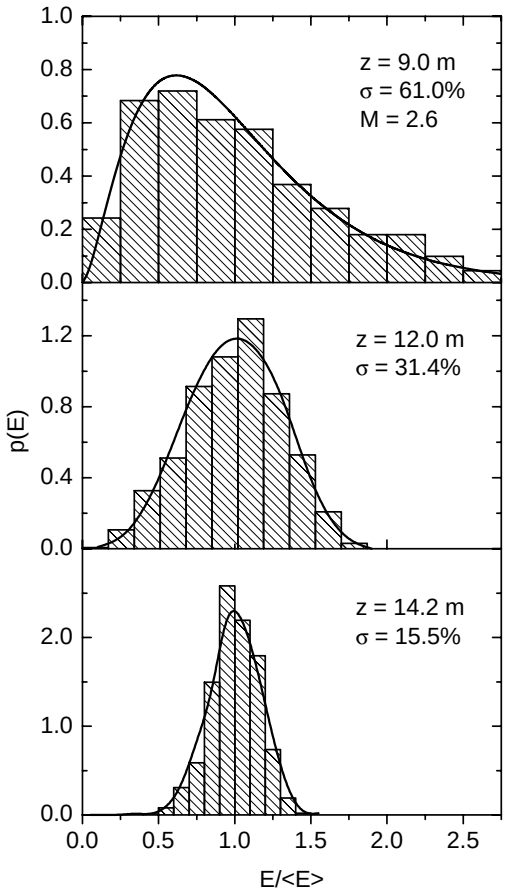

Figure 4. Probability density distributions of the energy in the radiation pulse at the undulator lengths $z = 9$, 12, and 14.2 m. The upper plot corresponds to the high-gain linear regime, the lower plots to the nonlinear regime. The solid curves are the results of simulations with the code FAST [7].

Measurements of the energy fluctuations of the

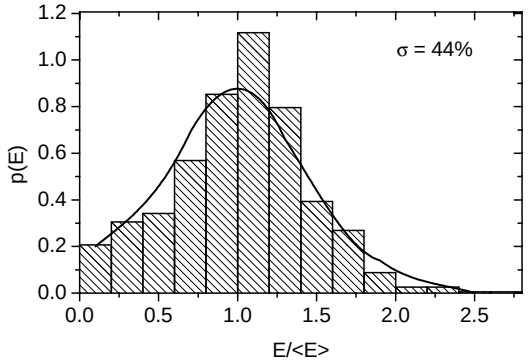

Figure 5. Probability density distribution of the pulse energy behind a narrow-band monochromator. The SASE FEL has been operated in the nonlinear regime; the active undulator length was 14.2 m. The solid curve represents simulations with the code FAST [7].

SASE FEL radiation in the nonlinear regime have also been performed behind a narrow-band monochromator (Fig. 5). The theory of SASE FELs predicts that the fluctuations should drop noticeably when the pulse duration $\tau_{\rm rad}$ is such that $\rho\omega\tau_{\rm rad} \lesssim 3$ [12] with ρ being the FEL parameter. The fluctuations increase drastically for larger values of $\rho\omega\tau_{\rm rad}$ and approach quickly the 100% level. Since the radiation pulse length at the TTF FEL is about twice the coherence time ($\rho\omega\tau_{\rm rad} \simeq \tau_{\rm rad}/t_{\rm c} \simeq 2.6$) [15], we should expect a significant suppression of the fluctuations in the nonlinear regime. It can be seen from Fig. 5 that the measured fluctuations of the pulse energy are only $\sigma = 44\%$ for the nonlinear mode of operation. There is both qualitative and quantitative agreement of the experimental results with calculated probability density distribution. It is worth to mention that such a reduction of the fluctuations is a further, independent indication for very short pulse durations $\tau_{\rm rad}$ [12].

Acknowledgements

The authors are indebted to all members of the TESLA collaboration for their contributions to the TTF at DESY.

REFERENCES

1. A.M. Kondratenko, E.L. Saldin, Part. Accelerators **10,** (1980) 207.
2. Ya.S. Derbenev *et al.*, Nucl. Instr. and Meth. **193,**(1982) 415.
3. R. Bonifacio *et al.*, Opt. Commun. **50** (1984) 373.
4. C. Pellegrini, J. Opt. Soc. Am. **52** (1985) 259.
5. E.L. Saldin *et al.*, Opt. Commun. **148** (1998) 383.
6. M.V. Yurkov, Nucl. Instrum. and Methods **A 483** (2002) 51.
7. E.L. Saldin *et al.*, Nucl. Instrum. and Methods **A 429**, (1999) 233.
8. V. Ayvazyan *et al.*, Eur. Phys. J. D **20** (2002) 149.
9. B. Faatz *et al.*, DESY Print TESLA-FEL 2001-09, 62-67.
10. B. Faatz *et al.*, Nucl. Instrum. and Methods **A 429** (1999) 424.
11. Ch. Gerth *et al.*, Nucl. Instrum. and Methods **A 475** (2001) 481.
12. E.L. Saldin *et al.*, "Statistical properties of radiation from SASE FEL driven by a short electron bunch", these Proceedings
13. E.L. Saldin *et al.*, Opt. Commun. **186** (2000) 185.
14. E.L. Saldin, E.A. Schneidmiller, M.V. Yurkov, "The Physics of Free Electron Lasers" (Springer-Verlag, Berlin, 1999).
15. V. Ayvazyan *et al.*, Phys. Rev. Lett. **88** (2002) 10482.

FIRST BEAM MEASUREMENTS AT THE PHOTO INJECTOR TEST FACILITY AT DESY ZEUTHEN*

R. Bakker, M.v. Hartrott, E. Jaeschke, D. Krämer, BESSY, 12489 Berlin, Germany
J.P. Carneiro, K. Flöttmann, P. Piot, J. Roßbach, S. Schreiber, DESY, 22603 Hamburg, Germany
K. Abrahamyan[&], J. Bähr[#], I. Bohnet, V. Djordjadze[$], U. Gensch, H.J. Grabosch, Z. Li[§], D. Lipka, A. Oppelt, B. Petrossyan[&], F. Stephan, DESY, 15738 Zeuthen, Germany
P. Michelato, C. Pagani, D. Sertore, INFN Milano, 20090 Segrate, Italy
V. Miltchev, I. Tsakov, INRNE Sofia, 1784 Sofia, Bulgaria
A. Liero, H. Redlin, W. Sandner, R. Schumann, I. Will, Max-Born-Institute, 12489 Berlin, Germany
R. Cee, M. Krassilnikov, S. Setzer, T. Weiland, TU Darmstadt, 64289 Darmstadt, Germany

Abstract

The **P**hoto **I**njector **T**est facility at DESY **Z**euthen (PITZ) was built to develop electron sources for the TESLA Test Facility Free Electron Laser (TTF-FEL) and future linear colliders. The main goal is to study the production of minimum transverse emittance beams with short bunch length at medium charge (~1nC). The facility includes a 1.5 cell L-band cavity with coaxial rf coupler, a solenoid for space charge compensation, a laser capable to generate long pulse trains, an UHV photo cathode exchange system, and different diagnostics tools. Besides an overview of the facility, its main components and their commissioning, this contribution will concentrate on the first measurements at PITZ with photo electrons. This will include measurements of the transverse and longitudinal laser profile, charge and quantum efficiency, momentum and momentum spread, transverse electron beam profiles at different locations and first results on transverse emittance.

PACS codes: 29.25 Bx electron sources, 29.27 Fh beam characteristics, 41.60 Cr Free electron Laser, 41.75 Fr electron and positron beam, 41.85 Ew beam profile

Keywords: rf photoinjector, test facility, gun optimization, Free Electron Laser, linear collider, transverse emittance

*** The project is funded partially by the HGF Vernetzungsfond.**
 # presenting author: juergen.baehr@desy.de
& on leave from YERPHI, 375036 Yerevan, Armenia.
$ on leave from HEPI, 380086 Tbilisi, Georgia.
§ on leave from CAEP, 621900 Mian Yang, China.

1. INTRODUCTION

In autumn 1999 it was decided to build a photo injector test facility at DESY Zeuthen [1]. In January 2002 the first photo electrons were produced. The current major goal is to develop and study an electron source for the TESLA Test Facility Free Electron Laser (TTF-FEL). Here, emphasis is taken on the production of minimum transverse emittance beams at a charge of about 1 nC. Detailed experimental analysis of the transverse and longitudinal phase space will allow benchmarking tests of the theoretical understanding of photo injectors. Using PITZ extensive R&D work on rf guns will be possible at DESY in parallel to the operation of TTF-FEL. This includes the test of new developments on e.g. lasers, beam diagnostics, and photo cathodes. In future, investigations on the production of flat beams and polarized electrons for the TESLA project are foreseen.

A description of the set-up and of the hardware components of PITZ are described elsewhere [2]. The schematic overview is presented in Fig. 1.

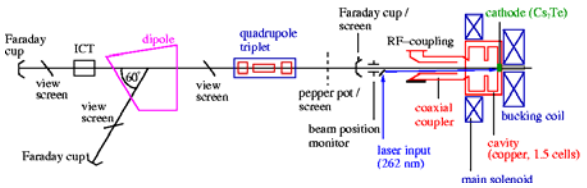

Figure 1: Schematics of the current set-up.

2. ACHIEVEMENTS ON RF COMMISSIONING

In a smooth commissioning procedure using an automatic conditioning program [3] a stable operation with a 400 µs long rf pulse at a 5 Hz repetition rate and a gradient of 34 MV/m has been obtained. In future, the rf pulse length will be extended to above 800 µs. The maximum gradient achieved by the existing rf system was about 37 MV/m at 100 µs pulse length and 1 Hz repetition rate. A more detailed description of the conditioning procedure, its results and dark current measurements is given in [4].

The dark current emission from the cavity has been measured as function of the electric field gradient at the cathode position for different settings of the main solenoid. The bucking magnet current was chosen accordingly to give a zero static magnetic field at the cathode plane. Measurements were performed using the photo emission Cs_2Te cathode. A maximum dark current of about 180 µA was observed for gradients of 35 MV/m, 1Hz repetition rate and 100 µs pulse length. For the conditioning work the usual Cs_2Te-cathode is replaced by a Mo-cathode [5,6]. The dark current emission from this cathode was measured to be a factor of 2 lower than for the Cs_2Te-cathode.

3. THE LASER SYSTEM

The schematic of the laser system currently in operation is shown in Fig. 2. The laser is able to generate trains of micro pulses of up to 800 µs length.

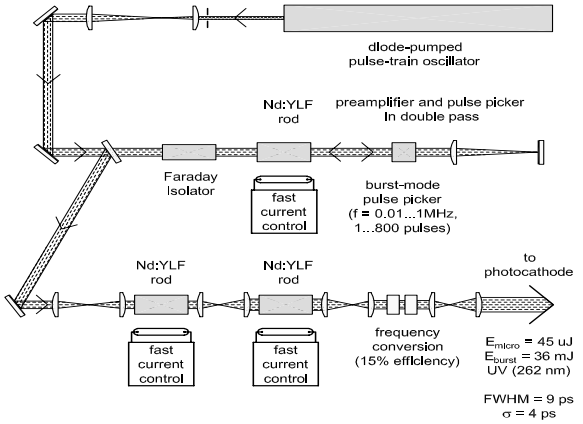

Figure 2: Optical scheme of the current PITZ laser.

The temporal profile (gaussian shape) of the laser micro pulses in the UV was measured using a streak camera to be about 10 ps FWHM.

The transverse profile of the laser beam at the position of the cathode is measured by means of a splitting plate just before the laser beam enters the vacuum system. The rms laser spot size at the so called 'virtual cathode' [7] was measured to be about 0.6 mm in general. For the beam size and emittance measurements a rms transverse size of 0.25 ± 0.15 mm was obtained (gaussian shape in all cases).

Simulations have shown, that a smaller emittance is achievable, if both, the transverse and longitudinal laser profile are flat [8, 9]. Therefore, an important goal of the ongoing laser development at the Max-Born-Institute is to produce a longitudinal flat profile

of a length of about 20 ps and a rise time below 2 ps.

4. MEASUREMENTS WITH ELECTRON BEAM

4.1 Charge and quantum efficiency

The charge of the electron beam is measured using a Faraday Cup which collects the beam charge and an oscilloscope to integrate over the current signal. Mean charges from the pC scale up to 4.7 nC were obtained.

A first measurement of quantum efficiency for only one value of charge was performed. For 36 MV/m and a main magnet current of 240 A a mean charge per bunch of (0.9 ± 0.1) nC was measured. The laser pulse energy of a single bunch in a bunch train of ten bunches was estimated to be (1.0 ± 0.1) μJ at the cathode. This results in a quantum efficiency of the order of 0.5 %.

4.2 Momentum

In Fig. 3 the momentum distribution of the electron beam accelerated at a gradient of about 35 MV/m and measured using the dipole spectrometer is shown. The mean charge is about 0.4 nC. A detailed methodical outline of the momentum measurement can be found in [10]. For a gradient of about 37 MV/m the current maximum beam momentum of about 4.3 MeV/c is obtained.

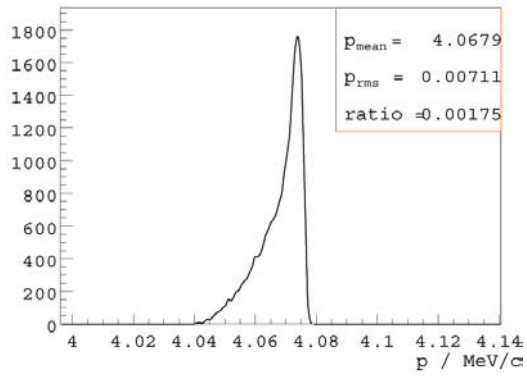

Figure 3: Momentum distribution for a gradient of about 35 MV/m and a mean charge of about 0.4 nC.

The rms momentum spread as function of the number of pulses in a bunch train of constant charge is shown in Fig. 4. It is about 8 keV/c for a low number of pulses. The increase of the measured overall momentum spread with the number of pulses could be caused by an instability of the rf gradient or of the phase relation between laser and rf or by a transverse beam jitter.

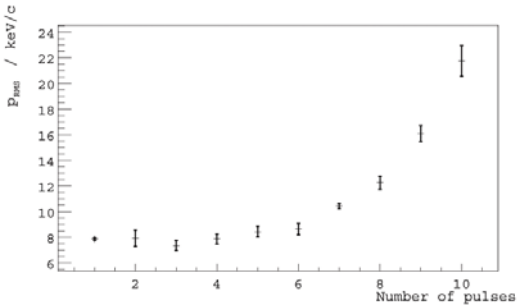

Figure 4: Momentum spread as function of the number of pulses in the laser bunch train at a bunch charge of about 0.4 nC.

4.3 Electron Beam Size and Simulations

The size of the electron beam was measured at different screen locations along the beam line, see Fig. 5. The measurement conditions are summarized in Table 1 and in the chapter on the laser system. For these conditions ASTRA simulations were run and compared to the data.

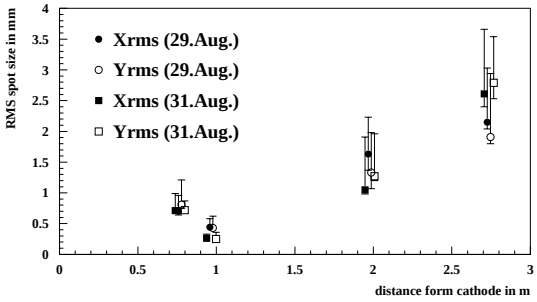

Figure 5: Two measurements of beam spot sizes along the beam line under similar operation conditions. The measurements at each of the four locations are slightly displaced to show them more clearly.

All the simulations with input parameters according to the measured numbers (Tab. 1) can predict a beam waist around 1 m distance from the photo cathode but the absolute beam size is not good reproduced, especially for the last two points of

observation. Here, the simulation always predicts larger sizes. Also the measured momentum distributions and emittances (see Table 1) can not yet be reproduced by the simulations. These problems need more study in future. They might be related to the very high space charge effects at the cathode (note small laser beam size) which could also explain the loss of charge from the cathode down the beamline.

4.4 Transverse emittance measurements

Measurements of the transverse emittance were performed using a multi-slit diagnostics. Beamlet profiles were observed 1010 mm downstream of a multi-slit mask (1 mm thick tungsten plate, 50 µm slit opening, slit-to-slit separation: 1.0 mm for vertical slits and 0.5 mm for horizontal slits).

The emittance was evaluated as a product of the RMS beam size and the RMS uncorrelated divergence. The beam size is measured directly at the location of the multi-slit mask, the divergence is determined by analysing the beamlet profiles. Since the beamlets are partially overlapping, their individual sizes are deduced by fitting the overall profile to a mixture of gaussian functions. For the final calculation, the weighted average of the rms width of all beamlets is used.

The results of two independent measurements at similar operation conditions of PITZ are summarized in Table 1. The largest uncertainty on the measured emittance comes from the noise threshold of the camera readout of the beam size and beamlet measurements. Although our CCD cameras [7] have a remote controllable gain which allows the observation of pictures with and without saturation in a large dynamic range, an industrial set noise threshold cuts the low intensity tails of distributions. The uncertainty from this effect is estimated for each beam measurement separately.

date	charge [nC]		momentum	solenoid		laser pulses			RMS	RMS	norm.
dd-mm-yy	z-position [mm]		[MeV/c]	current [A]		num.	$\sigma_{x,y}$		beam size	divergence	emittance
	768	2736		main	buck.		[mm]		[mm]	[mrad]	[mm mrad]
29-08-02	1.44 ± 0.14	0.65 ± 0.07	4.04 ± 0.08	301	170	5	0.25 ± 0.15	X	$0.44^{+0.14}_{-0.02}$	0.45 ± 0.09	$\mathbf{1.6^{+0.6}_{-0.3}}$
								Y	$0.43^{+0.19}_{-0.02}$	0.45 ± 0.09	$\mathbf{1.5^{+0.7}_{-0.3}}$
31-08-02	1.45 ± 0.15	0.90 ± 0.09	2 peaks at 4.26 ± 0.08 and 3.98 ± 0.08	300	170	1	0.25 ± 0.15	X	$0.26^{+0.07}_{-0.02}$	0.55 ± 0.12	$\mathbf{1.2^{+0.4}_{-0.3}}$
								Y	$0.25^{+0.11}_{-0.02}$	0.64 ± 0.14	$\mathbf{1.3^{+0.6}_{-0.3}}$

Table 1: Emittance measurements and operation parameters.

5. SUMMARY AND OUTLOOK

The photo injector test facility at DESY Zeuthen is now in operation. First measurements with and without photo electrons after several months of commissioning and running are presented.

The rf commissioning of the gun reached up to 5 Hz repetition rate with a pulse length of 400 µs and a gradient of about 34 MV/m. The maximum gradient of about 37 MV/m was measured at 100 µs pulse length and 1 Hz repetition rate.

A first version of the photo cathode laser system was commissioned, delivering up to 800 µs long pulse trains with a micro pulse length of about 10 ps FWHM. Beam charges from the pC scale up to 4.7 nC have been produced and the evolution of the beam along the beam line has been measured. The maximum electron momentum obtained was about 4.3 MeV/c. First results from the emittance measurement system have been presented. A longer program of operation and optimization is ongoing.

Until spring 2003 the complete characterisation of the rf gun is foreseen and afterwards the set-up will be extended by the installation of a booster cavity.

6. References

[1] F. Stephan et. al., "Photo Injector Test Facility under construction at DESY Zeuthen", Proc. FEL2000, Durham, August 2000.

[2] PITZ Collaboration, "Commissioning of the Photo Injector Test Facility at DESY Zeuthen", paper in preparation.

[3] I. Bohnet et. al., "Photo Injector Test Facility in commissioning phase at DESY Zeuthen", Proc. EPAC2002, Paris, June 2002.

[4] I. Bohnet et al., "RF Commissioning of the Photo Injector Test Facility at DESY Zeuthen", these proceedings.

[5] P. Michelato, C. Gesmundo, D. Sertore, "High Quantum Efficiency Photocathode Preparation System for TTF Injector II", Proc. FEL1999, Hamburg, August 1999.

[6] D. Sertore, S. Schreiber, K. Flöttmann, F. Stephan, K. Zapfe, P. Michelato, "First Operation of Cesium Telluride Photocathodes in the TTF Injector RF-Gun", Proc. FEL1999, Hamburg, August 1999.

[7] J. Bähr et. al., "The Diagnostics System for the Photo Injector Test Facility at DESY Zeuthen", Proc. EPAC2002, Paris, June 2002.

[8] S. Setzer, R. Cee, M. Krassilnikov, T. Weiland, "FEL Photoinjector Simulation Studies by Combining MAFIA TS2 and ASTRA", Proc. EPAC 2002, Paris, June 2002.

[9] M. Ferarrio, K. Flöttmann, T. Limberg, Ph. Piot, B. Grigoryan, "Conceptual Design of the TESLA XFEL Photoinjector", TESLA-FEL report 2001-03.

[10] D. Lipka et. al., "Measurement of the Longitudinal Phase Space at the Photo Injector Test Facility at DESY Zeuthen", Proc. EPAC2002, Paris, June 2002.

Scheme for Time-Resolved Experiments Based on the Use of Statistical Properties of the Third Harmonic of the SASE FEL Radiation

W. Brefeld[a], B. Faatz[a], J. Feldhaus[a], M. Körfer[a], J. Krzywinski[b], T. Möller[a], J. Pflueger[a], E.L. Saldin[a], E.A. Schneidmiller[a], S. Schreiber[a], M.V. Yurkov[c]

[a] Deutsches Elektronen-Synchrotron (DESY), Notkestrasse 85, D-22607 Hamburg, Germany

[b] Institute of Physics, Polish Academy of Sciences, Warsaw, Poland

[c] Joint Institute for Nuclear Research, Dubna, 141980 Moscow Region, Russia

A closer inspection of the statistical properties of the third-harmonic radiation from the SASE FEL reveals that it is possible to select single, temporary coherent radiation spikes by using a simple intensity trigger. A carefully designed optical system for splitting, delaying, filtering, and recombining the radiation would then allow time-resolved measurements with resolution down to the coherence time of the FEL, i. e. a few femtoseconds in the case of the TTF FEL.

The field of synchrotron radiation research has grown rapidly over the last 30 years due to push of the electron (positron) storage ring technology. Three successive generations of synchrotron radiation facilities have provided an increase in brilliance by more than ten orders of magnitude. However, the storage ring technology itself approaches its theoretical limits of performance with respect to average and peak brilliance, as well as to minimal pulse duration. Recently a new era of synchrotron radiation research has begun with first user experiments on the free electron laser (FEL) based on self-amplified spontaneous emission (SASE). The results have been obtained at the Tesla Test Facility (TTF) at DESY using radiation pulses of 80-120 nm wavelength with 30-100 fs pulse duration and peak power at GW level [1]. Compared to present day synchrotron radiation sources its peak brilliance is more than a 100 million times higher, the radiation has full transverse coherence and pulse duration is reduced from the 100 picoseconds down to the sub-100 femtosecond time domain. Furthermore a soft X-ray SASE FEL project with wavelengths down to 6 nm was started at DESY. Commissioning of this facility starts in year 2003.

The discussion in the scientific community over the last two years has produced many ideas for novel applications of the soft X-ray SASE FEL at the TESLA Test FAcility. Brilliance, coherence, and timing down to the femtosecond regime are the three properties which have the highest potential for new science to be explored with soft X-ray FEL. It is obvious that studies of time dependent phenomena can be tackled for the first time which relate the structural aspects with the transition states of those electrons which are responsible for the formation process of intra-molecular bonds, clusters, nanoparticles, liquids, solids and hot dense plasmas. This can possibly show us directly how matter is formed out of atoms.

In this paper we describe a new scheme for time resolved experiments. SASE FELs are capable to produce powerful radiation not only at fundamental frequency, but also at higher harmonics. When a beam is strongly bunched in the sinusoidal ponderomotive potential (formed by the undulator field and the radiation field of the fundamental frequency), the electron beam density spectrum develops reach harmonic contents. Coherent radiation at the odd harmonics can be generated in a planar undulator and significant power levels for the third harmonic can be reached before the FEL saturates [2]. It is expected that the power of the transversely coherent third-harmonic radiation can approach 1% of the fundamental power level at the TTF FEL [3,4].

Using the results of numerical simulations, we illustrate statistical properties of the third-harmonic of SASE FEL radiation. Analysis of data obtained shows that the statistical properties of the third-harmonic radiation from the SASE FEL, operating in

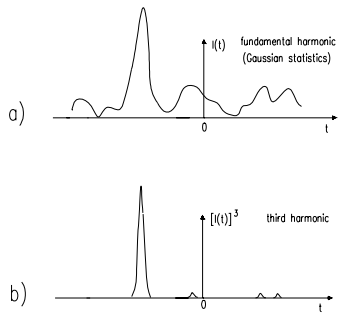

Figure 1. *Illustration of the results of a nonlinear transformation (a) sample function of fundamental harmonic instantaneous intensity for SASE FEL; (b) the nonlinear transform of Fig. (a) representing the third harmonic instantaneous intensity*

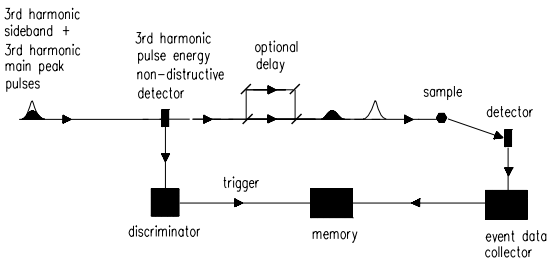

Figure 2. *Experimental setup to obtain single spike pulse duration. Signals from a non-destructive third-harmonic energy pulse detector are used to give trigger. The energy threshold is used to reject events with* E *smaller than* $10\langle E_3\rangle$

the linear regime, can be used for selection of radiation pulses with a single spike in time domain (of about few femtoseconds in the TTF FEL case). The selection of a single third harmonic radiation spike is based on the specific, instantaneous intensity variation within the radiation pulse. This is illustrated in Fig. 1 for a simple example. Consider the intensity function $I(t)$ of a SASE FEL pulse at the fundamental frequency shown in Fig. 1 (a). In the linear regime of the SASE FEL, the instantaneous intensity of the third harmonic is proportional to $[I(t)]^3$ plotted in Fig. 1 (b). Due to the nonlinear transformation the intensity variation becomes much more pronounced, leading to a distribution which is dominated by a single spike in this case. In practice this will not occur for every pulse, and for those cases where single spike is left, we expect a large intensity fluctuation from pulse to pulse. The main question is how likely we are to observe a single bright spike in the intensity of the third harmonic radiation. Clearly, a necessary condition for this event is that the energy $E_{(3)}$ in the third-harmonic radiation pulse is much larger than the average energy $\langle E_{(3)}\rangle$. The results of numerical simulations confirm these simple physical considerations. The predicted probability for the TTF FEL is about 1 %. This is completely acceptable for practical applications because the superconducting TTF accelerator can deliver up to 72 000 electron bunches per second such that a kHz-level average repetition rate of femtosecond third harmonic pulses can be obtained

In practice single-spike third-harmonic pulses can be identified by measuring their total pulse energy $E_{(3)}$ using a nondestructive technique such as gas ionization. The schematic arrangement of a pump-probe experiment employing these femtosecond pulses is shown in Fig. 2. A multilayer singles out the third harmonic radiation, a gas cell at low pressure measures the pulse energy, then the pulse is split into two parts which are delayed with respect to each other and then recombined on the sample. Only such data are selected for which the pulse energy exceeded a certain threshold, typically of the order of 10 $\langle E_{(3)}\rangle$.

To describe the single-spike selection, we should define the degree of contrast. Because of our lack of knowledge of the detailed microscopic structure of the radiation pulse intensity profile, it is necessary to discuss the properties of single-spike selection in statistical terms. SASE radiation is a stochastic object and at a given time it is impossible to predict the amount of energy which flows to a detector. First we should remember that the initial modulation of the electron beam is defined by the shot noise and has a white spectrum. Second, we obtain that the high-gain FEL amplifier cuts and amplifies only a narrow frequency band of the initial spectrum $\Delta\omega/\omega \ll 1$. In the time domain, the temporal structure of the funda-

mental harmonic radiation is chaotic with many random spikes, with a typical duration given by the inverse width of the spectrum envelope. Even without performing numerical simulations, we can describe some general properties of the fundamental harmonic of the radiation from the SASE FEL operating in the linear regime. Indeed, in this case we deal with Gaussian statistics. As a result, the probability distribution of the instantaneous radiation intensity I should be the negative exponential probability density distribution: $p(I) = \langle I \rangle^{-1} \exp(-I/\langle I \rangle)$. Here one should realize clearly that the notion of instantaneous intensity refers to a certain moment in time, and that the analysis must be performed over an ensemble of pulses. Also the energy in the radiation pulse E should fluctuate in accordance with the gamma distribution [5]:

$$p(E) = \frac{M^M}{\Gamma(M)} \left(\frac{E}{\langle E \rangle} \right)^{M-1} \frac{1}{\langle E \rangle} \exp\left(-M \frac{E}{\langle E \rangle} \right) ,$$

where $\Gamma(M)$ is the gamma function of argument M, and $1/M = \langle (E - \langle E \rangle)^2 \rangle / \langle E \rangle^2$ is the normalized dispersion of the energy distribution. These properties are well known in statistical optics as properties of completely chaotic polarized radiation [6].

If we define the contrast C as the ratio of number of photons in main spike to the total number of photons in the pulse we find that $\langle C \rangle$ asymptotically approaches unity at the ratio $E_{\rm th}/\langle E_3 \rangle$ increases, where $E_{\rm th}$ is the threshold level of the third-harmonic energy pulse discriminator. Clearly, the larger the threshold level of discriminator $E_{\rm th}/\langle E_3 \rangle$, the larger the number of shots per one trigger pulse $N_{\rm sh}$. Note that the number of degrees of freedom M of the fundamental radiation pulse is a parameter of the functions $\langle C \rangle = F(M, E_{\rm th}/\langle E_3 \rangle)$, $\langle N_{\rm sh} \rangle = f(M, E_{\rm th}/\langle E_3 \rangle)$ as indeed we might have anticipated.

In Fig. 3 and 4 one can see the basic characteristics of the single-spike pulse selection process. The dependence of the degree of the contrast $\langle C \rangle$ on the value of energy threshold $E_{\rm th}/\langle E_3 \rangle$ is presented in Fig. 3. It is seen that the contrast increases with an increase in the value of energy threshold and it asymptotically approaches to unity. Simulations at different values of M show that the degree of contrast does not differ significantly when the number of modes is within the limits $10 < M < 20$. Figure 4 shows plots

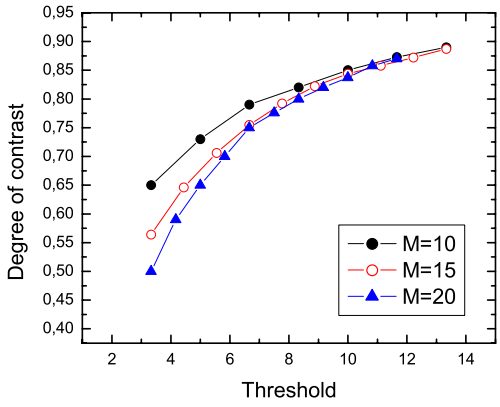

Figure 3. *Degree of contrast* $\langle C \rangle$ *versus energy threshold* $E_{\rm th}/\langle E_3 \rangle$

of the number of shots per one trigger pulse $\langle N_{\rm sh} \rangle$ on the $E_{\rm th}/\langle E_3 \rangle$ for several values of parameter M. From Fig. 4 it is quite clear that the dependence of $\langle N_{\rm sh} \rangle$ on the number of modes M is rather strong and can not be ignored.

With the preceding results in hand, it should now be possible to estimate, for example, the pump-probe pulse repetition rate. In the TTF SASE FEL case, the number of modes in the fundamental radiation pulse at wavelength 30 nm is about $M \simeq 10 - 20$. Suppose that we wish to achieve a degree of contrast of 80%. The discriminator threshold required to achieve this contrast is about $E_{\rm th}/\langle E_3 \rangle \simeq 9$. If the number of modes is close to $M \simeq 15$, plot in Fig. 4 shows that number of shots per one trigger pulse required is about 500 shots. Hence the pump-probe pulse repetition rate is still high (of about 50 single-spike pulses per second). On the other hand, if the contrast of interest is only 70% , the number of shots is about $\langle N_{\rm sh} \rangle \simeq 100$ and pump-probe pulse repetition rate increases up to a few hundred per second.

Acknowledgments

We thank R. Brinkmann, J. Rossbach, J.R. Schneider and D. Trines for useful discussions.

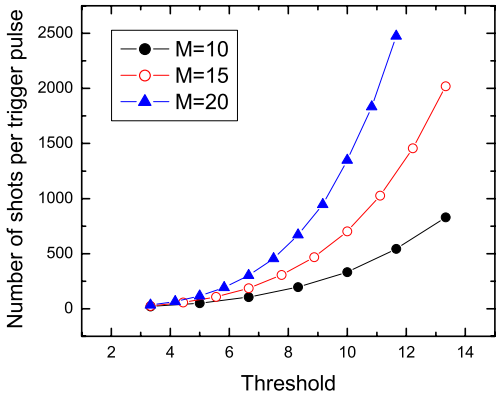

Figure 4. *Number of shots per one trigger pulse* $\langle N_{\rm sh}\rangle$ *versus energy threshold* $E_{\rm th}/\langle E_3\rangle$

REFERENCES

1. V. Ayvazyan et al., Phys. Rev. Lett. 88(2002)104802
2. R. Bonifacio, L. De Salvo, and Pierini, Nucl. Instrum. and Methods A 293,627(1990)
3. H. P. Freund, S. G. Biedron, and S. V. Milton, Nucl. Instrum. and Methods A 445,53(2000)
4. Z. Huang and K.-J. Kim, Phys. Rev. E 62, 7295(2000)
5. E. L. Saldin, E. A. Schneidmiller, and M.V. Yurkov, "The Physics of Free Electron Lasers" (Springer-Verlag, Berlin-Heidelberg-New York, 1999)
6. J. Goodman, Statistical Optics (Willey, New York, 1985)

The SASE FEL at the TESLA Test Facility as user facility

B. Faatz for the TTF-FEL team*
Deutsches Elektronen Synchrotron (DESY), Notkestr. 85, 22603 Hamburg, Germany

Abstract

During the past years, the experience gained with the TESLA Test Facility FEL resulted in several changes of its design. In addition, as the FEL is developed further to become a user facility during 2003, more details of future development of the FEL and the complete experimental hall for the users is taking shape. In this contribution, some of the aspects re briefly mentioned.

1. Layout of the facility

The TTF-FEL experimental hall will give space to 5 user experiments (see fig. 1). Each position has its specific characteristics of offered radiation properties, such as radiation spotsize and spectral properties. In addition, space is foreseen for preparation of experiments, on-line diagnostics and a synchronized optical laser for pump-probe experiments.

2. Electron Beam parameters

As compared to the original TTF-FEL design, there are now tree modes of operation foreseen

- Short wavelength mode (<30 nm), which uses full compression and the 3rd harmonic RF section.
- Long wavelength mode (>30 nm), which uses only the first compressor.
- Femtosecond mode (>30 nm, <100 fs), using a leading spike in the bunch profile, using only the first.

Phase-1 of the TTF-FEL has been run in the last mode, which will also be the starting point for commissioning of the user facility. Further details can be found in Ref. [1].

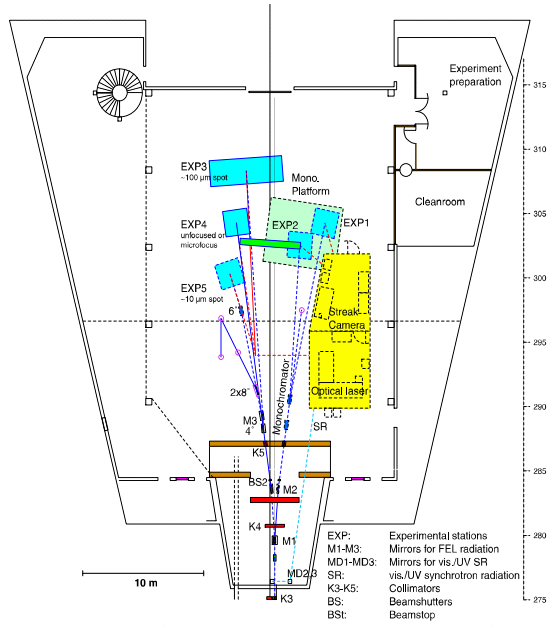

Figure 1: Layout of the experimental hall with space for 5 experiments

3. Proposed Experiments

So far, a number of experiments have been proposed, of which a fraction is shown in the table below. Requested is a variety in power, spectral properties, timing/pulse structure and pulse length.

* Deutsches Elektronen Synchrotron (DESY), Notkestr. 85, 22603 Hamburg, Germany, e-mail: bart.faatz@desy.de, phone: +49 40 8998 4513

Project Title	Photon Energy	Intensity		Pulse Timing & Pump-Probe		Category
	Preferred energy range (eV)	Acceptable spot size	Intensity variation	FEL pulse timing requirements	Requirements for Optical laser	
Pump-Probe Experiments in the Gas Phase	15-200					Developments for pump-probe
Single-Shot FEL Cross Correlator	>12	30 m		up to 9 MHz	10 J	
Quantitative Investigation of Photoionisation Processes on Free Atoms in a Focused VUV FEL Beam	>12		up to 1E16 W/cm^2			Atoms, ions, molecules, non-linear effects
High-Frequency Stabilisation of Li	>10,<70	several m	>1E16 W/cm^2	<50 fs	own diode and YAG laser	
Multiphoton Ionisation and Excitation	10-150	up to 1 mm	<1.5 mJ, 1E13-1E17 W/cm^2	100-200 fs, 200ns distance		
Resonant Single- and Multiphoton Excitation and Photoionisation of Highly charged Ions by FEL Radiation	20-140	100 m	>0.05 mJ, >1E15 W/cm^2 desirable	<100 fs preferable		
Multi-Photon Multiple Ionisation	30-70	<20 m	0.05-1 mJ, 1E13-1E17 W/cm^2	< 250fs		
Molecular Ion Photodissociation	7-40	~3 mm	0.1-1.6 mJ	1-10 kHz at 5 Hz		
Cluster FEL Interaction: Interaction of Intense Soft X-Rays with Atomic and Molecular Clusters	>12	~10 m	>1E14 W/cm^2	<100 fs, 10 s distance		Clusters
Structure of Mass-Selected Clusters	10-100	0.1-1mm, down to 10 m	>10-100	single pulse or 10 s separation	0.1-1 mJ	
XUV Laser Desorption	8-20	1-5 mm	>100 J, >factor 100	<300 fs, <1 s distance in pulse trains	own ns-laser	Surfaces and solids
VUV FEL Nanospectroscopy	10-200	several 100 m, info on beam profile and	some orders of magnitude	none initially	not needed	
IHED-DESY Beam Investigation	10-400	1-20 m	1-100% of full intensity	50fs	<1mJ	
Warm Dense Matter Creation: Isochoric Heating of a Thin Foil	60-400	uniform spot up to 100 m	none	timing of FEL to optical laser with the accuracy of .le. pulse length	0.1J	
Equation of State Measurements	60-400	uniform spot up to 100 m	none	timing of FEL to optical laser with the accuracy of .le. pulse length	0.1J	
Coulomb Explosions of Biological Samples	20-600	1-20 m	1%-100% of full intensity	no special requirements	N/A	
Diffraction Imaging of Biological Samples	100-600	1-10 m	1%-100% of full intensity	no special requirements	N/A	
Studies of Interactions of XUV-FEL Pulses with Solids: Optics Damage and High-Field Effects	85-600	1-20 m	1%-100% of full intensity	50 fs	< 1 mJ	

4. References

[1] The TTF-FEL team, 'SASE FEL at the TESLA Facility, phase-2', TESLA-FEL report 2002-01 (see also http://www-hasylab.desy.de/facility/fel/

VUV FEL Driven RF Gun

B. Faatz[a], A.A. Fateev[b], K. Flöttmann[a], D. Nölle[a], Ph. Piot[a], E.L. Saldin[a], H. Schlarb[a], E.A. Schneidmiller[a], S. Schreiber[a], D. Sertore[c], K.P. Sytchev[b], M.V. Yurkov[b]

[a]Deutsches Elektronen-Synchrotron (DESY), Notkestrasse 85, D-22607 Hamburg, Germany

[b]Joint Institute for Nuclear Research, Dubna, 141980 Moscow Region, Russia

[c]INFN Milano-LASA, via Fratelli Cervi 201, 20090 Segrate, Milano, Italy

In this paper we describe the regeneration of electron bunches from the RF gun by back-reflected radiation from VUV SASE FEL at the TESLA Test Facility (TTF) at DESY. The SASE FEL was running at the wavelength 96 nm with 30-100 femtosecond pulses, SASE pulse energy was up to 20 μJ. "Nominal" electron bunches for lasing were produced by RF gun with Cs_2Te photocathode driven by UV quantum laser system. "Parasitic" bunches with a charge up to 1-1.5 nC were extracted from the RF gun due to VUV FEL radiation reflected from the mirror (placed downstream of the undulator) to the cathode. Nontrivial dependence of a charge on a SASE pulse energy was found.

1. Introduction

Successful operation of a vacuum ultraviolet (VUV) free electron laser (FEL) with unique parameters (wavelength range 80-120 nm, 30-100 femtosecond pulses, gigawatt level of power) [1,2] has allowed to perform pioneering experiments [3,4] at the TESLA Test Facility (TTF) at DESY.

In this paper we present the results of an experiment which was not originally planned at TTF. Moreover, the effect, described in this paper, was discovered by chance at the end of FEL run (February 2002). SASE FEL radiation, reflected back to the photocathode of the RF gun, has regenerated electron bunches with a reasonable charge. It is worth mentioning that for the first time an RF gun was driven by

- VUV laser ($\lambda = 96$ nm),
- free electron laser,
- femtosecond laser (30-100 fs FWHM).

Experimental demonstration of a regenerative mode of electron beam production can be considered as a milestone towards realization of the Ignited Feedback Regenerative Amplifier concept [5] for high average power CW FELs. This concept assumes that a fraction of FEL radiation is used to drive the RF photocathode gun thus producing the next electron bunches that drive the FEL. A conventional laser system is supposed to be used only for the start-up (ignition), otherwise the required average power would be difficult to reach.

2. Experimental set-up

The layout of the TESLA Test Facility (phase 1) is shown in Fig. 1. The gun [6,7] is a $1\frac{1}{2}$-cell RF cavity operating at 1.3 GHz with a peak field of 35-40 MV/m at the photocathode. The Cs_2Te cathode [8] with diameter of 1 cm is illuminated by a UV laser system ($\lambda = 262$ nm) [9] with the spot size of 3 mm on the cathode. A quantum efficiency of the cathode in UV is 0.5%. A charge up to 3-4 nC could be extracted from the gun under these conditions, electron energy is 4 MeV. The gun is followed by a 9-cell superconducting capture cavity where the beam is accelerated up to 16 MeV. In addition, an energy chirp along the bunch is induced for compression in the first bunch compressor (BC1).[1]

The beam is then accelerated off-crest in the superconducting TESLA module (ACC1) [10] up to 130 MeV with the energy chirp for further compression in the second bunch compressor (BC2). After acceleration in the second TESLA module (ACC2) up to 250 MeV the beam passes the collimator and the

[1] In the nominal mode of FEL operation [1] the first bunch compressor was switched off

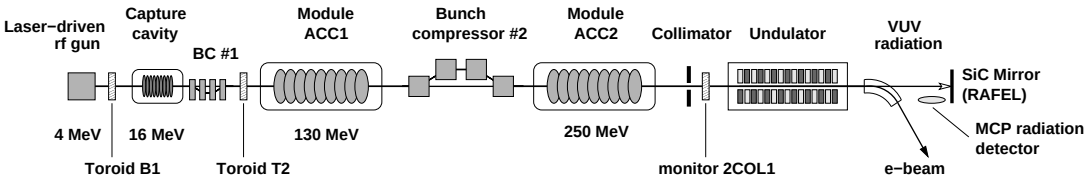

Figure 1. The layout of the TESLA Test Facility

undulator [11,12]. In the latter a short intense pulse of VUV radiation is generated due to SASE process [1,2]. Then electron and photon beams are separated: electron beam is deflected in the spectrometer dipole and goes to the beam dump while the photon beam goes straight downstream to the plane SiC mirror and is reflected back to the cathode of the RF gun.

The plane mirror is one of the elements of Regenerative Amplifier FEL (RAFEL) optical feedback system [13,14]. In the vicinity of the mirror, a thin golden wire is placed which reflects a tiny fraction of radiation to the micro-channel plate (MCP) detector [15]. The charge, regenerated from the cathode by VUV radiation, was detected by toroids in the injector (B1 and T2), and by the cavity monitor 2COL1 at the undulator entrance. The signal of the latter monitor was integrated into the RAFEL control system as well as the MCP signal, thus allowing to study correlation between energy of SASE pulses and charge of electron bunches, regenerated by these pulses.

3. Experimental results

During the measurements the generated wavelength was 96 nm, pulse duration was within the range of 30-100 fs (FWHM). First evidence of charge regeneration appeared as signals on photomultipliers that detect beam losses in the collimator. These signals were separated by about 650 ns (round-trip time between the cathode and the RAFEL mirror) from loss signals of nominal bunches and could be eliminated by closing the valve in the straight section behind the spectrometer dipole (or, by a distortion of the beam orbit in the undulator in order to suppress SASE process).

For the following measurements we increased the launch phase for nominal bunches in the gun by $5\,^\circ$. In addition, path length in BC2 was increased by about 7 mm what gave 10° delay for a VUV pulse to arrive to the cathode. At this operating point, therefore, a launch phase for regenerated bunches was at least 15°. Field gradient at the cathode was 39 MV/m. After optimizing SASE signal we measured reasonably high charge at the injector toroids: up to 1.5 nC at B1, and up to 1 nC at T2 (see Fig. 2). Maximal SASE pulse energy was about 20 μJ.

Since SASE pulse energy was fluctuating, regenerated charge was also fluctuating. Fortunately, it was possible to do correlation measurement using MCP signal and the signal from the monitor 2COL1 because both signals were integrated into the RAFEL control system. The results of such measurement for the first bunch are presented in Fig. 3. Similar correlation plots were obtained for the other bunches. From peak values of the charge measured by the monitor 2COL1 and by injector toroids we estimate the transmission from the gun exit to 2COL1 at 30%. A reason for the dip and the following growth of charge in Fig. 3 is not yet understood. Note that the spread of the data points in Fig. 3 is mainly due to electronic noise.

One can estimate a quantum efficiency of the cathode at $\lambda = 96$ nm during the measurement. First, we determine the fraction of a measured SASE pulse energy which reaches the cathode. From geometrical optics (since the divergence of radiation and the distance from source - undulator exit - are known) we estimate that the cathode accepted about 10% of photons in a radiated pulse.[2] A reflection coefficient of

[2] For more accurate estimate one should take into account diffraction on apertures in accelerator. Of major importance is the collimator aperture with the 6 mm diameter. Calculations show that diffraction effects can change the geometrical optics results by some 20% and lead to an inhomogeneous distribution of intensity on the cathode

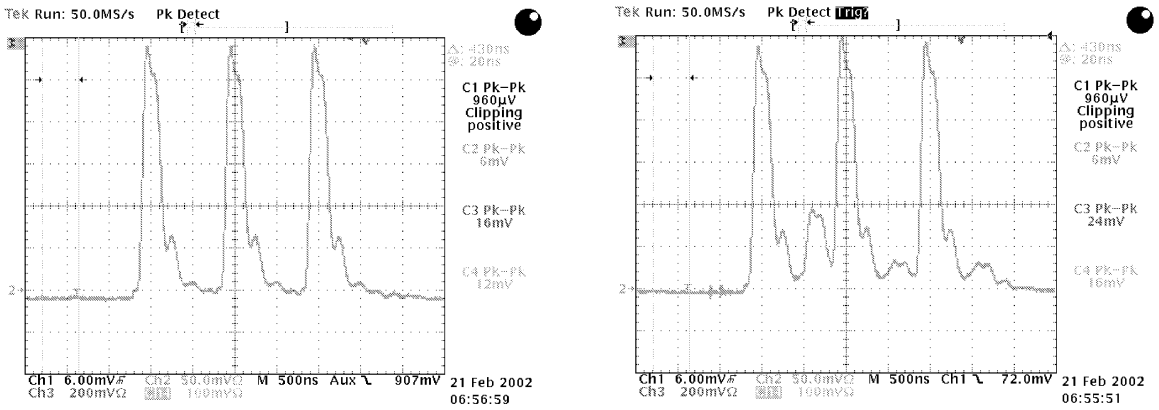

Figure 2. Signals from the toroid T2. Left: SASE off, right: SASE on. Charge of ”nominal” bunches is 3 nC

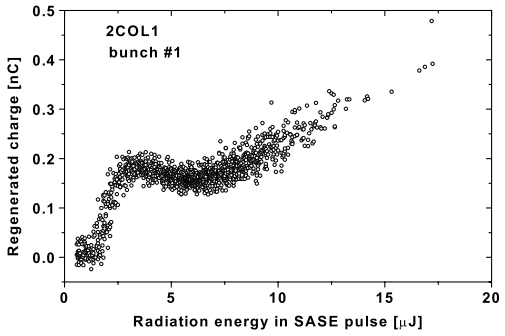

Figure 3. Charge measured at the monitor 2COL1 versus SASE pulse energy

the RAFEL mirror was 0.3 ± 0.1. Thus, one gets about 1.4×10^{10} photons incident on the cathode per 1 μJ of radiated energy (a photon energy is 13 eV). Taking into account the above mentioned charge transmission from the gun to the monitor 2COL1 (30%), from the slope in the initial part of the correlation plot one estimates the quantum efficiency at 15 ± 5 %.

Acknowledgments

The authors would like to thank TTF team at DESY for the valuable contribution to this work.

REFERENCES

1. V. Ayvazyan et al., Phys. Rev. Lett. **85**(2002)104802
2. V. Ayvazyan et al., Eur. Phys. J. **D20**(2002)149
3. T. Laarmann et al., ”Coulomb Explosion of Rare Gas Clusters Irradiated by Intense VUV Pulses of a Free Electron Laser”, these Proceedings
4. J. Krzywinski et al., ”Interaction of Intense, Femtosecond Soft X-ray Pulses with Solids: Desorbtion, Ablation and Plasma Formation by TTF FEL SASE Radiation”, these Proceedings
5. K.-J. Kim et al., Nucl. Instruments and Methods **A407**(1998)380
6. J.-P. Carniero et al., Proc. 1999 Part. Acc. Conf., New York, 1999, pp. 2027-2029
7. S. Schreiber, Proc. EPAC2000, Vienna, p.309
8. D. Sertore et al., Nucl. Instruments and Methods **A445**(2000)422
9. S. Schreiber et al., Nucl. Instruments and Methods **A445**(2000)427
10. H. Weise, Proc. 1998 Linac Conf., Chicago, 1998, pp.674-678
11. J. Pflüger et al., Proc. FEL 18 Conf., Rome, 1996, II-107

12. See http://www-hasylab.desy.de/facility/fel/main.htm for a compact description of the undulator for TTF (Phase 1)
13. B. Faatz et al., Nucl. Instruments and Methods **A429**(1999)424
14. B. Faatz et al., Nucl. Instruments and Methods **A483**(2002)412
15. B. Faatz et al., ”Use of micro-channel plate for nondestructive measurement of VUV radiation from SASE FEL at the TESLA Test Facility”, DESY print TESLA-FEL 2001-09, pp. 62-67

Pump-probe experiments in the femtosecond regime, combining first and third harmonics of SASE FEL radiation

J. Feldhaus[a], T. Möller[a], E.L. Saldin[a], E.A. Schneidmiller[a], M.V. Yurkov[b]

[a]Deutsches Elektronen-Synchrotron (DESY), Notkestrasse 85, D-22607 Hamburg, Germany

[b]Joint Institute for Nuclear Research, Dubna, 141980 Moscow Region, Russia

Two-color pump-probe experiments combining optical femtosecond lasers with short wavelength radiation from a free electron laser (FEL) are very attractive for sub-picosecond time-resolved stadies. Since the synchronization between the two light sources to an accuracy of 100 femtoseconds is not yet solved, it is proposed to derive both radiation pulses from the same electron bunch. In the present work we focus on the special case where pump and probe beams are generated by the same electron bunch in the same insertion device. Specifically we propose to combine GW-level VUV FEL pulses between 150 nm and 90 nm wavelength and 10 MW-level third-harmonic radiation between 50 nm and 30 nm. This scheme does not require any special synchronization nor additional FEL hardware components since the nonlinear third-harmonic generation occurs naturally in the planar FEL undulator. Reflection optics is used for beam splitting and tunable delay, the two harmonics are separated by using notch filters. The effect on the pulse duration is negligible.

1. Introduction

Over the last thirty years synchrotron radiation has become a very powerful research tool applied in many different fields of science, in physics, chemestry and biology. The rapid progress was driven by the development of new, increasingly brilliant synchrotron radiation sources based on electron or positron storage rings. Recently a new era of synchrotron radiation research has begun with first user experiments on a free electron laser (FEL) based on self-amplified spontaneous emission (SASE). The results have been obtained at the TESLA Test Facility (TTF) at DESY (Hamburg) [1,2] using radiation pulses of 100 ± 5 nm wavelength with 100 fs pulse duration and peak power of approximately 1 GW [3]. The peak brilliance of this SASE FEL is nine orders of magnitude higher than that of modern, third generation synchrotron light sources, and the light pulses are three orders of magnitude shorter. The average brilliance is orders of magnitude higher too, and the TTF FEL may thus be considered as the first 4th generation VUV light source in the world.

SASE FELs hold great promise as a source of short wavelength radiation down to 0.1 nm for a wide range of applications, particularly for the study of fast dynamic processes on a sub-picosecond time scale. The standard technique for high resolution time resolved measurements is a pump-probe scheme in which a process is started by a short pulse of radiation (pump) and the evolution of the process is then observed (probed) at a different times after the start by means of a second short pulse of radiation, generally at another photon energy. For very high resolution studies with optical lasers in the pico- and femtosecond regime the two radiation pulses are always derived from the same laser to ensure perfect synchronization, and the time difference is adjusted by changing the path length through an optical delay line. Pump-probe experiments combining pulses from a FEL and an optical laser are more difficult for two reasons. First, the linear accelerator is normally operated with a pulse-timing which is unusual for optical lasers. Second, the geometrical distance between the electron gun of the accelerator and the FEL user experiments can be hundreds of meters or even a few kilometers (for X-ray FEL) making perfect synchronization almost impossible. Two types of photon-pump-photon probe experiments have been proposed for the SASE FEL at the TTF:

1) independent pump and probe light sources employing a powerful optical laser system synchronized with the FEL [4],

2) pump and probe beams that are generated by the

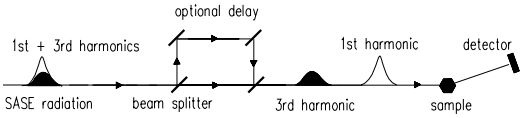

Figure 1. *Scheme for pump-probe experiments employing 1st SASE FEL harmonic radiation pulse as a pump and 3rd harmonic pulse as a probe or vice versa.*

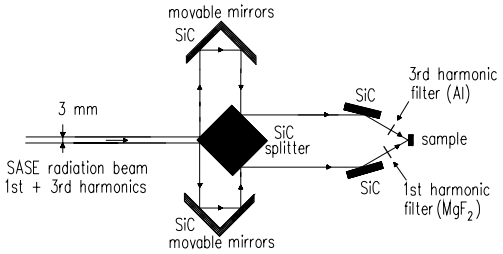

Figure 2. *Schematic setup of a delay line for pump-probe experiments. A SASE pulse passes a beam splitter, generating two pulses travelling different paths. After this, the two pulses impinge on the sample at the time difference which can be varied by changing the relative mirror position.*

same electron bunch but from two different insertion devices [5].

Independent pump and probe sources require synchronization to enable standard time-delay schemes, where the arrival time of the probe relative to the pump can be predetermined by using delay lines. The best synchronization between two sources achieved to date is of the order of a picoseconds [7]. Short wavelength SASE FELs can provide radiation pulses shorter than 100 femtoseconds, hence the synchronization should be better, possibly down to a few 10 femtoseconds. Even if the same optical laser used in the pump-probe experiment also generated the electron bunch producing the FEL radiation pulse, it is not clear how well the accelerator can be stabilized to keep the travel time of the electron bunches constant on a 100 fs-level or even better. Sub-picosecond synchronization certainly needs further research and development. On the other hand, if the two different frequencies were generated by the same electron bunch, the critical synchronization could be avoided and only stable optical delay would be required. This technique has been applied previously combining synchrotron radiation and VUV radiation from a storage ring FEL, although on a much longer time scale [6]. This method could be a very interesting alternative to the optical laser- SASE FEL approach, and it has the further advantage to make a wide frequency range accessible at very high average power not so easily available from conventional lasers. It should be possible to achieve a timing accuracy close to the duration of the radiation pulses (100 fs), allowing unprecedented insight into the dynamics of electronic exitations, chemical reactions and phase transitions of matter, from atoms, through organic and inorganic molecules and clusters, to surface , solids and plasmas.

In order to test this method it is proposed to exploit the ultrashort intense SASE radiation pulses from the TTF FEL and to start with a simple experiment combining pump and probe beams produced by the same electron bunch in the same insertion device. The analaysis shows that strong harmonic growth can be expected In SASE FELs. When a beam is strongly bunched in the sinusoidal ponderomotive potential formed by the undulator field and the radiation field of the fundamental frequency, the electron beam density spectrum develops reach harmonic contents. Coherent radiation at the odd harmonics can be generated in a planar undulator and significant power levels for the third harmonic can be reached before the FEL saturates [8]. Explicit calculations based on current SASE FEL projects show that the power of the transversely coherent third-harmonic radiation can approach 1 % of the fundamental power level [9,10]. The high harmonic power levels indicate the possibility of combining them with the FEL fundamental frequency in the pump-probe experiment.

It is therefore proposed to make use of the GW-

Table 1
Major parameters of VUV-EUV TTF SASE FEL pump-probe facility

Parameter	Value
Wavelength of the 1st harmonic	150 nm
bandwidth	1 %
SASE pulse duration	100 fs
number of photons at the FEL exit	
1st harmonic pulse	10^{14}
3rd harmonic pulse	10^{12}
number of pulses per train	100
repetition rate	1 Hz
delay line transmission	
for 1st harmonic	14 %
for 3rd harmonic	4 %

level VUV FEL pulse as a pump and 10 MW-level third-harmonic radiation from the same SASE FEL as a probe pulse or vice versa. Since the nonlinear harmonic generation occurs naturally in planar SASE FEL undulators, no special synchronization nor any additional FEL hardware components are required for this experiment. It is only necessary to develop components to select the 1st and 3rd harmonic pulses and combine them with a tunable delay.

2. Description of the pump-probe facility

A basic scheme of the proposed pump-probe facility is shown in Fig. 1. The general characteristics for a 1st harmonic wavelength of 150 nm are listed in the Table 1. For a test experiment in the range of 150 to 90 nm for the 1st harmonic and 50 to 30 nm for the 3rd harmonic the simplest way to separate the two frequencies is to use notch filters, such as MgF_2, In or Al. The specific design of a delay line with filters is shown in Fig. 2. A single FEL pulse passes beam splitter, generating two pulses travelling different paths. The two pulses are recombined on the sample with a time difference Δt which can be varied by changing the relative mirror position. Using beam splitting techniques, the time delay can be precisely controlled, and the temporal resolution is only limited by the stability of the optics used to relative to the other. A resolution of some ten femtoseconds should be achievable without much effort. The Al filter is useful in the 50-30 nm region. The transmission T of the 100 nm thick Al filter increases from 63 % to 72 % for wavelengths between 50 nm and 30 nm, while the fundamental is strongly suppressed (T varies from 1.6×10^{-6} to 1.5×10^{-3} for wavelengths between 150 nm and 90 nm). The SiC mirrors are best suited for delay lines in this spectral range. The mirror reflectivity for s-polarized light at an angle of incidence of 45° is about 60 % and 45 % for wavelengths of 150 nm and 50 nm, respectively. Consequently, the transmission of the delay lines are about 14 % and 4 % for 150 nm and 50 nm respectively.

For other wavelengths, or for very high power levels, simple transmission filters may not be available, and a monochromator has to the used to select the two wavelengths. In this case one has to take care that the short pulse duration is preserved. In principlpe, it is possible to design time-compensated spectroscopic configurations with gratings by using at least two gratings in a substrative fashion to compensate for the dispersion. This concept is well known in the study of ultrafast laser pulses, and has recently been extended to the EUV region [11].

Single harmonics can also be selected by using plane multilayer mirrors near normal incidence. The design of time-compensated monochromator without diffraction gratings has been presented in [12]. The monochromator is useful in the range 4-35 nm region, where multilayer mirrors have good performance. The pulse time duration is not altered up to a few femtoseconds, preserving the time resolution capability and the peak intensity.

Acknowledgments

We thank J.R. Schneider and D. Trines for interest in this work.

REFERENCES

1. J. Rossbach, Nucl. Instrum. and Methods **A375**(1996)269.
2. J. Andruszkow et al., Phys. Rev. Lett. **85**(2000)3825.
3. V. Ayvazyan et al., Phys. Rev. Lett. **88**(2002)104802.

4. ”Development of a pump-probe facility with subpicisecond time resolution combining a high-power optical laser and a soft X-ray free electron laser”: Joint DESY (Germany), Forshungszentrum Julich (Germany), Max-Born Institute Berlin (Germany), Dublin City University (Ireland), MAX-Lab/Lund Laser Centre (Sweden), and CNRS/LURE, orsay (France) Proposal. Available at DESY by request only.
5. B. Faatz et al., DESY-print 00-94(2000).
6. L. Nahon et al., Nucl. Instrum. Methods **A 429**(1999)489.
7. G. M. H. Knippels, M. J. van de Pol and A.F.G. van der Meer, Proceedings of the 20th International FEL Conference, Williamsburg, USA, 1998, Elsevier Science B.V., Amsterdam, 1999, p. II-97
8. R. Bonifacio, L. De Salvo, and P. Pierini, Nucl. Instrum. Methods **A 293**(1990)627.
9. H. P. Freund, S. G. Biedron, and S. V. Milton, Nucl. Instrum. Methods **A 445**(2000)53.
10. Z. Huang and K. -J. Kim, Phys. Rev. **E 62**(2000)7295.
11. P. Viloresi, Appl. Opt. 23, 293 (1999)
12. L. Poletto and G. Tondello, Journal of Opt. A **3**(2001)374.

Photon Ring Multi-User Distribution System for Soft X-ray SASE FEL Laboratory

J. Feldhaus[a], E.L. Saldin[a], E.A. Schneidmiller[a], M.V. Yurkov[b]

[a]Deutsches Elektronen-Synchrotron (DESY), Notkestrasse 85, D-22607 Hamburg, Germany

[b]Joint Institute for Nuclear Research, Dubna, 141980 Moscow Region, Russia

It is shown that although the soft X-ray SASE FEL photon beam from undulator is in principle a single user tool, just like an optical laser, the optical distribution system based on multifacet reflectors provide efficient ways to generate a multi-user facility – very similar to present day synchrotron radiation facilities. Multifacet reflectors involve multiple reflections from a series of plane mirrors. These make use of the principle of total external reflectance. The candidate mirror materials include C, Mo, and Si which should yield a reflectance of 40 - 80 % for an arc angle of 90° in the wavelength range 6-100 nm. Multifacet reflector arcs can be repeated a number of times to form a complete ring. In order to make efficient use of the new SASE FEL source it is proposed to install this photon ring distribution system in the experimental hall of soft X-ray FEL laboratory. A few tens beam lines with different experiments can be served by a single FEL source. Using movable mirrors in each photon ring cell it is possible to quickly switch the FEL photon beam from one experiment to the other, thus providing simultaneous multi-user capability.

1. Introduction

Free electron lasers (FEL) based on self-amplified spontaneous emission (SASE) represent a new source of high-brightness short wavelength radiation with unprecedented properties in terms of coherence and peak intensity. Today SASE FELs have already operated successfully at VUV wavelengths [1,2] and will soon produce radiation in the EUV and soft X-ray regions [3]. The preferred layout of a SASE FEL is a linear arrangement in which the injector, accelerator, bunch compressors and undulators are nearly collinear, and in which the electron beam does not change the direction between accelerator and undulators. On the other hand, a soft X-ray FEL laboratory needs to serve many, up to few ten of, experimental stations which can be run independently according to the needs of the user community. The present paper describes a beam distribution system which allows to switch the FEL beam quickly between many experiments in order to make efficient use of the source.

The technical approach adopted in this design makes use of multifacet reflectors i.e. a sequence of plane mirrors [4,5]. Previously, Vinogradov, et al., [6] had recognized the potential of whispering gallery optics in the soft X-ray range. In their theoretical analysis, they derived an analytical expression for the net reflectance after a near-infinite number of grazing-incidence reflections from cylindrical reflectors. Subsequently, Newnam [4] proposed a multiple-facet arrangement of flat mirrors for the end reflectors in FEL resonators operating in the VUV wavelength range. The flat mirror configuration practically eliminates the problem of astigmatism that is inherent in large-angle reflections from a cylindrical reflector.

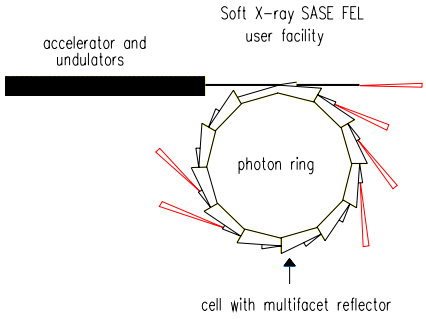

Figure 1. *A bird's view of a soft X-ray FEL laboratory showing a possible layout*

A possible layout of a soft X-ray FEL laboratory based on photon ring distribution system is shown in

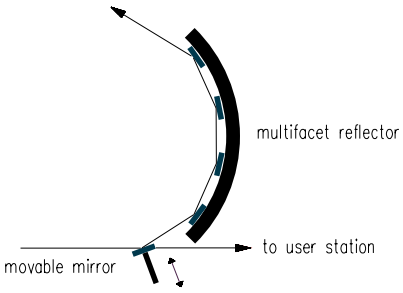

Figure 2. *Optical design of the photon ring cell*

Fig. 1. The layout of the laboratory follows a similar approach as used for the synchrotron light sources. The SASE FEL user facility consists of an SASE radiation source and photon beam distribution system. The SASE radiation source is composed of a 1-1.5 GeV linac, bunch compressors and undulators. After the SASE undulators the electrons are stopped in the beam dump while the photons are transferred to the experimental hall. In order to make efficient use of the new source it is proposed to segment the full circumference of a distribution system into arcs which are repeated a number of times to form a complete ring. Each photon ring sector or cell includes multifacet reflector as "bending" element and a movable mirror. Specific realization of the photon ring cell is sketched in Fig 2. Mirrors are mounted in place in ultra-high vacuum. The radiation beam transport line guiding photons from the SASE FEL to the experimental hall is connected tangentially to one of the straight sections of the photon ring, and the beam is injected by a deflecting mirror. In order to obtain a useful separation between the experimental areas behind the beam lines, an angle of 15 degrees between two neighboring lines would be desirable. Thus, twenty-four beam lines can be installed on a complete photon ring. Using movable mirrors in each photon ring cell, as shown in Fig. 2, it is possible to quickly switch the FEL photon beam from one experiment to the other thus providing multi-user capability.

Multifacet reflectors involve multiple reflections from a series of plane mirrors. These make use of the principle of total external reflectance which occurs for angles of incidence beyond a critical angle (often near 10° grazing-incidence) when the reflective index is less than unity and the material has zero absorption. Any material absorbs light to some degree, but over certain spectral ranges in the VUV-EUV, in which the extinction coefficient is sufficiently less than unity, a few materials do exhibit very high reflectance. Thus, with a sequence of reflections, surprisingly high values of reflection of optical beam by large angle are possible. Multifacet reflector transmission is determined by the total (arc) angle of the cylindrical surface, number of facets and the optical constants of the mirror material. At the same time, transmission is independent of the radius of the curvature of the multifacet reflector, because the number of reflections is independent of the radius value.

The multifacet reflector optics has two fundamental features which consist in the following:

1. Multifacet reflectors can deflect a soft X-ray beam through a large total turning angle (up to 360°) with an efficiency comparable to that obtained by normal incidence multilayer mirrors. Note that the usual grazing incidence elements deflect soft X-rays through an angle smaller than $2\theta_c$, where θ_c is the critical angle of the total external reflection, with is small in the soft X-ray region.

2. Multifacet reflectors like any kind of grazing incidence optics are wideband, unlike an interference multilayer mirror which has a high spectral selectivity.

Hence, multifacet reflector optics unites some useful features of multilayer and grazing incidence optics. This unique property allows one to use multifacet reflectors to solve problems which can not be solved in any other way. It is therefore proposed to make use of the multifacet reflectors in a soft X-ray SASE FEL user facility. In contrast to multilayer mirrors, the high reflectance of multifacet mirrors can be extended over a relatively broad range, a feature that well suits in inherently broad tunability of SASE FELs. Additionally, the radiation load on the multifacet reflector is rather low because the absorbed power is distributed along the whole number of facets.

The highest efficiency of a multifacet reflector transportation is achieved if a low-absorbing mirror material and a sufficient large number of facets are

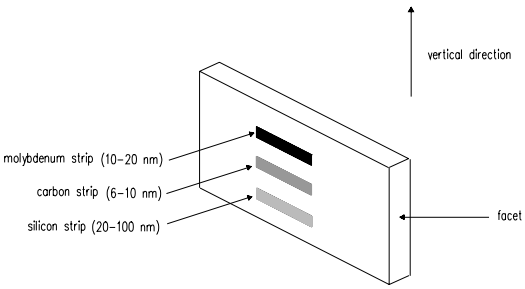

Figure 3. *View of a facet of the reflector system optimized for the wavelength range 6-100 nm. Each facet has three different coatings (C, Mo and Si strips) separated in the vertical direction. The photon beam can be injected into the photon ring at three different vertical positions*

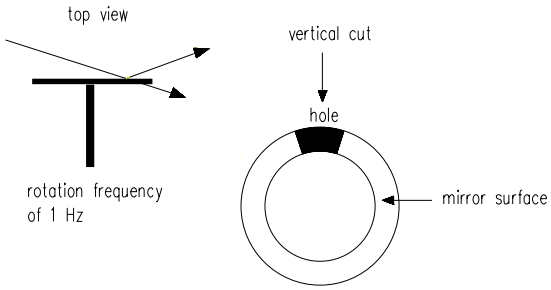

Figure 4. *Different views of a rotating deflector mirror. Using rotating mirrors as switching elements between the photon ring cells makes it possible to provide soft X-ray radiation for many user stations. The distribution of photons is achieved on the basis of pulse trains and it is possible to serve one user station with repetition rate up to 1 Hz*

used. For low-absorbing materials the transportation efficiency is approximately equal to

$$R_0(\psi) \simeq \exp(-\psi\gamma/\delta^{3/2}), \quad \text{for} \quad \gamma \ll \delta\ , \quad \epsilon = 1 - \delta + i\gamma$$

where ψ is the arc angle and ϵ is the complex dielectric constant. The candidate mirror materials include C, Ag, Pd, Mo, Al and Si which, based on measured values of the optical constants, should yield high reflectance [7]. In the wavelength range 6-10 nm carbon is preferable which gives a multifacet reflector efficiency $R_0 \simeq 40$ % for an arc angle $\psi = 90^\circ$. In the wavelength range 10-20 nm the most interesting element is Mo, which gives a transportation efficiency $R_0(90^\circ) > 40$ % . In the long wavelength range the best material is Si with $R_0(90^\circ) > 40$ % in the wavelength range 20-100 nm.

In order to obtain effective reflection in a broad wavelength range it is necessary use different mirror materials. This is easily possible in the proposed distribution system. The plane facets can be used at different vertical level. For example, the photon beam could be injected into the photon ring at three different vertical positions. Figure 3 shows a view of a facet with three different strip coatings in order to cover the wavelength range 6-100 nm. The best optical coatings for this use are C (6-10 nm), Mo (10-20 nm) and Si (20-100 nm). The proposed substrate material for the plane mirrors is silicon because it can be well polished, and has excellent thermal properties. Therefore we need only two strip coatings, C and Mo, and have one strip uncoated for the range 20-100 nm. Users can define the radiation wavelength for their experiment independent of each other to a very large extent, since they use three different vertical levels in the photon ring. This design made it possible to make various wavelengths of SASE radiation available in the FEL laboratory quasi-simultaneously.

The system, described above, can provide FEL radiation for 24 user experiments in a quasi-simultaneous mode. Let us discuss the problem of a simultaneous mode operation of users. Many applications require only very high peak brilliance. Such experiments for which average brilliance and wavelength are not critical, can operate simultaneously at the same radiation wavelength. This could be realized, for instance, by means of rotating deflector mirrors. The principle design is sketched in Fig. 4. Let us assume that the superconducting accelerator operates with duty factor 1 % at a repetition rate of 24 Hz. In this case the initial photon beam is transformed into 24 beams. The switching mirrors need to rotate on frequency of 1 Hz such that each user actually receives one train of pulses with a full duration of 0.5 ms per second. This procedure of pulse train distribution reduces the average brilliance of the SASE FEL, but the peak brilliance remains untouched. Note also

that even if the beam is distributed among 24 users , the average brilliance per user will still be three orders of magnitude higher than that of state-of-art 3rd generation synchrotron radiation sources.

In addition to quasi-simultaneous operation at different wavelengths or simultaneous operation with the same wavelength, the SASE FEL with photon ring distribution system also offers a possibility for simultaneous multi-user mode operation at different wavelengths. At a fixed electron energy the magnet gap of the FEL undulator can be varied mechanically for wavelength tuning. The wavelength range 6-100 nm at fixed electron energy of 1.5 GeV can be covered by operating the SASE FEL with four undulators which have different periods. These SASE undulators can be placed behind each other at the condition that the subsequent undulator radiates at longer wavelength. Normally if a SASE FEL operates in saturation, the quality of the electron beam is too low for the generation of SASE radiation in a subsequent undulator which is resonant at a different wavelength. However, it is indeed possible to generate low intensity radiation in the linear SASE regime simultaneously in a sequence of undulators which are resonant at different wavelengths. This procedure reduces the peak brilliance of the SASE FEL radiation by about of factor 10, but this is still 9 orders of magnitude higher than that of 3rd generation synchrotron radiation sources. The wavelength selection can be done by suitable filters. Broad band notch filters exist for the VUV and soft X-ray ranges. For example, a (Zr) filter is useful in the 6-18 nm region, (Se + Al) in the 18-35 nm region, (Ti) filter for 35-50 nm region, (Pb) filter for 70-75 nm region, (In) for 75-90 nm, etc. If the power density is too high for transmission filters, one can use reflection filters based on multilayers or gratings.

In conclusion, it should be reemphasized that although the soft X-ray SASE FEL photon beam from each undulator is in principle a single user tool, just like an optical laser, the optical distribution system based on multifacet reflectors, movable mirrors and filters provide efficient ways to generate a multi-user facility – very similar to present day synchrotron radiation facilities. It is a great advantage that accelerator and electron beam transport lines in a new scheme of multi-user facility operate at fixed parameters and ”electron switchyard” is not required.

Acknowledgments

We thank J.R. Schneider and D. Trines for interest in this work.

REFERENCES

1. J. Anduszkow et al., Phys. Rev. Lett. 85(2000)3825
2. V. Ayvazian et al., Phys. Rev. Lett. **88**(2002)10482.
3. M. Koerfer, Nucl. Instrum. and Methods **A 483**(2002)34.
4. B. E. Newnam, in: Laser-Induced Damage in Optical Materials, eds. H. E. Bennett, et al., NBS Special publications, 1985, p. 161
5. B. E. Newnam, SPIE Vol. 738 Free Electron Lasers (1987), p.1
6. A. V. Vinogradov, A. V. Kozhevnikov, and A. V. Popov, Opt. Commun. 47(1983)361
7. I. N. Bukreeva, I. V. Kozhevnikov, and A. V. Vinogradov, Journal of X-ray science and technology 5(1995)396

Transverse self-fields within an electron bunch moving in an arc of a circle

G. Geloni, [a] J. Botman[a], J. Luiten[a], M. v.d. Wiel[a], M. Dohlus[b], E. Saldin[b], E. Schneidmiller[b]and M. Yurkov[c]

[a]Department of Applied Physics, Technische Universiteit Eindhoven,
P.O. Box 513, 5600MB Eindhoven, The Netherlands

[b]Deutsches Elektronen-Synchrotron DESY,
Notkestrasse 85, 22607 Hamburg, Germany

[c]Particle Physics Laboratory (LSVE), Joint Institute for Nuclear Research,
141980 Dubna, Moscow Region, Russia

Self-interaction within an electron bunch moving under the action of external forces may spoil the high brightness required for a SASE-FEL operating in the x-ray regime. Here we present part of the results achieved in [1], which deals with transverse self-interactions. We address the problem of a 1D line bunch moving in an arc of a circle analytically and from a fully electrodynamical viewpoint comparing our results with the code TRAFIC^4.

1. TWO PARTICLES IN AN ARC OF A CIRCLE

We follow [1] (see the latter for detailed treatment and references), starting from the expressions of the Lorentz force in the transverse (in the orbital plane, orthogonally with respect to the test particle velocity) direction:

$$\vec{F}_{\perp C[orR]} = e\vec{E}_{\perp C[R]}(\vec{r_{\rm T}},t)+ec[\vec{\beta_{\rm T}}\times\vec{B}_{C[R]}(\vec{r_{\rm T}},t)]_{\perp}. \quad (1)$$

Here the subscript T stands for test particle, C and R stand for Coulomb and Radiative field. $\vec{B}$ and $\vec{E}$ are understood to be the Lienard-Wiechert formulae for the electromagnetic fields. Using explicit expressions for the quantities in Eq. (1) together with the proper retardation conditions we found analytic equations for the transverse force exerted by a source electron on a test particle in all the cases in Fig. 1, both with the test particle in front (the cases actually depicted in the figure) or behind the source. These expressions are in perfect agreement with simulations by the code TRAFIC^4 (see [1]). As an example we show, in Fig. 2, the normalized transverse force ($\hat{F} = F_{\perp}/[e^2/(4\pi\varepsilon_0\Delta s)]$) for a two-particle system entering a hard-edge bending magnet (situation in Fig. 1a) as a function of the position after injection. The solid lines show analytical results; the circles describe the outcome from TRAFIC^4. We plotted several outcomes from different values of the normalized distance between the two particles.

2. LINE BUNCH AND TEST PARTICLE

By integration of the latter results over a given bunch density distribution function one can calculate analytical expressions for the transverse force acting on a test particle behind or in front of the bunch (Tail-Head interaction). Fig. 3 shows the normalized transverse force $F_{\perp}/f_2$ ($f_2 = e^2\lambda_0/(4\pi\varepsilon_0 R)\ln(\Delta\hat{s}_{\rm max})$, $\Delta\hat{s}_{\rm max}$ being the maximal source-test distance) acting on a test particle in front of a bunch with rectangular density distribution which enters a hard-edge bending magnet as a function of the position of the test particle inside the magnet. The solid lines show analytical results; the circles describe the outcome from TRAFIC^4. We choose $\Delta s_{\rm max} = 100\mu$m, $\gamma = 100$, $R = 1$ m; graphs are plotted for several values of the parameter $\Delta\hat{s}_{\rm min}$. Similar studies can be performed with the test particle behind the bunch (giving completely different results, due to the change of the retardation condition, [1]). In the case of tail-head interaction, by composition of rectangular bunches we found an expression for

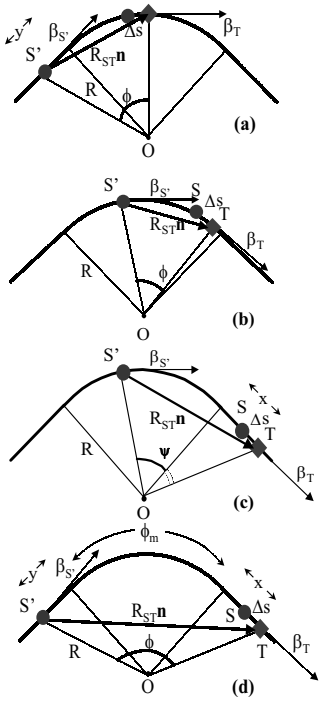

Figure 1. Possible configurations source-test particle.

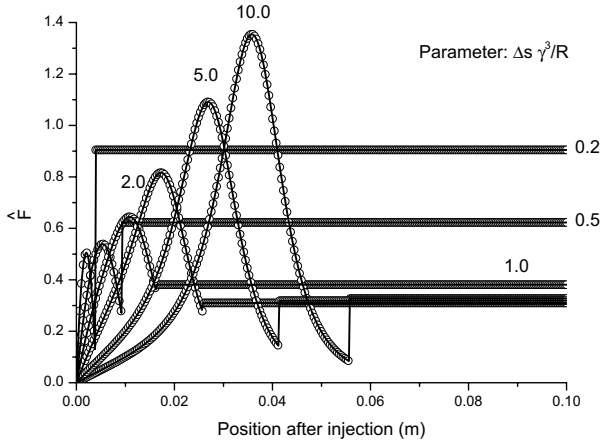

Figure 2. Example of transverse self-force for a two-particle system. The source particle is behind the test electron (Tail-Head interaction).

the transverse force exerted by a bunch with arbitrary density distribution. Such expression is regularized to a formula independent of the distance between test particle and bunch by subtraction of the steady-state transverse self-interaction:

$$\widetilde{F}_{\perp}^{\rm tot} \simeq \frac{e^2}{2\pi\varepsilon_0 R}\left[\lambda(s - R\phi^3/6) - \right.$$

$$\left. -\frac{1}{6}\int_{-\infty}^{s-R\phi^3/24} \ln\left(\frac{24(s-s')}{R\phi^3}\right)\frac{d\lambda(s')}{ds'}ds'\right], \qquad (2)$$

λ being the particle density distribution, s being the test particle position in the bunch, and ϕ the retarded angle (see [1]).

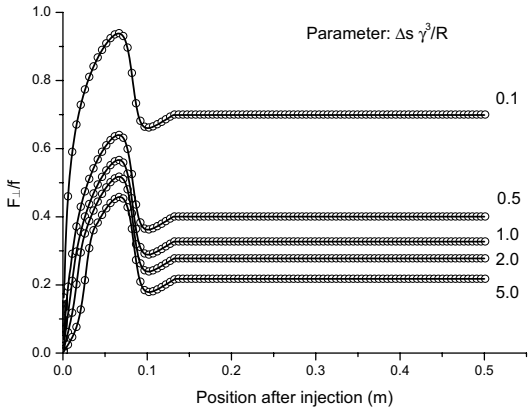

Figure 3. Example of transverse self-force acting on a self particle in front of a rectangular bunch (Tail-Head interaction).

REFERENCES

1. G. Geloni et al., DESY 02-048, May 2002. Also, to be submitted to Phys. Rev. E

Bunch Length and Phase Stability Measurements at the TESLA Test Facility

Ch. Gerth[a*], J. Feldhaus[a], K. Honkavaara[a], K.D. Kavanagh[b], Ph. Piot[a], L. Plucinski[a], S. Schreiber[a], I. Will[c]

[a]Deutsches Elektronen-Synchrotron (DESY), Notkestraße 85, D-22603 Hamburg, Germany

[b]School of Physical Sciences, Dublin City University, Dublin 9, Ireland

[c]Max-Born-Institut, Max-Born-Straße 2a, D-12489 Berlin, Germany

Electron bunch lengths and time jitters have been measured with sub-ps resolution at the TESLA Test Facility at DESY. Synchrotron radiation emitted from a dipole magnet reflects the longitudinal charge distribution of the electron bunch and can also be used as a timing reference of the radiation pulses produced by the free-electron laser. For sub-ps time resolution, dispersion effects of the spectrally broad-band synchrotron radiation have to be suppressed. The phase stability of the FEL pulses with respect to the radio-frequency master oscillator has been studied with a streak camera operating in synchroscan mode.

1. Introduction

Single-pass free-electron lasers (FEL) operating in self-amplified spontaneous emission (SASE) mode are promising sources for the generation of tunable, short-pulse, laser-like radiation in the VUV and X-ray region (Ref. [1] and references therein). The SASE process requires a high-quality electron beam and a long, precise undulator. Presently, only laser-driven radio-frequency (rf) electron guns in combination with bunch compression schemes can produce ultra-short bunches with high peak currents and small emittances. Much work has been devoted to the development of diagnostic techniques for electron bunches with sub-ps duration (for an overview see Refs. [2,3]). In this paper, we report on electron bunch length measurements at the TESLA Test Facility (TTF) with a high-resolution streak camera.

In order to exploit the short pulse length of the FEL radiation, an optical fs laser system will be synchronized to the TTF FEL for sub-ps two-colour pump-probe experiments [4]. A crucial issue is the synchronization of the optical laser to the FEL pulses [5–8] with an accuracy of approximately the pulse length (200 fs (rms)). To fulfil such a requirement, the time (or phase) stability of the FEL pulses must be on the same timescale. In this paper, we report on phase stability measurements of the electron bunches with respect to the rf of the linear accelerator that dives the FEL. Under SASE conditions, the phase jitter of the electron bunches is a fingerprint of the time jitter of the FEL pulses.

*Corresponding author. Tel.: +49-40-8998-1841; fax: +49-40-8998-4475.
E-mail address: christopher.gerth@desy.de (Ch. Gerth)

2. Experimental set-up

A schematic overview of the main components of the TTF (phase 1) is depicted in Fig. 1. Electron bunches were generated from a Cs_2Te cathode located in an L-band (1.3 GHz) rf gun. The cathode was illuminated by frequency-quadrupled UV laser pulses (262 nm) of a mode-locked Nd:YLF laser. The laser has been synchronized to the rf and its measured (rms) pulse length in the UV is 7(1) ps [9]. The rf gun is followed by a super-conducting TESLA cavity which boosts the electron energy up to 16.5 MeV. Two super-conducting accelerating modules (ACC1 and ACC2) further accelerate the electron bunches up to 300 MeV. Two magnetic chicanes (BC1 and BC2) have been installed to compress the electron bunches: BC1 is located downstream from the booster cavity and BC2 between the two accelerating modules. For a detailed discription of the set-up refer to Ref. [1].

Synchrotron radiation (SR) emitted by the dipole magnet has been utilized to study the electron bunch length and the phase stability with respect to the rf master oscillator. The temporal distribution of the SR pulse, which mirrors the longitudinal charge dis-

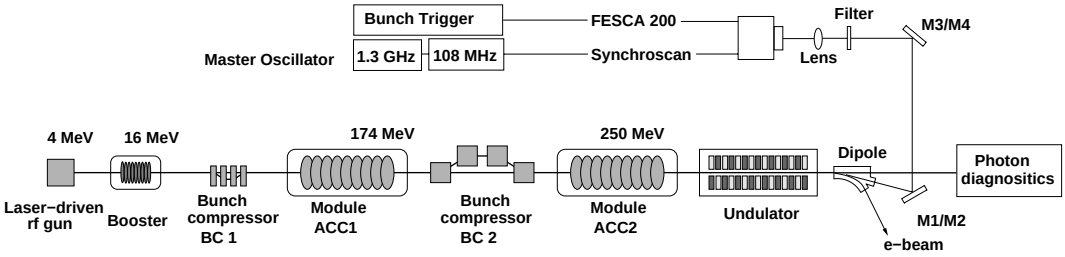

Figure 1. Schematic layout of the TTF (phase 1). The total length is about 100 m (not to scale).

tribution of the electron bunch, has been measured with a streak camera. The spectrally broad-band SR has been transported by four plane Al mirrors from the accelerator tunnel through 15 m of air to a diagnostic hutch and focused with an achromatic lens ($f = 0.2$ m) onto the entrance slit of the streak camera. The CCD image produced by the streak camera has been binned in order to get the temporal profile.

To reduce chromatic effects, a narrow band-pass filter has been employed [10]. Figure 2 demonstrates the broadening of the profiles which is mainly due to dispersion effects in the vacuum window of the dipole magnet and the focusing optics of the streak camera. The profiles have been recorded during FEL operation in the saturation regime for three different radiation bandwidths. The asymmetric profile is only resolved if a narrow band-pass filter is used. The width of the leading peak has been determined to be 0.6(1) ps (rms) if the filter $\lambda = 515 \pm 5$ nm (Fig. 2(c)) is used and 1.0(1) ps (rms) if the filter $\lambda = 500 \pm 40$ nm (Fig. 2(b)) is used. Without applying any filter, the leading peak smears out completely (Fig. 2(a)).

The FESCA-200 camera [11] employed for the bunch length measurements has a resolution of 0.22 ps (rms) at the second fastest streak speed of 50 ps/10.29 mm. A bunch signal with a jitter of about 50 ps served as a trigger for the streak.

A streak camera operating in synchroscan mode [12] was utilized for the study of the phase jitter of the FEL pulses. Instead of using a trigger signal, the streak repetition rate of the camera was synchronized to the sub-divided 108 MHz of the rf master oscillator of the accelerator. The rf signal was transported from the master oscillator located in the injector region to the synchroscan camera by a temperature stablilized, 100 m long cable.

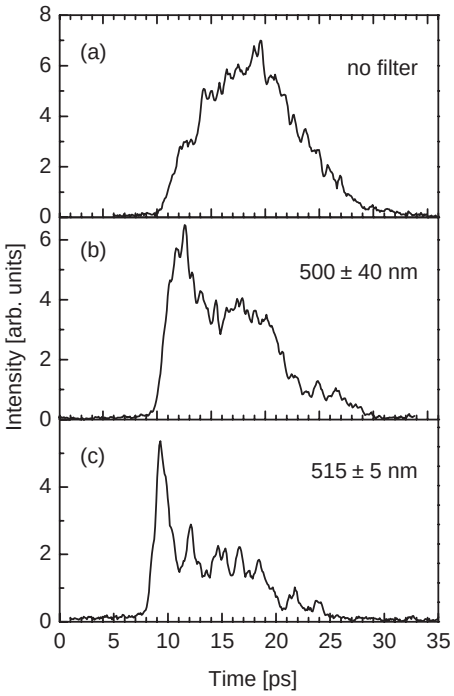

Figure 2. Temporal profiles of the synchrotron radiation pulses emitted by the dipole magnet. The profiles have been recorded for different bandwiths of the radiation. The profile in part (c) is an average of six single-shot profiles.

3. Bunch length measurements

Figure 3 compares the longitudinal bunch profiles measured for three different phase settings of module ACC1 with the results of numerical simulations. The experimental data represent the longitudinal charge distribution of single electron bunches. For these measurements, a filter with a bandwidth

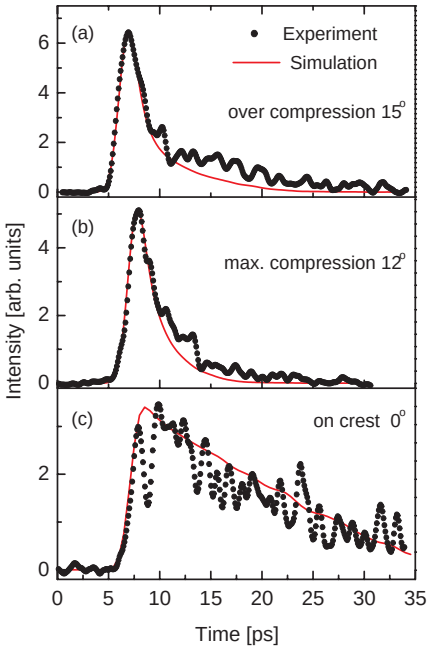

Figure 3. Profiles of the longitudinal charge density distribution of single electron bunches for different phase settings of the accelerating module ACC1. Dots: experiment; solid line: simulation.

$\Delta\lambda = \pm 40$ nm and a streak speed of 50 ps/10.29 mm have been used. Bunch compressor BC2 was operated at its nominal bending angle of 20° whereas BC1 was switched off during these measurements.

The beam dynamics was simulated with the set of computer tracking codes Astra [13] and Elegant [14]. The former programme includes a mesh-based space-charge algorithm and is used for the beam generation and transport at low energies. The latter programme is used to track through the accelerating module ACC1 and the bunch compressor BC2. It incorporates a simple model for bunch self-interaction induced via coherent synchrotron radiation (CSR) in the bunch compressor. The profiles generated by the simulations have been convolved with Gaussian profiles to account for the experimental resolution.

All profiles exhibit a distinct asymmetry. Figure 3(b) shows the profile at maximum compression which has experimentally been determined to be $12(1)^\circ$ off maximum acceleration (on crest). The profile comprises a narrow leading peak and a long tail. The width of the peak amounts to 0.9(1) ps. This corresponds to an electron bunch length of $\sigma_z = 0.27(3)$ mm. The longitudinal bunch profile presented in Fig. 3(c) has been recorded for a module ACC1 phase at on-crest acceleration (0°) whereas the profile in Fig. 3(a) is slightly overcompressed (15°). The rms bunch lengths of the entire profiles are in good agreement with the results of previous measurements [15] in which the asymmetric shape of the profiles could not be resolved due to a limited resolution at that time.

Since the bunch length is not negligible compared to the rf wavelength, off-crest acceleration for maximum bunch compression induces a curvature in the longitudinal phase space distribution (see Fig. 1 in Ref. [16]). This together with the small uncorrelated energy spread of less than ≈ 20 keV give rise to a spike in the longitudinal charge distribution. The longitudinal slices with extremely high peak currents (1–1.5 kA) lead to the SASE process producing ultrashort FEL pulses in the fs regime (≈ 100 fs) with GW peak powers [1,16].

4. Phase jitter measurements

Due to the dispersive sections (bunch compressors) in the accelerator, an energy variation of the electron beam results in a time jitter of the electron bunches and hence the FEL pulses. For instance, an energy variation of $\Delta E/E = 0.1\%$ would lead to a time jitter of the electron bunches with respect to the rf of $\Delta t = R_{56}/c \cdot \Delta E/E = 0.8$ ps behind bunch compressor BC2 with a longitudinal dispersion of $R_{56} = 227$ mm.

To study the time jitter between subsequent bunch trains with respect to the rf master oscillator, the accelerator was operated with single bunches at a 1 Hz repetition rate. A shot-to-shot variation of the centre position of the profiles directly reflects the time jitter with respect to the rf master oscillator. A histogram of the center positions of 100 subsequent pulses together with a Gaussian fit is shown in Fig. 4. The rms width of the Gaussian fit amounts to 0.7(1) ps. However, the latter value can only be regarded as an upper limit for time jitter, since it corresponds to the camera resolution.

A statistical energy jitter that results in a time jitter of about 1 ps could not be corrected for in a synchronization scheme. In this case it is necessary to mea-

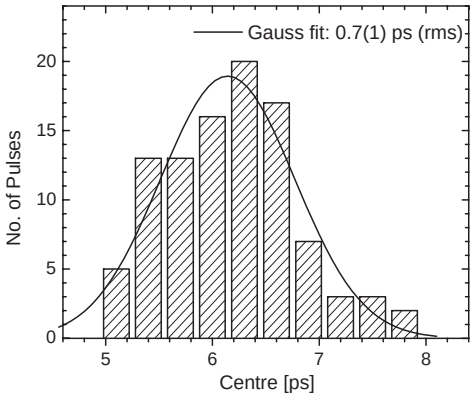

Figure 4. Histogram of the centre positions of 100 subsequent electron bunches. The width of the Gaussian fit amounts to 0.7(1) ps (rms).

sure the exact timing of the FEL and optical pulse (see Sec. 1) for each shot and to bin the data for different time delays. An upgrade of the present set-up will measure both the FEL and optical pulse on a single streak of a high-resolution FESCA-200 streak camera [5–8]. The time difference between the pulses will then provide the necessary information for implemanting a feedback correction for slow drifts.

Acknowledgements

The authors are thankful to A. Liero, M. Wendt and S. Simrock for their help and contributions to the successful performance of the phase jitter measurements. The authors are indebted to all members of the TESLA collaboration for their contributions to the TTF at DESY. Financial support for the pump-probe facility from the European Community within the Fifth Framework Programme (contract No. HPRI-CT-1999-50009) is gratefully acknowledged.

REFERENCES

1. V. Ayvazyan *et al.*, Eur. Phys. J. D **20** (2002) 149.
2. G.A. Krafft, Proc. DIPAC 97, Frascati, (1997) 48.
3. M. Geitz *et al.*, Nucl. Instr. and Meth. A **445** (2000) 343.
4. Project within the Fifth Framework Programme of the European Comission under contract No. HPRI-CT-1999-50009.
5. R.J. Stanley *et al.*, Opt. Commun. **115** (1995) 87.
6. M. Uesaka *et al.*, J. Nucl. Mat. **248** (1997) 380.
7. G.M.H. Knipples *et al.*, Opt. Lett. **23** (1998) 1754.
8. Y. Tanaka *et al.*, Nucl. Instr. and Meth. A **467-468** (2001) 1451.
9. S. Schreiber *et al.*, Proc. EPAC 2002, Paris, 1804.
10. M. Uesaka *et al.*, Nucl. Instr. and Meth. A **406** (1998) 371.
11. Hamamatsu CS6138 FESCA-2000.
12. Hamamatsu Synchroscan Camera.
13. K. Flöttmann, Astra user manual `www.desy.de/~mpyflo/Astra_dokumentation`
14. M. Borland, APS note LS-287, Argonne National Laboratory IL, USA.
15. K. Honkavaara *et al.*, Proc. PAC 2001, Chicago, 2341
16. V. Ayvazyan *et al.*, Phys. Rev. Lett. **88** (2002) 10482.

Study of the Transverse Coherence at the TTF Free Electron Laser

R. Ischebeck[a*], J. Feldhaus[b], Ch. Gerth[b], E. Saldin[b], P. Schmüser[c], E. Schneidmiller[b], B. Steeg[b], K. Tiedtke[b], M. Tonutti[a], R. Treusch[b], M. Yurkov[d]

[a]Rheinisch-Westfälische Technische Hochschule Aachen, III. Physikalisches Institut, Sommerfeldstraße 14, 52056 Aachen, Germany

[b]Deutsches Elektronen-Synchrotron DESY, Notkestraße 85, D-22603 Hamburg, Germany

[c]Universität Hamburg und DESY, Notkestraße 85, D-22603 Hamburg, Germany

[d]Joint Institute for Nuclear Resaerch, Dubna, 141980 Moscow Region, Russia

Double slits with different separations, crossed slits and circular apertures have been used to study the transverse coherence of the VUV light of the SASE Free Electron Laser at the TESLA Test facility at DESY. The resulting diffraction patterns are converted to visible light by a Ce:YAG crystal and imaged by a high resolution CCD camera. The visibility of the diffraction patterns indicates a high degree of transverse coherence. Measurements have been taken at various operating modes and wavelengths of the FEL. A numeric FEL simulation code (FAST) has been used to calculate the wavefronts of the light at the exit of the undulator. By propagating the wavefronts through the optical setup, the diffraction at the double slits is computed with the code GLAD. Good agreement with the measurements is found.

1. Transverse Coherence

Transverse coherence is one of the key features of a free electron laser. The particles in each microbunch oscillate synchronously; this is the reason for the enormous brilliance growth as compared to a conventional undulator light source. At the same time, the synchronized motion creates a radiation with a high degree of transverse coherence. The coherence increases as the FEL reaches saturation.

A light pulse can be characterized by its longitudinal and transverse coherence properties[2]. The transverse coherence has been investigated with the classical Young double slit experiment. The FEL beam propagates in free space behind the undulator, and the transverse coherence length increases together with the beam width during propagation of the light pulse. Hence the position must be specified at which the coherence length is determined. In the present expertiment, we choose the position of the double slits, 11.84 m downstream of the undulator exit. The complete setup is enclosed in the ultra high vacuum environment of the accelerator to avoid absorption of the VUV light.

2. TTF Accelerator and Free Electron Laser

The linear accelerator at the TESLA Test Facility TTF [1], [2] is equipped with 17 nine-cell superconducting cavities and serves both as a test accelerator for the superconducting linear electron-positron collider TESLA and as a drive linac for a VUV free electron laser which is based on the Self Amplified Spontaneous Emission (SASE) principle. The maximum electron energy is 260 MeV, the maximum bunch charge 5 nC. For the present measurements, photon wavelengths between of 80 and 120 nm have been used. The total pulse energy can reach 10 μJ.

*Corresponding author. E-mail: Rasmus.Ischebeck@desy.de

[2]These are also called temporal and spatial coherence.

3. Photon Diagnostics

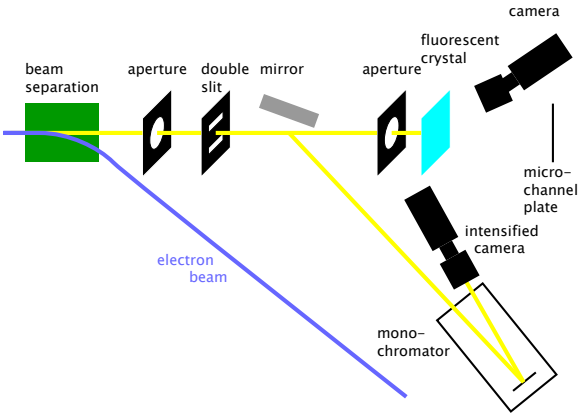

Figure 1. *Experimental setup for the SASE FEL photon diagnostics at the TTFL. For details, see [3].*

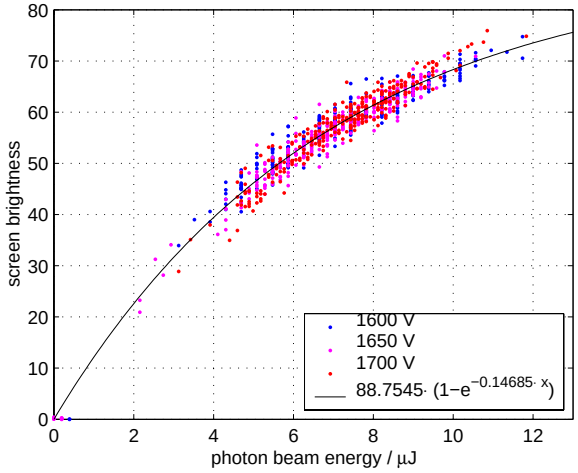

Figure 2. *Correlation of the Ce:YAG crystal brightness with the calibrated signal of the multi channel plate detector. The MCP has been operated at three different operating voltages; the results have been scaled according to a previous calibration [4]. The black line gives the fitted curve.*

Various devices are installed to analyze the properties of the FEL light. Figure 1 shows an overview of the experimental setup. A grating spectrometer [3], equipped with an intensified CCD camera, is used to measure the spectral distribution. The intensity is monitored over a wide range with a calibrated micro-channel plate (MCP) [4], detecting the light which is scattered on a thin gold-plated tungsten wire. A fluorescent Ce:YAG crystal (cerium activated yttrium aluminum garnet $Y_3Al_5O_{12} : Ce$) can be inserted to observe the spatial distribution of the FEL light as well as interference patterns. Ce:YAG is a fast scintillator (decay time constant 80 ns) with excellent mechanical properties. A crystal made of lead tungstenate ($PbWO_4$) is also available. However, in light yield it is much inferior to the Ce:YAG screen.

The light output of the Ce:YAG crystal is a non-linear function of the incident photon pulse energy, see Fig. 2. The MCP detector has been used to determine the light pulse energy.

The crystal is observed by a CCD camera, having 1280×1024 pixels with a size of $(6\,\mu\mathrm{m})^2$. A Peltier element cools the CCD in order to reduce noise and to make use of the full range of the 12 bit ADC. The camera is controlled and read out by a fiber optical link. The CCD chip employs the interline transfer technique to achieve exposure times below one microsecond and the lens-on-chip technique to increase the sensitivity. The CCD signal is digitized in the camera itself. In comparison with conventional video technology, where an analogue signal is transmitted to a frame grabber outside of the accelerator area, the digital readout reduces crosstalk to a minimum and permits a precise timing between the charge transfer in the CCD and the digitization of the ADC.

The space behind the Ce:YAG screen is occupied by an MCP detector. Therefore, the CCD camera is mounted at an angle of approximately 35° with respect to the normal of the screen. A shift-tilt lens (Nikon 85mm f/2.8D) is used to achieve good focusing over the entire crystal area. Different apertures can be moved into the beam at a position 3.1 m in front of the screen and

11.84 m behind the undulator exit. Circular apertures and double slit arrangements with different separations are mounted on two actuators. They can be moved to an arbitrary position with stepper motors. The slits are 2 mm long and 100 μm respectively 200 μm wide.

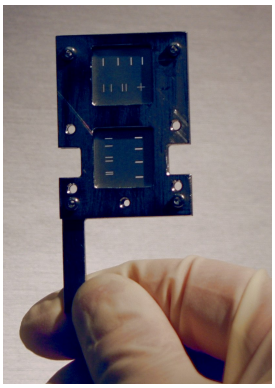

Figure 3. *The double slits, cut in stainless steel foil.*

Due to the high absorption of 100 nm radiation by almost any material, it is not possible to extract the radiation from the accelerator beam tube through an optical window. Therefore, the entire setup is incorporated into the accelerator vacuum system. As a consequence, the slit arrangement and the distance between slits and screen cannot be varied easily. The CCD camera is protected against radiation damage by a 20 cm thick lead shielding.

4. Image Processing

The image Φ recorded by the CCD is the convolution of the actual diffraction pattern Ψ with the point spread function P of the lens:

$$\Phi(x,y) = \int_{-\infty}^{\infty}\int_{-\infty}^{\infty} P(x-u, y-v)\cdot\Psi(u,v)\mathrm{d}u\ \mathrm{d}v$$

or, if we use discrete distributions

$$\Phi_{i,k} = \sum_{m,n} P_{i-m,k-n}\cdot\Psi_{m,n} \qquad (1)$$

The finite resolution smears out details in the images and reduces the apparent visibility of the diffraction patterns.

The system of equations (1) can in principle be solved for Ψ by matrix inversion if the point spread function P is accurately known. However, noise in the measured image distribution has a strong impact on the solution and will inevitably lead to negative values for Ψ. More appropriate are methods based on the maximum likelihood principle, imposing additional constraints on the smoothness and non-negativity of the reconstructed distribution. Originally developed by Lucy [5] and Richardson, such methods are widely used to correct for lens errors.

The point spread function may depend on the position in the image. Lens errors, for example, become more important in the outer part of the observed field. In our case, the tilt of the lens was not completely sufficient to correct for the inclination of the Ce:YAG crystal. A deconvolution with a spatially varying point spread function is numerically elaborate since it cannot be done in Fourier space [6].

The point spread function (PSF) of our setup has been measured in the center of the image with the lens focused onto an aperture with 1 μm diameter, illuminated from the back side by incoherent light. The width of the PSF increases as one moves away from the center. The narrow PSF has been used in the data analysis in order to avoid that an image is reconstructed with a higher contrast than is present in the real diffraction pattern (Fig. 4). The nonlinear response of the Ce:YAG has been corrected for using the fit curve in (Fig. 2).

It should be noted that the Ce:YAG crystal has another effect on the measured contrast of the interference pattern. The visible photons produced by fluorescence are emitted with an isotropic distribution. Only part of them enter the camera directly while many others are internally reflected at the surface of the crystal and emerge at the edges. On their path some are scattered inside the crystal and generate thereby an overall light background that reduces the modulation visibility of the diffraction pattern. The effect is under study but the data presented here are not yet cor-

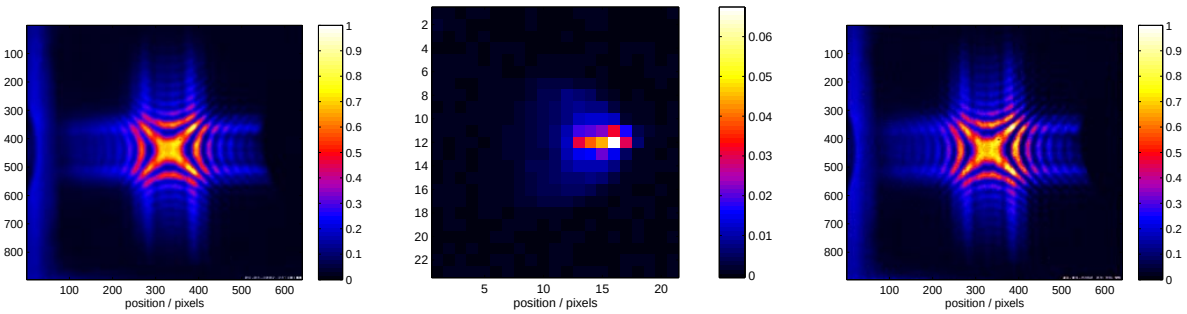

Figure 4. Left: *Raw image, averaged from 100 pictures; units: ADC counts.* Middle: *Point spread function of the tilted lens, measured under the same conditions as in the FEL.* Right: *The image has been deconvoluted with the camera resolution (10 iterations of the Lucy-Richardson algorithm [5]).*

rected for this background.

5. Image Analysis

To extract a quantitative measure for the transverse coherence from the images, the following analysis routine is applied. A slice perpendicular to the slits is selected and projected onto an axis along the slit direction. The resulting curve is smoothed with a fifth order lowpass Butterworth filter. One defines the *visibility* as the modulation depth of the intensity:

$$\mathcal{V} = \frac{I_{max} - I_{min}}{I_{max} + I_{min}}$$

and is computed for each interference fringe. For a perfectly coherent beam, we expect $\mathcal{V} = 1$ in the center of the pattern. Due to near field effects, the visibility drops to zero towards the sides (see section 6). Its peak value can be taken as a measure for the transverse coherence of the FEL beam at the given slit separation. The dependence of $\mathcal{V}$ on the slit separation is shown in Fig. 6. The measured [7] and simulated [8] beam profiles are shown for comparison.

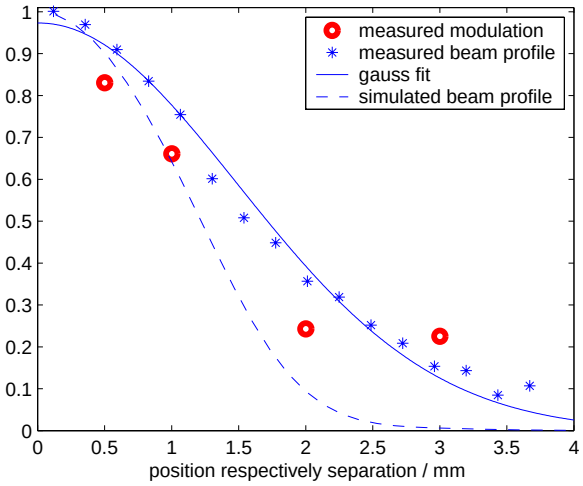

Figure 6. *Central modulation as a function of slit separation. For comparison, the beam profile (measured with the MCP detector) is also shown.*

6. Simulations

At a distance of 3.1 m behind the double slit one has not yet arrived in a region where far field diffraction theory (Fraunhofer diffraction) is applicable. Therefore, the diffraction effects are simulated with the program GLAD [9] which takes into account near field effects by solving

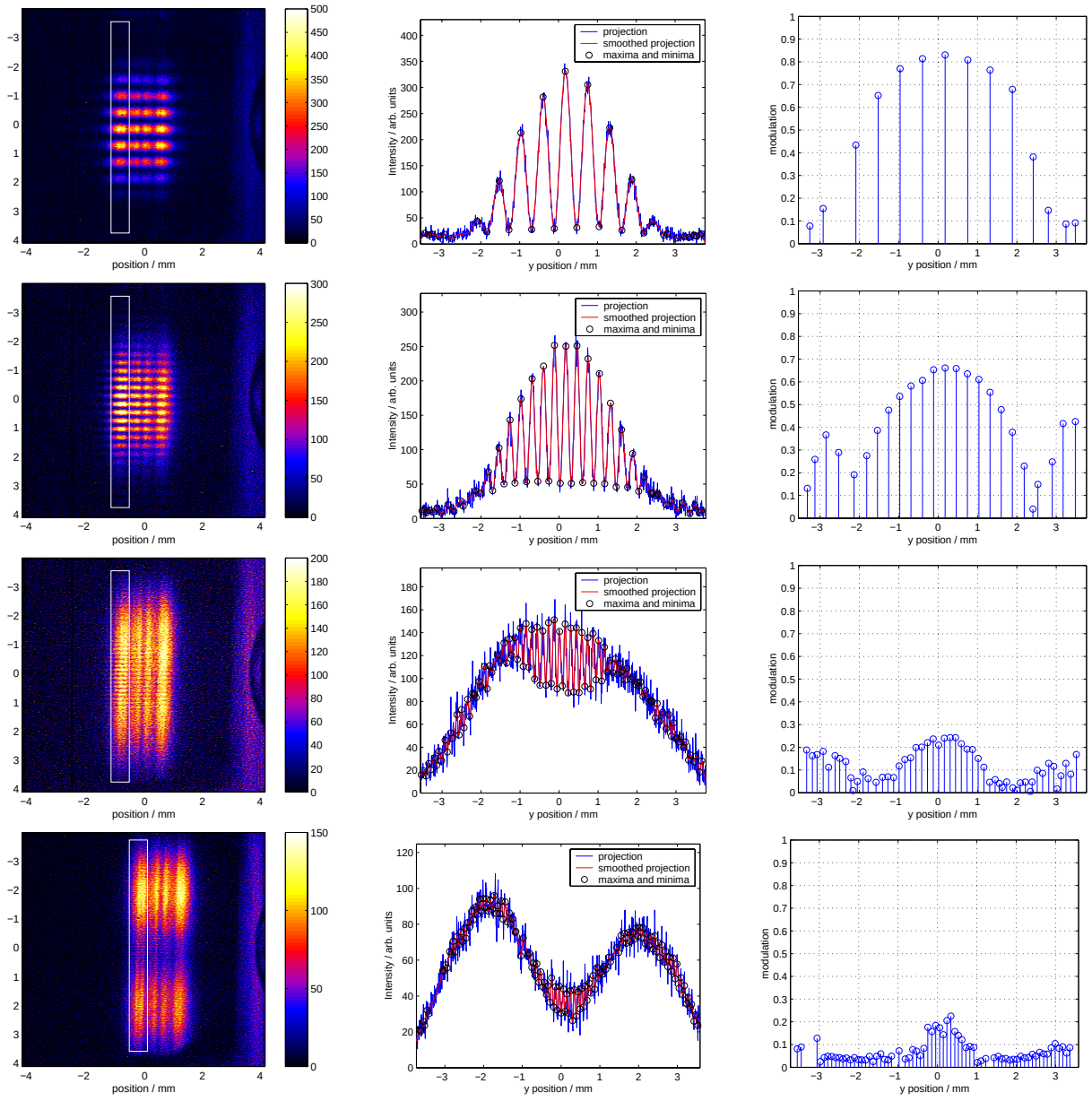

Figure 5. *Diffraction pattern for horizontal double slits with 0.5, 1, 2 and 3 mm separation.* Left: *Camera images*, middle: *Projection of the selected region*, right: *Visibility of the diffraction fringes.* First row: *0.5 mm*, second row: *1 mm*, third row: *2 mm and* fourth row: *3 mm slit separation. The visibility is highest in the middle of the field (although the envelope of the pattern has a minimum for the slits separated by 3 mm). The data are preliminary since a correction for background light in the Ce-YAG screen has not yet been applied.*

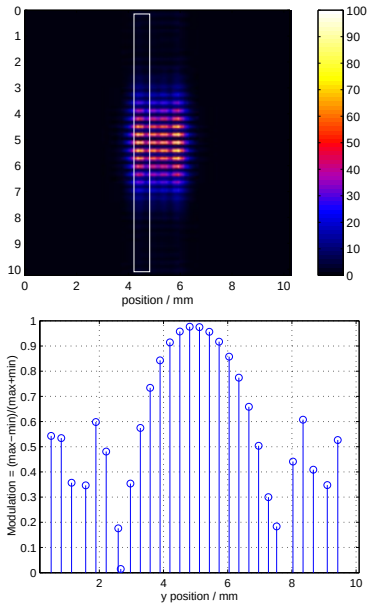

Figure 7. *Simulated diffraction pattern for the double slits with 1 mm separation.* Top: *Intensity distribution.* Bottom: *Visibility of the diffraction fringes.*

the Maxwell equations on a discrete grid that is propagated through space. The simulations are done on a grid of 2048 × 2048 points with a separation of 5 μm. The output wave front of the three-dimensional FEL simulation code FAST [8] is propagated from the end of the undulator through the slits up to the Ce:YAG screen. Fifty slices, equally spaced over the bunch, are propagated individually and their intensity at the screen is added incoherently. The resulting visibility (Fig. 7) is only slightly lower than unity.

7. Conclusion and Outlook

We have installed and successfully operated a double slit experiment at the 100 nm FEL at DESY. The observed diffraction pattern is quite similar to a numerical simulation in the near-field regime. The measured modulation depth exceeds a value 0.8 at 0.5 mm slit separation and goes down with increasing separation. It sould be noted though that the true modulation depth will be larger since a correction for the background light in the Ce:YAG screen has not yet been applied. From a statistical analysis of the FEL data almost full transverse coherence can be derived [10].

Beyond the saturation point of the FEL, the number of transverse modes grows, leading to a decrease of the transverse coherence. The TTF FEL can be virtually shortened by kicking the beam away from the undulator axis at various positions along the undulator. Thereby, it was possible to record diffraction patterns with different effective undulator lengths. The analysis of these data is underway.

REFERENCES

1. The Conceptual Design Report for the TESLA Test Facility, http://tesla.desy.de/TTF_Report/CDR/TTFcdrTab.html
2. P. Castro, Performance of the TESLA Test Facility Linac EPAC 2002
3. Ch. Gerth et al., Nucl. Instr. and Methods **A 475** (2001) 481
4. B. Faatz et al., TESLA-FEL 2001-09, 62 – 67
5. L. B. Lucy, The Atronomical Journal Vol. 79, Nb. 6, (1974) 745.
6. A.F. Boden, D.C. Redding, R.J. Hanisch, and J. Mo J. Opt. Soc. of America A, V 13 No 7 (1996) 1537 – 1545.
7. V. Ayvazian et al., Phys. Rev. Lett. **88** (2002) 10482.
8. E. L. Saldin, E. A. Schneidmiller, M. V. Yurkov, Nucl. Instrum. and Methods **A 429**, 233 (1999)
9. Applied Optics Research, http://www.aor.com
10. E.L. Saldin, E.A. Schneidmiller, M.V. Yurkov, these Proceedings.

Ablation of various materials with intense XUV radiation

Libor Juha[1,2], Josef Krása[1], Andrea Cejnarová[1], Dagmar Chvostová[1], Vladimír Vorlícek[1], Jacek Krzywinski[2,3], Ryszard Sobierajski[2,5], Andrzej Andrejczuk[3,4], Marek Jurek[2,3], Dorota Klinger[3], Henryk Fiedorowicz[6], Andrzej Bartnik[6], Miroslav Pfeifer[1], Pavel Kubát[7,8], Ladislav Pína[9], Jozef Kravárik[10], Pavel Kubeš[10], Yuri L. Bakshaev[11], Valeri D. Korolev[11], Andrei S. Chernenko[11], Mikhail I. Ivanov[12], Marek Scholz[13], Leszek Ryc[13], Josef Feldhaus[2], Jiri Ullschmied[8], Frederick P.Boody[14]

[1]*Institute of Physics, Czech Academy of Sciences, Na Slovance 2, 182 21 Prague 8, Czech Republic*
[2]*Deutsches Elektronen-Synchrotron DESY, Notkestrasse 85, 22603 Hamburg, Germany*
[3]*Institute of Physics, Polish Academy of Sciences, Al. Lotników 32/46, PL-02-668 Warsaw, Poland*
[4]*Institute of Experimental Physics, University of Bialystok, Lipowa 41, PL-15-424 Bialystok, Poland*
[5]*Warsaw University of Technology, Pl. Politechniki 1, PL-00-661 Warsaw, Poland*
[6]*Military University of Technology, Ul. Kaliskiego 2, PL-00-908 Warsaw, Poland*
[7]*J. Heyrovky Institute of Physical Chemistry, Czech Academy of Sciences, Dolejskova 3, 18223 Prague 8, Czech Republic*
[8]*Institute of Plasma Physics, Czech Academy of Sciences, Za Slovankou 3, 182 21 Prague 8, Czech Republic*
[9]*Czech Technical University, Brehova 7, 115 19 Prague1 – Stare Mesto, Czech Republic*
[10]*Czech Technical University, Technicka 2, 166 27 Prague 6, Czech Republic*
[11]*Russian Research Center "Kurchatov Institute", 123182 Moscow, Russia*
[12]*Research Institute of Pulsed Systems, 115304 Moscow, Russia*
[13]*Institute of Plasma Physics and Laser Microfusion, Hery 23, PL-00-908 Warsaw, Poland*
[14]*Ion Light Technologies GmbH, Lessingstrasse 2c, 93077 Bad Abbach, Germany*

Abstract

Ablation behavior of organic polymer (polymethylmethacrylate - PMMA) and elemental solid (silicon) irradiated by single pulses of XUV radiation emitted from Z-pinch, plasma-focus, and laser-produced plasmas was investigated. The ablation characteristics measured for these plasma-based sources will be compared with those obtained for irradiation of samples with XUV radiation generated by a free-electron laser (FEL).

PACS: 52.38.Mf; 81.65.Cf; 41.60.Cr; 52.50.Jm

Keywords: Ablation; XUV radiation; Z-pinch; Free electron laser; Laser-produced plasma

Corresponding author. Tel.: +42-2-66052741; Fax: +42-2- 86890265
E-mail address: juha@fzu.cz

1. Introduction

From earlier experiments [1-3] using intense XUV radiation, it was recognized that the interaction of short-wavelength radiation with organic polymers in vacuum results in the reduction of a layer thickness due to the transfer of macroscopic amounts of irradiated material into the vacuum.

Short wavelength radiation sources used for material removal (for a review see [4]) emit at both low (synchrotron radiation - SR) [1,2] and high (FEL and hot dense plasmas) [3] peak powers. With low-peak-power sources, material is removed by photon-induced desorption of material components from the irradiated surface (often called direct dry etching or SR evaporation). Each XUV photon can break any chemical bond and its energy is usually higher than any crystal's cohesive energy. XUV photons excite electrons from inner atomic shells, followed by an Auger cascade of other electrons. This leads to the formation of electron-depleted regions in the material structure, which rapidly decompose by Coulomb explosion. Thus, photons absorbed in the near-surface region may split the sample material into tiny pieces, which are ejected into vacuum. It is necessary to stress that, in the case of low peak intensity irradiation, material is removed only from the surface and a very thin near-surface layer. Quite a different situation is expected when a high-peak-power source delivers a single high-energy pulse onto the sample. The sample is exposed to a high local radiation dose (given by the energy content of the pulse and the absorption length of the radiation in the irradiated material) and dose rate (given by the short pulse duration). Thus, a large number of events which cause radiation-induced structural decomposition occur almost simultaneously, in a relatively thick layer of irradiated material, provided the absorption is not too high. Since a significant part of the radiation energy absorbed in the material is thermalized, sudden overheating of the layer, which is simultaneously chemically altered by the radiation, must be taken into account. The overheated fragmented sample region represents a new phase, which tends to blow off into the vacuum. Last but not least, the ultrashort, ultraintense FEL pulses can cause an immediate disintegration of the irradiated solids transferring a significant amount of electrons from valence to conduction band.

We present results for the ablation of organic polymer (PMMA) and elemental solid (silicon) induced by a single shot of intense XUV radiation emitted from discharge and laser-produced plasmas. The PMMA samples were also irradiated at high intensities by coherent 86-nm radiation delivered in many very short FEL pulses.

2. Experimental

The PMMA samples were 1-mm thick sheets, fabricated into 5x5-mm^2 chips purchased from Goodfellow (UK). 420 μm thick wafers of silicon (001) were cut from a single crystal supplied by the Chemistry Department of the Institute of Physics (Prague) and manufactured into 5x5-mm^2 chips. A piece of PMMA, 13x32-mm^2, was cut from the sheet mentioned above, mounted in a 27x32-mm^2 stainless steel frame and irradiated by XUV FEL radiation (TTF-FEL; for more details see [5-7]). The irradiation, the results of which are presented here, was carried out without masks at intensity ~ 10^{12} W/cm^2. All samples irradiated with other sources were placed behind a contact mask. Other sources of intense XUV radiation used were based on hot dense plasma produced by either a strong current pulse or a focused laser beam. The discharge plasmas used included Z-pinch plasma, which was formed from a single 120-μm diameter copper wire and driven by the S-300 pulsed-power machine [8], and a deuterium plasma focus, driven by the PF-1000 facility [9].

Higher temperature plasma was obtained by focusing a near-infrared laser (PALS [10]) into single and double gas puff targets. The single-stream gas-puff targets were realized by pulsed injection of xenon from an electromagnetic valve through a 2.0-mm diameter circular nozzle. For double-stream gas puff targets, the nozzle setup consisted of two coaxial nozzles [11]. The annular outer nozzle produced a hollow cylinder of helium, suppressing sideways expansion of the xenon. The outer nozzle orifice is a ring with an outer and inner

diameter of 3.0 mm and 2.5 mm respectively. Double-stream gas puffs have been demonstrated [11,12] to improve IR to XUV conversion radiation efficiency, compared to conventional single-stream gas puffs. For the experiments reported here the conversion efficiency reached 30% [12].

In our experiments we are taking into account that hot dense plasma is a source not only of photons but also of highly charged ions. For large-scale gas-puff targets, ion emission seems to be suppressed by the outer gas envelope surrounding the plasma, formed close to the gas stream center. Absence of ion current was checked using ion collectors. For the discharge plasmas, choosing suitable irradiation geometry, the ion bombardment of the sample surface was reduced. This means that the samples looked at the pinching plasma perpendicularly to the main axis of the plasma column. It is widely recognized that ion emission in that direction is much weaker than along the plasma column. In case of plasma focus charged particle emission from the plasma was stopped before arriving at the sample surface by a deuterium gas fill in PF-1000 chamber while a significant portion of the photons was transmitted.

Depth profiles of the structures formed due to ablation and expansion of the irradiated material were measured using an Alpha-Step 500 Surface Profiler (Tencor; USA). Raman measurements were made with an Ar^+ laser (514.5 nm) microbeam in the usual back scattering geometry (Model 1000 Renishaw Ramascope; U.K.). The system was equipped with a CCD camera and the Leica microscope DMLP. This tool enables the probing of chosen places on the sample surface. Typically, laser spots with diameter of 4 μm were used.

3. Results and discussion

Silicon was successfully ablated using the XUV source based on laser-produced plasma only. Profile and optical micrograph of a structure formed at the silicon surface irradiated through the contact mesh mask by XUV radiation emitted from a single stream gas-puff target driven by 0.5-kJ laser pulse are shown in Fig. 1. The structure looks not very smooth and its edges do not seem very

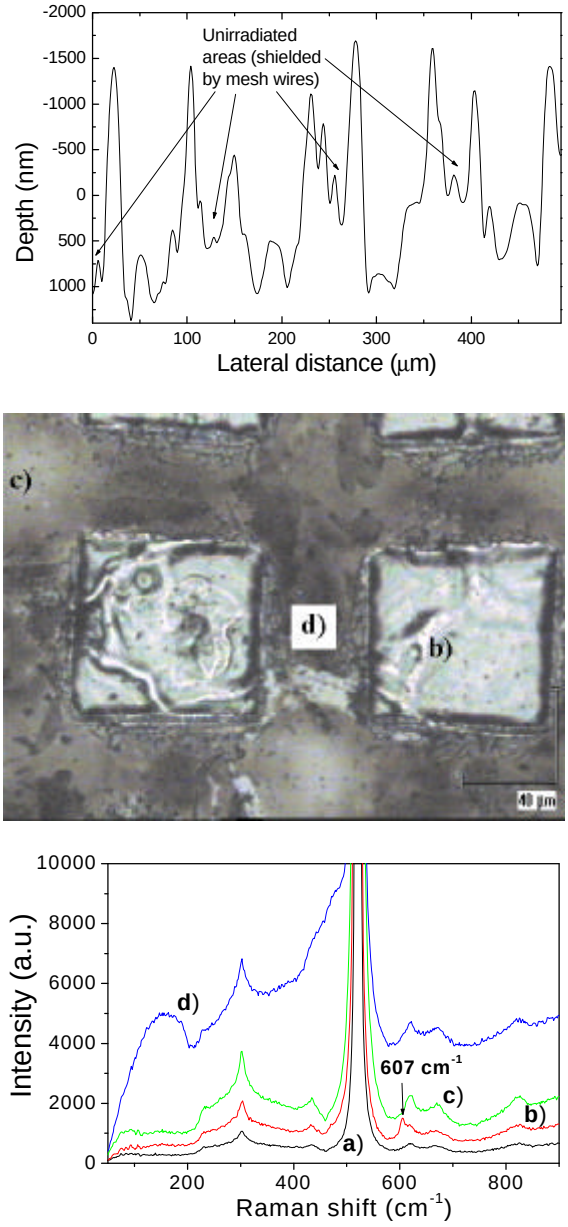

Fig. 1. Profile (top), optical micrograph (middle), and Raman spectra (bottom) of the silicon sample irradiated through mesh contact masks by XUV radiation emitted from a single-stream Xe gas-puff target driven by PALS. Two shots were accumulated (Nr. 23489 with pulse energy of 564 J and Nr. 23490 providing 519 J). Distance between the source and the sample was about 2.5 cm.

sharp. Its depth profile demonstrates this finding too. Raman spectra summarized in Fig. 1 (bottom) were taken at chosen places (they are marked in Fig. 1: middle; spectrum a) was measured on a surface of unirradiated silicon sample) on silicon sample surface. Strong amorphization can be seen in center of a strip between two ablated square wells [Fig. 1: d)]. Surprisingly, such an amorphization is not observed on the bottom of ablated well, i.e. below the ablated material layer [Fig. 1: b)]. Nevertheless, a new band (not yet assigned) appeared at 607 cm^{-1} in the spectrum measured on the bottom of the well. In center of the cross between four neighboring wells [Fig. 1: c)] can some amorphization be registered but is not so remarkable like in d). Irradiation of silicon with long XUV pulses from both discharge sources did not cause material ablation at a sample distance of about 50 cm from the source. Therefore we moved with the sample towards the plasma focus adjusting the distance at about 25 cm. Then some material removal was observed but the sample was destroyed (cracked) by a shock wave propagated in the deuterium gas.

Irradiated PMMA was affected by radiation in a different way than silicon. Formation of numerous small bubbles can be seen in Fig. 2 (top). Increase of a fluence (Fig. 2: bottom) leads to decrease of a number of bubbles, which are now spread over whole area of the sample. It means the bubbles were formed not only at directly irradiated squares between mesh wires, but also below the wires. This behavior indicates the secondary character of their origin. The bubbles shown in Fig. 2 (top) are due to the massive appearance of polymer chain radiolysis gaseous products in a high-dose-rate irradiated volume of material, while the bubbles in Fig. 2 (bottom) are formed due to local accumulation of the gaseous products transported from a deep irradiated volume by diffusion. A weak signal at 1580 cm^{-1} appeared in the Raman spectrum taken in a dark region of the bubble carpet in Fig. 2 (top). It testifies to a presence of graphitic carbon traces. Both surfaces shown in Fig. 2 look very different with respect to surfaces of PMMA irradiated by conventional, long wavelength lasers [13,14]. The XUV-radiation-induced bubbles are much finer than that produced by UV laser radiation. They are more similar to that formed by irradiation of

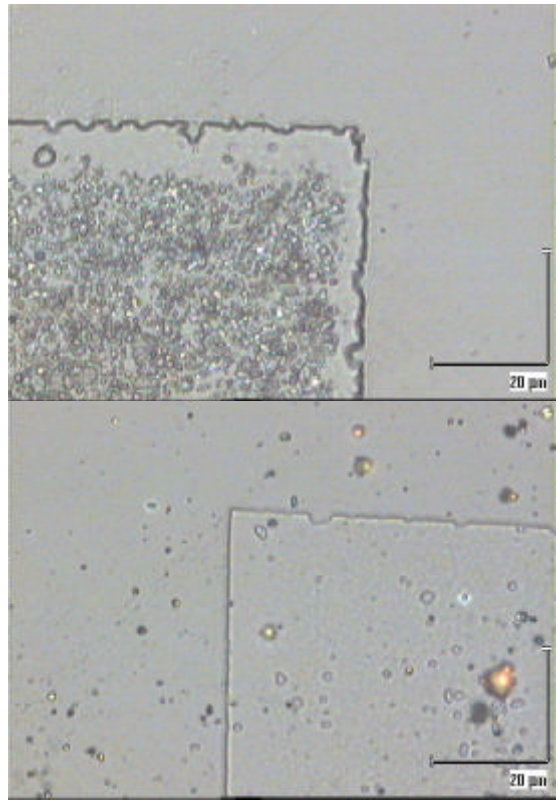

Fig. 2. Surface morphology of PMMA sample after irradiation by a single pulse of XUV radiation emitted from copper plasma driven by the S-300 pulsed power machine. The samples were placed behind mesh contact masks at six various distances from the source. The results shown here are for samples located at 59 cm (top) and 34 cm (bottom) from the source.

PMMA with ionizing radiation and subsequent heating of the sample [15]. An expansion of irradiated PMMA followed by an increase of irradiated surface roughness was reported for 800-nm 150-fs pulses [16]. Absence of such a process in the 86-nm FEL beam interaction with PMMA is demonstrated in Fig. 3 (top) and confirmed by a measurement with profiler. The FEL irradiated surfaces look very clean. According to the Raman measurements (Fig. 3: bottom) the material below ablated layers was not significantly radiation chemically altered. A length of about 25 µm was determined by optical microscopy for the hole drilled by the FEL beam in the material. It means that 70-nm layer of PMMA was removed by one FEL shot. An attenuation length of 86-nm radiation

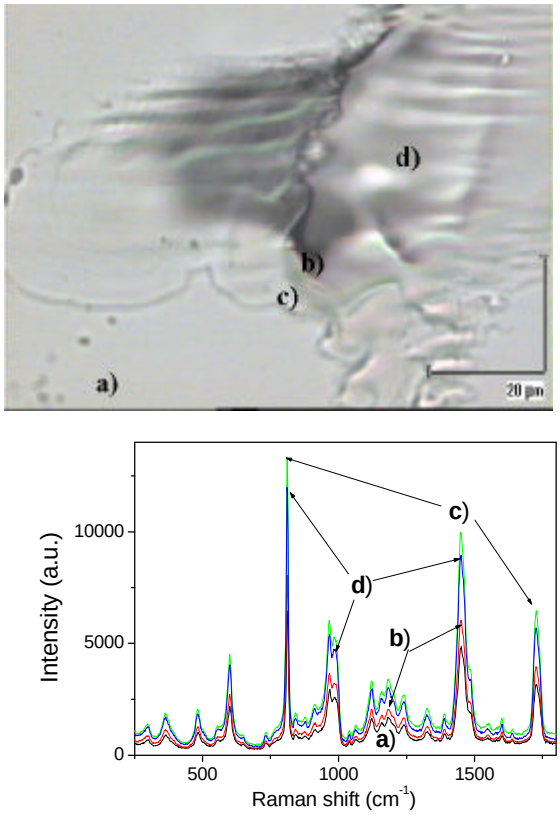

Fig. 3. Optical micrograph (top) and Raman spectra (bottom) of a crater induced in PMMA by 380 accumulated 5-μJ pulses of 86-nm FEL radiation. Angle of incidence was about 55°.

was in PMMA found to be about 10 nm [17]. It means that FEL intensity applied to PMMA surface in this particular case, is high enough to ablate PMMA even if reduced by three orders of magnitude due to absorption.

4. Conclusions

The silicon layers with thicknesses of several hundred nanometers can be ablated by a single shot of XUV radiation emitted from single- and double-stream He-Xe gas-puff targets irradiated by focused 0.5-kJ near-infrared laser pulse. The energy content of the XUV pulses is high enough to induce a heat flux sufficient to amorphize unirradiated silicon located below the shielding wires, however, the silicon material remaining below the ablated layer was found to be crystalline. This is surprising because a material below a layer ablated by XUV FEL radiation seems to be amorphized [18]. A possible explanation could offer an idea that harder, more penetrating components of the broadband XUV emission from the plasma induce a recrystallization of the amorphized layer. The long XUV pulses initiated remarkable morphological changes on the irradiated PMMA surfaces. Contrary to that, the FEL-induced ablation of PMMA seems to be clean and followed by a negligible alteration of remained material. This finding is very encouraging for prospective applications of short-wavelength FEL radiation in micromachining.

Acknowledgements

This work was funded by the Czech Ministry of Education within the framework of programs INGO (Grant LA055) and National Research Centres (Grant LN00A100), EC within 5th EU-FP (Project HCPRI-CT-1999-00053), and the State Committee for Scientific Research in Poland (Grant 217/E-284/SPUB-M).

References

[1] S. Ichimura et al., J. Vac. Sci. Technol. B1 (1983) 1076.
[2] K. Saito, A. Yoshikawa, Jpn. J. Appl. Phys. 26 (1987) L1428.
[3] B. Yaakobi et al., Appl. Phys. Lett. 43 (1983) 686.
[4] L. Juha et al., Surf. Rev. Lett. 9 (2002) 347.
[5] V. Ayvazyan et al., Eur. J. Phys. D20 (2002) 149.
[6] R. Treusch et al., Nucl. Instrum. Meth. Phys. Res. A467-8 (2001) 30.
[7] A. Andrejczuk, U. Hahn, M. Jurek, J. Krzywinski, J. Pelka, H. Reniewicz, E. A. Schneidmiller, W. Sobala, R. Sobierajski, M. Yurkov, TTF FEL team, HASYLAB Annu. Rep. (2001) 117.
[8] Yu. L. Bakshaev et al., Rev. Sci. Instrum. 72 (2001) 1210.
[9] M. Scholz et al., Nukleonika 45 (2000) 155.
[10] K. Jungwirth et al., Phys. Plasmas 8 (2001) 2495.
[11] H. Fiedorowicz et al., Opt. Commun. 184 (2000) 161.
[12] H. Fiedorowicz et al., to be published.
[13] T. Efthimiopoulos et al., Can. J. Phys. 78 (2000) 509.
[14] Z. Q. Liu et al., Appl. Surf. Sci. 165 (2000) 303.
[15] M. Ross, A. Charlesby, Atomics 4 (1953) 189.
[16] S. Badauch et al., Appl. Surf. Sci. 154-5 (2000) 555.
[17] I. E. Ferincz et al., J. Vac. Sci. Technol. B14 (1997) 828.
[18] R. Sobierajski, J. Krzywinski et al., this issue.

VUV Lithography Based on SiC Reflective Optical Systems and SASE FEL Coherent Light Sources as a Natural Extension to Shorter Wavelengths of Present-Day Optical Lithography Technology

C. Pagani[a], E.L. Saldin[b], E.A. Schneidmiller[b], M.V. Yurkov[c]

[a]INFN Milano - LASA, Italy

[b]Deutsches Elektronen-Synchrotron (DESY), Notkestrasse 85, D-22607 Hamburg, Germany

[c]Joint Institute for Nuclear Research, Dubna, 141980 Moscow Region, Russia

The semiconductor industry growth is driven to a large extent by steady advancements in microlithography. According to the newly updated industry roadmap, the 50 nm generation is anticipated to be available in the year 2012. This paper discusses the basic concepts of VUV lithography (VUVL), a relatively new form of lithography that uses vacuum ultraviolet radiation (VUV) with a wavelength in a range of 50 to 100 nm to carry out projection imaging. This approach uses a Self Amplified Spontaneous Emission (SASE) Free Electron Laser (FEL) as a source of radiation, a reflective mask, and a 4X reduction all reflective imaging system. The reflective elements for VUVL use SiC mirrors to produce normal incidence reflectivities nearly 40% . The mask in a VUV system also uses the same type of SiC material. Recent advances in SASE FEL systems suggest the feasibility of flexible sources for microelectronic production facilities. Any lithography must satisfy cost-ownership requirements. A VUV SASE FEL source is economical for high-volume production, because it can feed multiple steppers. The average SASE radiation on wafers is about 1 W, and throughput of each stepper is 90 wafer/hr. Estimated SASE FEL source portion of total cost is about $ 0.5 per 300 mm wafer. We believe that the underlying simplicity of the technology, particularly the mask and mirror and low source portion of total cost will make VUVL a cost effective solution for lithography at 100 nm and below. Since the wavelength of SASE FEL source is adjustable, selection of new materials needed for photoresists may be much easier than for the case of fixed wavelength source. SiC mirrors with characteristics required for VUVL optics are produced by industry. All components of the proposed SASE FEL source equipment have been demonstrated in practice. This is guaranteed success in the time requirement.

1. Introduction

The electronic industry is supported by the semiconductor industry, and the semiconductor industry is supported by the equipment industry where lithography has been the critical link. The speed and performance of the chips are dictated by the lithographic minimum printable size. Lithography, which replicates a pattern rapidly from chip to chip, also determines the throughput and the cost of electronic systems. Lithography is perhaps the most critical of the processing steps since about half of the capital equipment cost for a wafer fabrication is in lithography. Any future lithography technology must address the issues of a tool cost, throughput, mask costs, and process costs in order to be viable.

Current lithography for high-volume manufacturing employs optical projection. In projection photolithography, the mask is moved to near the light source. The presence of the different transparent and opaque regions patterns the light source. This patterned light beam is then passed through a reducer lens, which is focussed on the sample. The reducer acts to decrease the size of the light beam, and hence the size of the pattern. The pattern that is written on the sample is therefore smaller than the pattern than is in the mask. The actual size of the pattern is determined by the reducing factor of the lens, and can be a factor of four or more smaller than the mask pattern. The most advanced lithography tools use a wavelength of 193 nm. This will take the integrated circuit (IC) industry to 130 nm scale features. For IC features of 100 nm and beyond a new lithographic concept is required.

IC industry is willing to invest billions of dollars

to develop future lithographic technologies. There are four main next-generation lithography (NGL) technology contenders for 100-nm lithography and below. They are extreme ultraviolet lithography (EUVL), electron projection lithography (EPL), ion-beam projection lithography (IPL) and synchrotron-based proximity X-ray lithography (PXL). International SEMATECH hopes to build global consensus for a single NLG technology choice in near future. The huge cost of converting semiconductor manufacturing facilities to the new technology demands that the industry selects just one. In year 1999, International SEMATECH narrowed its choice of possible successors to optical lithography to two: EUVL and EPL [1]. Nevertheless, industry experts generally agree that it is too early to make a singular NLG decision. Now we can recognize the fallibility of recent NLG decision. Although, the recommendation for International SEMATECH to focus its funding efforts on the two selected technologies does not imply that development efforts in the other two selected technologies under consideration - X-ray and ion-beam projection lithography - should stop, the effect was to kill PXL development and infrastructure in the United States. However, at the XEL 2000 conference in Yokohama, where progress on all of four NLG technologies was reported, it was clear that Japan's PXL is many years ahead of the others. In contrast, the problems of EUVL and EPL are only slowly being revealed. It is not at all clear that either could succeed in semiconductor manufacturing, regardless of how much money and manpower is devoted to them [2].

The shift to smaller feature size traditionally was done by reducing the wavelength of optical lithography systems. As the wavelength becomes shorter, the light source become more complex and expensive. The present light sources under consideration for NGL include laser plasma sources and synchrotron radiation sources. A new era in the technology of powerful synchrotron radiation sources began in year 2000, with the first demonstration of the high gain linac-based SASE FEL at 100 nm wavelength. The experimental results presented in Ref. [3] have been achieved at the TESLA Test Facility (TTF) at DESY (Hamburg). The TTF team also demonstrated tunability of the SASE FEL in the wavelength range from 80 to 180 nm [4].

SASE FELs hold great promise as bright sources of VUV-EUV radiation for applications such as a projection lithography. This paper discusses the basic concepts of VUV lithography (VUVL), a relatively new form of lithography that uses VUV radiation with a wavelength in range of 50 to 100 nm to carry out projection imaging. This approach uses a SASE FEL source of radiation, a reflective mask, and a 4X reduction all reflective imaging system. The reflective elements for VUVL use SiC mirrors to produce normal incidence reflectivities nearly 40% . Recent advances in SASE FEL systems suggest the feasibility of flexible sources for microelectronic production facilities. In the Ref. [5] we presented design considerations of SASE FEL based on superconducting RF linear accelerator which provides in the 50-100 nm wavelength range average output light power up to 10 kW within 0.5% bandwidth. Any lithography must satisfy cost-ownership requirements. A VUV SASE FEL source is economical for high-volume production, because it can feed multiple steppers. We believe that the underlying simplicity of the technology, particularly the mask and mirror and low source portion of total cost will make VUVL a cost effective solution for lithography at 100 nm and below. Since the wavelength of SASE FEL source is adjustable, selection of new materials needed for photoresists may be much easier than for the case of fixed wavelength source. SiC mirrors with characteristics required for VUVL optics are produced by industry.

2. VUV lithography a reality for 100 nm production and beyond

VUV lithography, a novel approach to lithography that has been seen as the primary competitor to EUVL, is discussed in this section. In principle, VUVL is also a logical extension of optical lithography to short wavelengths. The wavelength range 40-120 nm is called Vacuum Ultraviolet, and the VUV-lithography utilizes light of 50-100 nm wavelength. This is the peak reflectivity wavelengths of silicon carbide (SiC). The idea of VUV lithography is to use SiC reflective optical systems and powerful VUV SASE FEL source [5]. SiC has a reflectivity at normal incidence of about 40% in the VUV wavelength range between 50 and 100 nm. It can be polished to a super-smooth surface with rms roughness of 2 $\AA$. This ma-

terial is very hard, stable and has high electrical conductivity and excellent thermal properties, such that surface distortions caused by high average absorbed power are negligible.

The mask in a VUV system is reflective and also uses the same type of SiC surface. A powerful SASE FEL source is used to illuminate the mask. Once the image is reflected from the mask, its travels through the projection optics system. The four SiC mirrors of the projection optics system reduce the image and form it onto the wafer with reduction factor of four. The resolution of a lithography system is usually expressed in terms of its wavelength and numerical aperture (NA) as

$$\mathrm{Resolution} = k_1 \frac{\lambda}{\mathrm{NA}} ,$$

where the k_1 is dependent on the process being used. In IC manufacturing, typical values of k_1 range from about 0.5 to 0.6 today. The idea of VUV lithography is to use large NA reflective optical elements at wavelength about equal to the smallest circuit dimensions. For example, an VUV system with wavelength of 50 nm and NA of 0.5 can yield 50-nm resolution. Another major limitation besides resolution in optical lithography is the depth of focus (DOF), which is governed by the equation

$$\mathrm{DOF} = k_2 \frac{\lambda}{(\mathrm{NA})^2} ,$$

where $k_2 \simeq k_1$ is a constant for a specific lithographic process. Historically, the "Comfort Zone for Manufacture" corresponds to the region for which DOF $>$ 0.5 μm [6]. Recently, however, it has been necessary to extend 193 nm imaging technologies to ever smaller DOF values down to 200 nm. Depth of focus values associated with VUVL for the printing of critical dimensions (CD) values ranging from 100 nm down to 50 nm will be DOF = 200 - 100 nm, i.e. comparable to the DOF associated with 193 nm lithography to print CD's down to 130 nm [6].

Compared to the multilayer EUV optics, a key advantage of VUV optics is the long history of technology development of SiC mirrors. Over this timeperiod a large experience base has accrued to clarify the key technical problems in detail. Now SiC mirrors with characteristics required for VUVL are produced by industry and are widely used at synchrotron radiation beam lines.

Industry experts generally agree that the biggest challenges and risks for the next generation lithography systems involve the mask. The technology that successfully overcomes the problems of mask production has a good chance of becoming the preferred choice. The VUV mask is produced by applying VUV-absorbing metal layer to flat SiC substrate and then etching away the metal to form the image of the circuit. We believe that the underlying simplicity of the mask technology will make VUVL a promising technology for lithography at 100 nm and below.

Present level of accelerator and FEL technique allows to solve the problem of powerful laser for VUV lithography. In [5] we performed design consideration of 10 kW-scale VUV SASE FEL. The design consists of a 12 MeV electron injector, a one pass 1 GeV accelerator, and a uniform undulator. The exhaust electron beam from the FEL is decelerated for the energy recovery and dumped at final energy 10 MeV. In this design the beam dump energy is below the photon-neutron production threshold, so the problem of radio-nuclide production in the dump does not exist. The technical approach adopted in this design makes use of superconducting RF linear accelerator (SRF accelerator). With SRF linac, a SASE FEL would acquire high average power, thanks to the input beam continuous-wave (CW) nature. The energy recovery of most of the driver electron beam energy would further increase the wall plug power to output VUV radiation power efficiency up to 1%. The electron beam qualities required for VUV SASE FEL operation can be met with a conservative injector design using a conventional thermionic DC gun and subharmonic bunchers. Average current produced by the injector is 10 mA. The SASE FEL provides a continuous train of 0.5 ps micropulses, with 2 mJ of radiation energy per micropulse at repetition rate 6 MHz. The radiation from SASE FEL is spatially coherent. The bandwidth of the output radiation would be about 0.5%. When considering a possible technical realization of the injector we have used only those technical solutions which have been used 10 years ago. The SRF modules for the main accelerator have been produced by industry. This is advantageous for compressing development time.

The development and test of the tools for VUVL

is greatly facilitated by the fact that required parameters of the radiation source are practically identical to those being developed in framework of SASE FEL user facility at DESY [7]. The SASE FEL user facility at DESY will produce in the VUV-EUV wavelength range (10-70 nm) train of 0.5 ps micropulses with about 1 mJ of radiation energy per micropulse at repetition rate of 9 MHz. The 1000 MeV SRF accelerator will operate at 1% duty factor. The average output radiation power can exceed 50-100 W. Commissioning of this facility could start in year 2003 [7]. The SASE FEL at TTF would allow to test various novel hardware components and could be used for pilot tests of the sub-100 nm lithography technology.

Estimating the cost of ownership (CoO) for any lithography system is always a risky business, fraught with the necessity of making numerous guesses. Nevertheless, analysis presented below indicates that the CoO for VUVL should be significantly lower than for EUVL technology.

Superconducting linear accelerator used to generate the high power of VUV SASE radiation is relatively expensive, approximately $ 150 million dollars. However, a SASE FEL source is economical for high-volume production, because it can feed multiple steppers. A SASE FEL source is assumed to yield 12 kW average power and is expected to support 100 steppers. Table 1 shows the result of VUVL stepper throughput estimation. The output dividing system produces 100 radiation beams which are directed to the steppers. The stepper exposure area is 26x27 mm2, and the exposure steps in a 300 mm wafer are 80, assuming 80% wafer area utilization. The average SASE radiation on wafers is 1 W, and the resist sensitivity 5 mJ/cm2. The exposure time thus obtained is 0.03 sec. Assuming stepping motion $W_{\rm s} = 0.2$ sec and overhead time 20 sec the raw throughput of this stepper is 90 wafer/hr

The accelerator, VUV beam line and accelerator building cost are $ 150M, $ 1.5M and $ 20M, respectively. The depreciation term for accelerator and beam line is 10 years, taking into account their application in plural device generations, and the depreciation term for building is 10 years. We assume that 5 persons takes care of accelerator by a cost of $ 50/hr. AC wall plug power consumption is about 1 MW.

Exposure cost can be acceptably low for high-volume production, where 100 steppers reduce the source portion of total cost to $ 0.5 per wafer single layer. The VUV mask and mirrors are significantly less expensive than EUV multilayer mask and mirrors and we believe that VUV lithography cost will be less than $ 20/wafer layer.

REFERENCES

1. R. DeJule, Semiconductor International, March 1999
2. H. I. Smith, Semiconductor International, February 2001
3. V. Ayvazian et al., Phys. Rev. Lett. **88**(2002)10482.
4. V. Ayvazian et al., Eur. Phys. J. D **20**(2002)149.
5. C. Pagani, et al., Nucl. Instrum. and Methods A 463(2001)9
6. J. E. Bjorkholm, Intel Technol. J. Q3(1998)1
7. M. Koerfer, Nucl. Instrum. and Methodods **A 483**(2002)34.

Radiation Exposure and Magnetic Performance of the Undulator System for the VUV FEL at the TESLA Test Facility Phase-1 after three years of operation *

J. Pflüger*, B. Faatz, M. Tischer, T. Vielitz
Hamburger Synchrotronstrahlungslabor, HASYLAB
Notkestr. 85, 22603 Hamburg

Abstract

Radiation damage to undulator systems made of permanent magnet materials like NdFeB or SmCo is a critical issue in SASE projects. It is of even more interest in high duty cycle machines using superconducting accelerators such as the TESLA Test Facility (TTF), which is a prototype for the future X-FEL at TESLA. This paper reports on experience made on the undulator system of the VUV-FEL of TTF-1, which ended on May6, 2002 after nearly three years of operation. The radiation exposure of the undulator system was recorded continuously and meticulously over the whole installation period in the TTF linac. Results of these dosage measurements as well as magnetic measurements after de-installation are reported. A comparison with magnetic field data taken prior to installation is given.

PACS codes:61.80-x, 87.66.Sq

Keywords: Physical radiation effects, Radiation damage, TLD

1. Introduction

Except for very special cases today's insertion device (ID) technology is almost entirely based on permanent magnet technology using mostly NdFeB and in some special cases SmCo. SmCo compounds, especially Sm_2Co_{17}, have higher Curie temperatures and therefore have better thermal stability. On the other side these compounds have a 30-40% lower energy product than NdFeB. Therefore, the field levels at otherwise constant parameters are 10-20% lower. In addition, SmCo is more expensive and much more brittle than NdFeB. Both NdFeB and SmCo can be partially demagnetized by exposing them to high energy particles such as neutrons, protons, γ rays or electrons. Generally SmCo, especially Sm_2Co_{17}, is known to be more resistant to radiation damage than NdFeB.

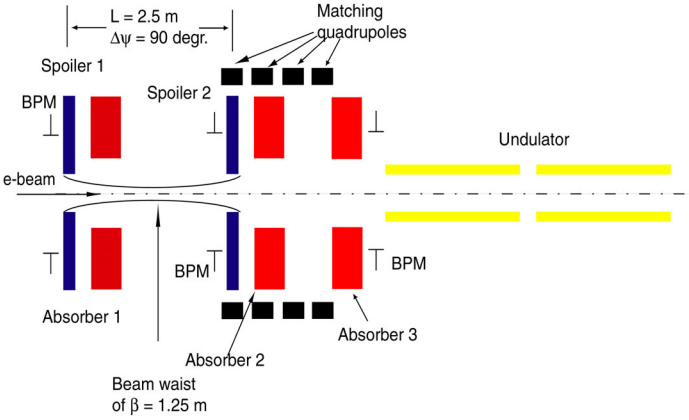

Figure 1: Schematic of the collimator system used in TTF-1. It effectively limits the horizontal and vertical phase space so that the adjacent undulator cannot be hit. The two spoilers separated by 90° Phase advance limit the phase space. The particle showers are absorbed in absorbers 1-3.

Over the past 20 years there were numerous publications on magnetization damage induced by neutrons [1-4], protons [5], hard γ rays [6] and electrons [7-9]. Several of these investigations were stimulated by a potential use of these materials for accelerator applications such as IDs or dipole, quadrupole or sextupole magnets. There is a general trend, which can be seen in these investigations: The amount of demagnetization depends on the type of particle, not on the deposited energy. As an example electrons are more detrimental than an equivalent dose of γ-quanta. Also, there is a close correlation to the coercive field of a specific material. The higher the coercive field, the higher the resistance to irradiation. There seems to be an analogy between

thermal stability, which for a given compound is determined by the coercive field and radiation hardness. At room temperature, for different NdFeB or SmCo compounds the coercive field $H_{C,J}$ may vary by more than a factor of three depending on the exact chemical composition and on details of the powder metallurgical process. There are ways to influence magnetic properties in such a way that a high remanent field can be balanced versus a low coercive field. It is therefore not too surprising that also different hardness to irradiation results.

In storage rings permanent magnet IDs are used successfully for more than 20 years. During routine operation no demagnetization has been observed. This was also verified in 1994 in a dedicated investigation [10]. However, by miss-steering the beam during injection severe radiation damage to IDs is possible as was shown in such an accident in 1993 at the ESRF [8].

A different situation arises in undulators for SASE FELs. They are operated in Linacs, which are single path devices. There the situation is very much different than in storage rings, where a very high transmission through the undulator is automatically enforced by the requirement for a long lifetime of the stored beam. Although in Linacs such as TTF the core of the beam may be much smaller than in a storage ring, it is nevertheless possible that a beam halo exists, which occupies a phase space, which can be many times larger than that of the beam core. Moreover, dark currents can be accelerated in a straight Linac without bending magnets.

A passive protection system, a collimator is therefore a prerequisite for a safe operation in a Linac. Such a system, which limits the phase space appropriately was built and installed in TTF-1 [11]. Because of length constraints it was not possible to install any kind of beam deflection. In this way dark current in the undulator region could not be avoided completely. Fig 1 shows a schematic of this system as it is installed in TTF-1. The collimator is straight, there is no dispersion because there is no space left for bending magnets. As a result dark current particles with less than the nominal energy may also pass through the collimator and eventually get lost inside the undulator. Control over dark current was therefore very important during TTF-1 operation.

2. Experimental

2.1 The Undulator

1. The undulator system is made of NdFeB material (VACODYM 396 produced by Vacuumschmelze GmbH, Hanau, Germany). It has a period length of 27.3 mm and a gap of 12mm. Its peak field is 0.47T. The system is subdivided in three segments of 4.492m length each. It is described in detail elsewhere [12-14]. Great care was taken in selecting a magnet material with high coercive field ($H_{C,J}$ =2070 kA/m).

2.2 Dosimetry

The radiation exposure was continuously monitored over the whole operation period of the undulator system, which began in July 1999 and ended in May 2002. Dosimeters were provided by the DESY radiation safety group. Radiophotoluminescence dosimeters (RPL's) with a large dynamic rang (10^{-2} to 10^{6} Gy) were used from July 1999 to August 2000. Starting in August 2000 Harshaw TLD-100 type Thermoluminescense Dosimeters (TLDs) were used. Both types of dosimeters are very small, round, about 1mm in diameter and about 5mm long. There were two reasons to switch from RPL to TLD's: First, dose rates were low enough to use TLDs and second, TLDs need less work for preparation and analysis. TLD's have a linear range of 10 Gy. By taking the non linearity into account, the usable range could be extended up to about 1000 Gy. Dosimeters were wrapped in aluminum foil, which allowed easy placement in between the poles. The distance to the beam axis was about 6.5mm. This was only possible on locations, where no focusing magnets were needed [12, 13]. In each undulator segment dosimeters were mounted on five positions. So there was a total of 15 positions for dosimeters distributed along the undulator system. Depending on the current accelerator conditions all dosimeters were exchanged frequently, typically once a week. Typical doses rarely exceeded 100 Gy, see below. Analysis of the dosimeters made by the DESY radiation safety group.

2.3 Magnetic Measurements

After de-installation the magnetic measurements were made in identical manner as in 1999 right before the installation of the undulator system into the linac. For this contribution they were restricted to the first upstream segment called SASE300, which suffered the highest radiation dose. The magnetic measurement bench, which was used, employs air bearings and guiding made of natural stone. This results in an ultra precise and very smooth movement. The verified flatness error of the bench over the length of the undulator is about 7μm. Longitudinally, the bench position is recorded by a

Heidenhain LIDA encoder system with an accuracy of 1µm/m. The resolution for the measurements is 1µm. A linear motor uses this position signal to position the probe with an accuracy of 1µm. It is a highly dynamic drive, providing fast positioning and a mechanical movement, which is completely free of any mechanical play. The hall probe was of type Bell HTL6-0608 together with appropriate electronics. It was carefully calibrated against a NMR system to correct for non-linearities.
The field was measured 'On the Fly' at intervals of 0.5mm. A full scan consisted of 10000 data points ranging from -2500 to +2500mm. The coordinate zero was at the center pole position of the structure.

The peak field values on all 327 poles were evaluated from these scans. For this purpose a procedure was employed using quadratic interpolation to precisely locate the position of the field extrema. Their absolute values were calculated. They are a precise measure of the 'local amplitude' and are sensitive indicators for changes due to demagnetization, very slight gap changes, etc.

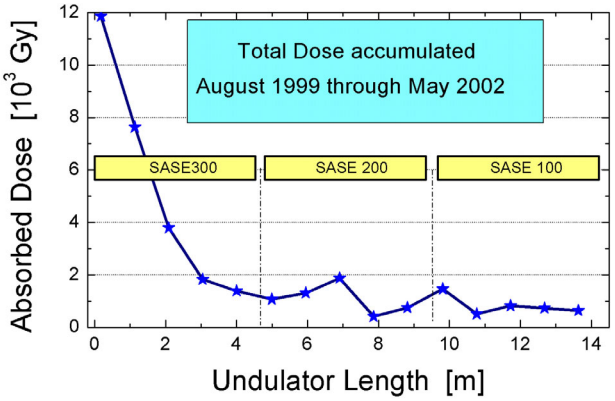

Figure 2: Total accumulated doses along the undulator system from August 1999 to May 2002. The beam enters from the left.

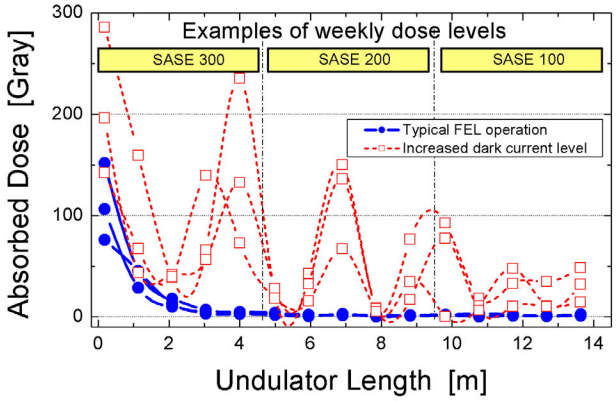

Figure 3: Examples of different weekly dose measurements at different operating conditions of the accelerators. The open squares correspond to increased dark current levels. Low energy particles enter the undulator and get unstable in the FODO lattice of the undulator and get lost. The full circles are typical for good FEL runs.

3. Results

The total accumulated dose since installation in 1999 is shown in Fig. 2. It is clearly seen that the dose decreases rapidly from about 12000 Gy at the beam entrance at the left side to about 640 Gy at the exit to the right. At about 1/4 of the SASE 300 segment the dose level is half of its initial value. To the end of the undulator systems doses get lower. It is important to note that these doses are by no way representative for an optimum operating mode. Although beam conditions for FEL runs were usually very good, Fig. 2 includes as well the initial commissioning phase of the accelerator, beam studies, different gun conditions, runs with high dark current levels etc. where beam conditions were not optimum and resulted in additional radiation exposure in the undulator. An impression of the variety of types of weekly radiation exposure is shown in Fig 3.: Six typical examples for weekly dose deposition patterns are shown. Good FEL beam condition was accompanied by pattern like the three full curves in Fig. 3. Entrance doses were in the order of a very few hundred Gray at most and the exit doses well below 10 sometimes even below one Gray. This demonstrates how well the beam can be collimated. The three dotted curves are patterns, which could be observed in conjunction with elevated dark current levels, i.e particles with less than the nominal energy, which can pass through the collimator, but become unstable in the FODO lattice of the undulator and hit the vacuum chamber. The exponential form in Fig.2 but especially the solid lines in Fig.3 suggest, that the source of radiation is not inside the undulator. It is inside the spoilers of the collimator, which is located about 4m upstream.
Fig.4 shows results of the magnetic measurements. The difference between the absolute peak field values of the data taken after de installation in May 2002 and those taken before installation in 1999 is

shown. In both cases data were taken on the 'naked undulator' this means the focusing magnets were not attached. The peak field level was 0.47T.
The data in Fig. 4 need some explanation. The overall shape is that of a very shallow parabola. This is a hint, that the girder has slightly deformed and the gap in the center of the structure is now slightly higher (about 8-10μm) than in the extremities. Most eye-catching are 10 regions where the deviation is significantly enhanced to about ±1 to 2 mT. At exactly these locations the focusing magnets arrays were previously attached. In between the deviation is much smaller. The reason for the enhanced deviation at these locations is presently not fully understood. There are at least two possibilities: Poles might have been moved by attaching and removing the focusing magnets. A 1mT peak field deviation would correspond to a local gap change of about 16μm.

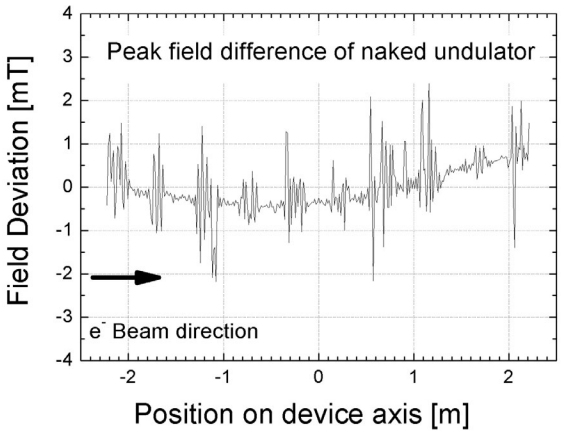

Figure 4: Absolute peak field difference of the 'naked' undulator, i.e. without focusing magnets attached. Measurements were taken before installation 1999 and after de-installation 2002. The locations where the focusing magnets where attached are still clearly visible by an increased deviation

Also slight hysteresis effects might play a role. In any case the curves are symmetric with respect to the center of the structure. If there would have been demagnetization, this curve should systematically show negative values at the beam entrance side Also there should be a correlation between dose rates and deviations. This is clearly not the case.

The detection limit for demagnetization can be estimated by the unperturbed regions to smaller than 0.1mT. Within this accuracy there is no evidence for any radiation induced demagnetization after almost three years of operation.

4. Summary and Outlook

The undulator system of the SASE FEL at the TTF is made of NdFeB. The magnetic field of the first, the SASE300 segment was carefully remeasured and compared to data taken before installation. We could not detect radiation induced demagnetization with an accuracy of about $2x10^{-4}$ at dose levels up to 12000 Gy. This was the maximum accumulated dose observed. It is still open at what dose levels observable damage occurs. Our operating conditions were that of a Linac in routine operation over the past three years. We believe that the passive beam protection by a collimator was essential. for the moderate doses. Our results support design efforts to reduce dose levels in future projects such as TTF-2 and the TESLA X-FELs: In TTF-2 collimator and undulator axis will not coincide anymore. To do so a dogleg type chicane will be built, which offsets the beam by about 400 mm. Its dispersion will be used for 'energy collimation' so dark current particles with less than the nominal energy cannot enter the undulator region. With such a collimating system we expect dose levels, which are significantly less than at the exit side shown in Fig.2., much less than 1 Gy/week.
A simple lifetime estimate based on the data of this report would result in a lifetime of the NdFeB material in the order of 200 Years or more under identical operation conditions, assuming 4Gy/week and a damage threshold of 12000 Gy. This gives the possibility of increasing the duty cycle of the accelerator by a factor of 10 but still stay within a lifetime limit of 20 years. If the level in TTF-2 could be lowered to 0.4Gy/week another factor of 10 would result. This is very likely, since dose level like this have already been observed. They have to be reproduced routinely. Also, the damage threshold of 12000 Gy is conservative and can be raised if better information is available, resulting again in an appropriately increased lifetime. Thus for TTF-2 the duty cycle can be increased by a factor >100 without jeopardizing the undulator leading to a lifetime of about 20 years. It should be noted that during the weeks of operation the number of bunches was increased by up to a factor of 100 Also the RF pulse lengths were increased. Both effects resulted in far less than an according increase in measured dose rate.

Finally the TESLA X-FELs undulator systems will be gap adjustable [15-16]. This offers an additional way to further minimize radiation exposure. For commissioning, electron beam alignment and other critical machine operations the undulator gap will be opened and radiation exposure is drastically reduced. Only if the machine is well adjusted, which can be supervised by a beam loss monitor system, the gap will be closed.

Our result indicate that operation conditions of a high duty cycle linac can be found so that conventional high coercivity NdFeB material can be used to built the insertion devices for the 4th generation light sources.

Acknowledgement:

We would like to thank N. Tesch, K.U. Hartz, K. P. Klimek and B. Racky from the DESY radiation safety group D3 for effective and continuous support of this work.

5. References

1. H. Spitzer, A. Weller, Report KFA Jülich (1984), SNQ1 NBH 22.05.84
2. K. Boden, H. Spitzer, Addendum to KFA Report SNQ 1 NBH 22.05.84
3. J. R. Cost, R.D. Brown, A.L. Giorgi, J.T. Stanley IEEE Trans. Magn. MAG-**24**, 3 (1987)
4. J. R. Cost, R.D. Brown, A.L. Giorgi, J.T. Stanley; Mater: Res. Soc. Symp.. Proc. **96** ,321 (1987)
5. F. Cominckx, W. Naegele, M. Reinharz, H. Schoenbacher, P. Seraphin, CERN Report SPS 83-1, TIS-RP(IR/83-07 (1983)
6. K. Boockman, H. Liehr, W. Rodewald, E. Salzborn, M.Schlupp, B. Wall, J. Magn. Mater. **101** (1991) 345
7. P. Colomp, T. Oddolaye, P. Elleaume, ESRF Report MACH-ID 93-09 (1993)
8. T. Ikeda, S. Okuda, Nucl. Instr. and Methods A407 (1998), 439
9. T. Bizen, T. Tanaka, Y. Asano, D.E. Kim, J.S. Bak, H.S. Lee, H. Kitamura, Nucl. Instr. and Methods A467-468 (2001), 185
10. J. Pflüger, G. Heintze, I. Vassserman, Rev. Sci. Instrum. **66** (1995),2
11. H. Schlarb, "Collimation System for the VUV Free-Electron Laser at the TESLA Test Facility" DESY-THESIS-2001-055 Nov. 2001 (ISSN 1435-8085; H. Schlarb "Design and performance of the TESLA Test Facility Collimation System" Proceedings of the EPAC 2002, June 3-7, 2002, Paris, France
12. J. Pflüger, Nucl. Instr. and Methods A445 (2000), 366
13. J. Pflüger, Y.M. Nikitina, B. Faatz, T. Teichmann, Proceedings of the FEL 18 conference Rome, August 26-31, 1996, II, 107
14. See: http://www-hasylab.desy.de/facility/fel/main.htm for a compact description of the undulator for Phase-1
15. TESLA Technical Design Report Part V: The X-ray Free Electron Laser , G. Materlik, T. Tschentscher, Editors, DESY 2001-011, ECFA 2001-209 TESLA FEL 2001-05, March 2001, available in the WWW under: http://tesla.desy.de

J. Pflüger, M. Tischer, Nucl. Instr. and Methods A483 (2002), 388

Undulator system for the VUV-FEL at the TESLA Test Facility Phase - 2

J. Pflüger*, U. Hahn, B. Faatz, M. Tischer *
Deutsches Elektronen-Synchrotron DESY, HASYLAB, Notkestrasse 85, 22603 Hamburg, Germany

Abstract

The Phase-1 of the VUV FEL at the TESLA Test Facility finishes in fall 2002. Phase-2, an extension of Phase-1 towards shorter wavelengths is under construction and will be ready for operation in 2003. A radiation wavelength as low as 6nm will be obtained by raising the electron energy to 1 GeV. There will be only minor changes to the undulator system. Compared to Phase-1 six instead of three undulator segments will be installed. The integrated focusing system will be replaced by an electromagnetic doublet structure. We report about the changes of the undulator, the undulator vacuum system, the separated quadrupoles including a stretched wire alignment systems and the modifications to the beam diagnostic system consisting of pick up monitors and wire scanners.

PACS codes:41.60.Cr, 41.85.Lc

Keywords: FEL, undulator, wire scanner, quadrupole alignment, TESLA TTF

1. Introduction

The goal of Phase-1 of the VUV FEL at the TESLA Test Facility was a proof of principles of the validity of the SASE concept in the VUV regime. Meanwhile Lasing was observed in Feb 2000 at 109nm [1] and most recently (Sep2001) saturation was obtained [2]. Thus, the design goals for Phase-1 were reached or exceeded [3].

Phase-2 is planned to be an extension of Phase-1 towards shorter wavelengths as low as 6nm. The option

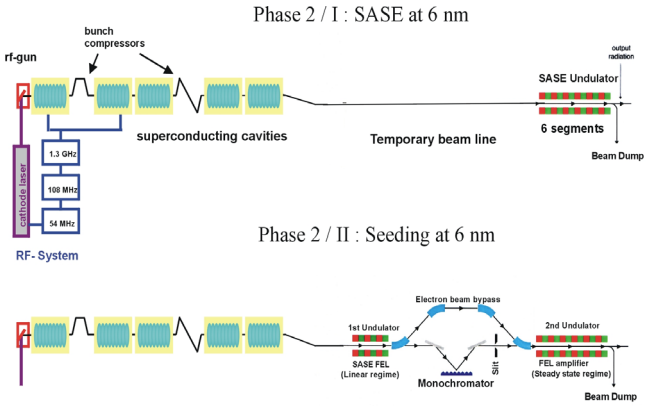

Figure 1: The two steps planned for Phase-2.:
Phase-2 /1 SASE at 6nm
Phase-2 /2 Seeding at 6nm

for this extension was kept in mind already from the very beginning of Phase-1 [4]. Expensive hardware components such as undulator magnet structures were designed to be used in Phase-2 as well. A radiation wavelength of about 6 nm could be obtained using the same magnet structure and gap by just raising the electron energy to 1 GeV. Two options will be realized:
In the first stage a 6 nm SASE FEL will be built as a straightforward extension of Phase-1 [4]. In order to reach saturation at 6nm the magnetic length of the undulator system has to be doubled to six undulator segments. The total length of the undulator section will be almost 30m.

In a second stage the so called seeding option will be built, which will provide a fully coherent beam with narrow bandwidth. Another three undulator segments with a total length of approximately 15 m are needed [5].

Fig 1 shows these two stages schematically.

2. Modifications of the Undulator System

The undulator system for Phase-1 was optimized without compromising on FEL performance and saturation length [6,7]. The result was a magnet structure with an integrated combined strong focusing FODO lattice consisting of 15 focusing and 15 defocusing quadrupoles. It allowed for an optimum average β function inside the undulator of only 1m at a beam energy of 0.3 GeV. By choosing a small quadrupole distance the influence of β-variations on the FEL process was kept negligibly small. Such a combined function undulator is much more difficult to design, build and tune than a conventional one. In addition for high accuracy electron beam orbit control one corrector and one beam position

Table 1: Undulator system parameters of Phase-1 and Phase-2

		TTF 1	TTF 2
Undulator Period Length	mm	27.3	27.3
Gap	mm	12	12
Peak field	T	0.47	0.47
K-Parameter		1.17	1.17
Electron beam energy	GeV	0.23	1.0
Segment length	m	4.4922	4.4922
Distance between Segments	mm	325	606
Focusing Type		integrated, FODO	separated, Doublet
Quadrupole type		Permanent magnet	Electro-magnet
Quadrupole distance	mm	477.75	4713 / 385 *
Quadrupole gradient	T/m	17	37
Quadrupole length	mm	163.8	120
Average β function	m	1	4.5
β_{Max} / β_{Min}	m	3.0	3.0
Saturation length	m	12	27

* distance between quadrupole doublets / quadrupoles in the doublets

monitor (BPM) per quadupole was required. They had to be integrated into the vacuum chamber inside the undulator gap, which therefore need a quite sophisticated design [8].

Based on the good and successful experience made in Phase-1 the requirements on undulator performance, temperature stability can be relaxed: In Phase-1 the stringent mechanical stability requirements lead to a temperature stability specification of ±0.3K. In Phase-2 this can be relaxed to ±1.0K. The smaller number of quadrupoles in the whole set up also simplifies commissioning and operation.

There are drawbacks, which have to be mentioned: First, debunching occurs in the quadrupole doublets. Second, the resulting average β-function is larger than its optimum values and for geometrical reasons cannot be made smaller. Both effects lead to an increase of saturation length of a few meters. These issues were worked out in detail in Ref [9]. A comparison of key device parameters between Phase-1 using the combined focusing and Phase-2 with the separated solution is shown in Table 1.

Fig. 2 shows a 3D view of the undulator system as it will be installed in the TTF tunnel.

average β function, β function beat, numbers of correctors and BPMs were revised [9]. For Phase-2 at 1 GeV an average β of ~3m would be possible with the present structure. A separated focusing system was investigated, in which the boundary conditions set by the already existing hardware were carefully considered. Full advantage will be taken from the modular magnet design used for Phase-1. The focusing magnets, which can be considered as additional attachments to a hybrid type magnet structure will be omitted. Thus period length, gap and total lengths of the magnet structures are kept unchanged and only the plain, conventional Halbach Type Hybrid Structure will be used further. The focusing will have to be accomplished by quadrupole doublets placed in between two neighboring undulator segments. Consequently the vacuum chamber design can be considerably simplified as compared to Phase-1. For electron optical reasons the quadrupoles of the doublets need to have a distance of 385mm. This gives space for electron beam diagnostic equipment such as beam position monitors (BPMs) and wire scanners in between.

Although a combined focusing solution used in Phase-1 offers the shortest overall system length there is much more effort needed for magnetic measurements, fine tuning magnetic as well as mechanical alignment, vacuum chambers, beam position monitors and correctors. Therefore the undulator system is considerable simplified by using separated focusing. In addition requirements on

3. Intersections

Fig.3 shows the components which will be placed in front, between and at the end of the undulator segments. For brevity these components will be called intersections. The vacuum chamber for the electron beam passes the assembly from the right to the left. The bore of the two quadrupoles is larger by 3 mm than the outer diameter of the vacuum chamber. In addition they are supported by a two axis drive system, which will allow to change the

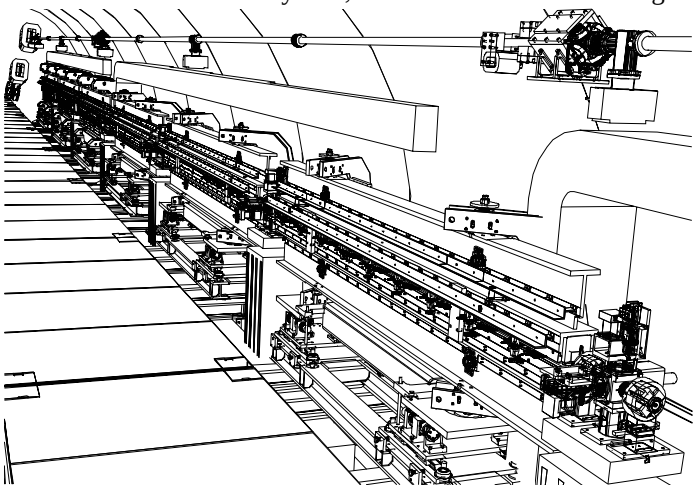

Figure 2: The FEL undulator set up in the tunnel for Phase-2. The beam enters the undulators from the left. The bending magnet at the end deflects the beam down towards the beam dump.

exact position of their axes by ±1.5mm in the horizontal and vertical direction with a relative precision better than 2 μm. The diagnostics block installed in the center of the whole device carries:

a cross of BPMs of the same type used already in the undulator vacuum chamber TTF Phase-1.

two wire scanners for horizontal and vertical scans of the electron beam

To reduce the size and the weight of the whole set up a new scanner type was developed. Fig. 4 shows a photograph of the prototype. First tests of the mechanics were done successfully at TTF Phase-1[10]. The fork with the wires (to be seen on the left side of the figure) is driven by a special reverse spindle drive powered by a stepping motor. The maximum design scanning speed of 1m/s was achieved. In the slow speed operation mode a linear resolution of 1 μm was obtained.

To fulfil the high demands on position stability and precision, all components are mounted on a granite base plate which in turn is supported by a concrete block. A stretched wire alignment system (see Fig. 3) consisting of two wires will be used. It connects all intersections in the undulator region [11]. It will be used for two purposes:

1. to increase the relative precision of the alignment to at least 50μm
2. to control the long term stability of all 7 devices relative to each other.

4. Vacuum Chambers

The new set up simplifies the requirements on the vacuum chambers. We nevertheless shall use the proven vacuum chamber design using extruded aluminium profiles developed at the APS [8]. It will fully based on the design used for Phase-1. However for Phase-2 only two BPMs and one corrector will be installed in the undulator vacuum chamber. These correctors will not be used during normal operation. They will be used only to analyze the FEL process by kicking off the beam in the center of an undulator segment. In addition the chamber will be equipped with a groove system to carry optical fibers to detect beam losses close to the beam pipe inside the magnet structures. Such systems have already been tested successfully in Phase-1 [12].

5. Beam based quadrupole alignment

One of the most important issues in a Free Electron Laser (FEL) is the transverse overlap of electron and photon beam. One main reason for electron beam misalignment is misalignment of quadrupoles. It is one of the great advantages of the separated focusing structure chosen for Phase-2 to have electromagnet quadrupoles. In contrast to permanent magnet (PM) quadrupoles used in Phase-1 their strength can be chosen independent of the electron beam energy. This will allow for better, faster and more efficient beam based alignment techniques. For the PM quadrupoles, as used in Phase-1 the only means of checking their offsets was the variation of the electron beam energy, which, in turn, requires very stable operating conditions. Appropriate alignment procedures have been proposed [13,14]. The advantage of the separated focusing is that on one hand less focusing elements are needed, resulting in less kicks of the electron beam. On the other hand, the alignment procedure can now be performed by varying the quadrupole strength by ±20% instead of changing the beam energy. Thus, the initial conditions do not have to be changed at all. The alignment procedure that has been tested is similar to one of the procedures proposed for TTF 1 [9]. As a result, initial beam dispersion does not play a role. Because of the larger distance between quadrupoles and BPMs, quadrupoles can be aligned with higher accuracy, and more modest demands on the resolution of the BPMs. Compared to the procedures described in refs [13,14] for TTF 1, where a 1 μm resolution was assumed, a 5 μm resolution now gives a comparable alignment precision of the electron beam[9]. Statistical simulations have been performed assuming randomly displaced quadrupoles with an RMS values between 200 to 600μm. It was demonstrated that after a single iteration step approximately 90% of the orbits are within an RMS orbit deviation of 15 μm, which would fulfil the overlap requirements [9]. Accuracy can be further improved by repeating this procedure several times. The ultimate accuracy is determined by the resolution of the BPMs

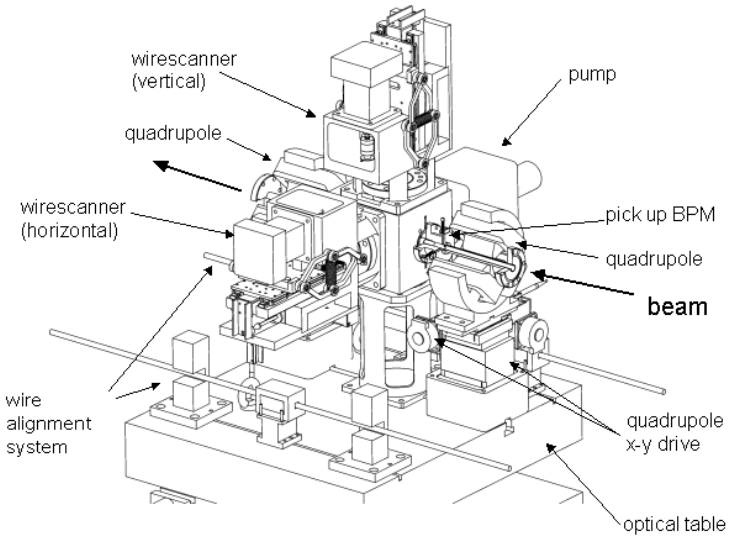

Figure 3: The 'Intersections': Adjustable quadrupoles, wire scanners, BPMs and vacuum components are mounted on a massive granite base plate, Its position can be monitored by a stretched wire system

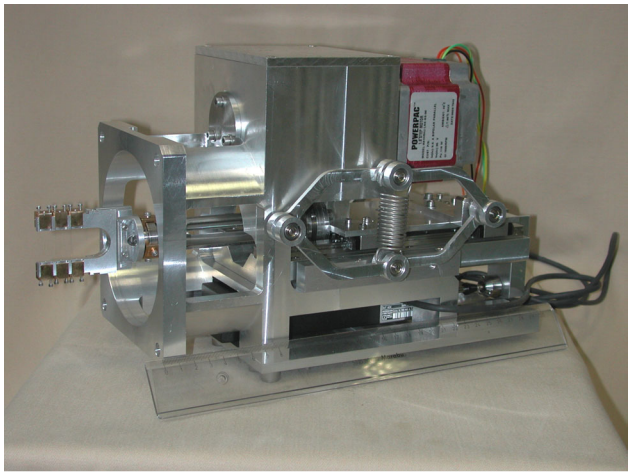

Figure 4: Prototype of the new wire scanner unit**.** Its maximum scanning speed is 1 m/s. A resolution of 1 μm has been obtained in slow motion mode.

which was assumed to be 5μm. Errors in the undulator structures have not been taken into account in this alignment procedure. Experience has shown, however, that these errors can be neglected in practice [15].

6. References

1. J. Andruskow et al. Phys. Rev. Lett. **85** (2000) 3825
2. V. Ayvazyan et al. Phys. Rev. Lett. **88** (2002) 104802
3. V. Ayvazyan et al.Europ. Phys. Journal D **20** (2002), 149
4. W. Brefeld, B. Faatz, Y.M. Nikitina, J. Pflüger, P. Pierini, J. Roßbach, E.L. Saldin, E.A. Schneidmiller, M.V. Yurkov, Nucl. Instr. and Methods A375 (1996), 295
5. J. Feldhaus, E.L. Saldin, J.R. Schneider, E.A. Schneidmiller, M.V.Yurkov, Opt. Commun. 140, 341-352 (1997)
6. J. Pflüger, Y. M. Nikitina, Nucl. Instr. and Methods A381 (1996), 554
7. See: http://www-hasylab.desy.de/facility/fel/main.htm for a compact description of the undulator for Phase-1
8. U. Hahn, P.K. den Hartog, J. Pflüger, M. Rüter, G. Schmidt, E.M. Trakhtenberg, Nucl. Instr. and Methods A445 (2000), 442
9. B. Faatz, J. Pflüger, Nucl. Instr. Meth. A475 (2001) 603
10. N. v. Bargen, U. Hahn, O. Hensler, S. Karstensen, M. Sachwitz, H. Schlarb, H.Thom, "Prototyp eines Wirescanners für TTF II“, TESLA Report 2002-08, DESY, Hamburg
11. J. Prenting, R. Ruhland in preparation
12. H. Henschel, J. Kuhnhenn, M. Koerfer, F. Wulf,"Fibre optic radiation sensor systems for particle accelerators", in preparation
13. P. Castro, "TTF FEL Beam-based Alignment by Dispersion Correction Using Micado Algorithm", TESLA FEL report 1997-04, DESY, Hamburg.
14. K. Flöttmann, B. Faatz, E. Czuchry and J. Roßbach, Nucl. Instr. Meth. A416 (1998) 152.
15. J. Pflüger, H. Lu, T. Teichmann, Nucl. Instr. Meth.A429 (1999) 386.

Demonstration of Gain Saturation and Controlled Variation of Pulse Length at the TESLA Test Facility FEL

J. Rossbach*, for the TTF FEL Group**
DESY, 22603 Hamburg, Germany

Abstract

We report on experimental evidence that the free-electron laser at the TESLA Test Facility has reached the maximum power gain of 10^7 while operating in the Self-Amplified Spontaneous Emission mode. Following request of first scientific users, the TTF FEL has been tuned in the wavelength range between 80 and 120 nm (vacuum ultraviolet, VUV), and saturation has been achieved in this entire wavelength range. At saturation the FEL emits short pulses with GW peak power and a high degree of transverse coherence. Also, the paper reports on the demonstration of controlled pulse length variation between 30 fs and 100 fs and on detailed intensity fluctuation studies in this operation mode.

PACS codes: 41.60.Cr, 29.17.+w, 29.27.-a

Keywords: Free-electron laser, VUV radiation, Self-Amplified Spontaneous Emission

* E-mail: joerg.rossbach@desy.de

** V. Ayvazyan, N. Baboi, I. Bohnet, R. Brinkmann, M.Castellano, P. Castro, L. Catani, S. Choroba, A. Cianchi, M. Dohlus, H.T. Edwards, B. Faatz, A.A. Fateev, J. Feldhaus, K. Flöttmann, A. Gamp, T. Garvey, H. Genz, Ch. Gerth, V. Gretchko, B. Grigoryan, U. Hahn, C. Hessler, K. Honkavaara, M. Hüning, M. Jablonka, T. Kamps, M. Körfer, M. Krassilnikov, J. Krzywinski, P. Kulinski, C. Lackas, M. Liepe, A. Liero, T. Limberg, H. Loos, M. Luong, C. Magne, J. Menzel, P. Michelato, M. Minty, U.-C. Müller, D. Nölle, A. Novokhatski, C. Pagani, F. Peters, J. Petrowicz, J. Pflüger, P. Piot, L. Plucinski, K. Rehlich, I. Reyzl, A. Richter, J. Rossbach, E. Saldin, W. Sandner, H. Schlarb, G. Schmidt, P. Schmüser, J.R. Schneider, E. Schneidmiller, H.-J. Schreiber, S. Schreiber, D. Sertore, S. Setzer, S. Simrock, R. Sobierajski, B. Sonntag, B. Steeg, F. Stephan, N. Sturm, K.P. Sytchev, K. Tiedtke, M. Tonutti, R. Treusch, D. Trines, D. Türke, V. Verzilov, R. Wanzenberg, T. Weiland, H. Weise, M. Wendt, T. Wilhein, I. Will, K. Wittenburg, S. Wolff, M. Yurkov, K. Zapfe

1. Introduction

For most FELs presently in operation [1], the electron beam quality and the undulator length result in a gain in radiation power of up to a few 100% per undulator passage, making it necessary to use an optical cavity and a synchronized multi-bunch electron beam to build up high brightness upon several round-trips of the radiation in the cavity.

If one aims at very short wavelengths, where good mirrors are unavailable, high-gain FEL amplification [2,3] up to laser saturation is required within a single passage of the electron beam. This requires extreme parameters of the electron beam and a long undulator. In this mode, the radiation power P(z) is expected to grow exponentially with the distance z along the undulator.

In order to become independent of the availability of a seed laser providing the input power at the desired wavelength, the spontaneous undulator radiation from the first part of the undulator can be used as an input signal to the amplification process. Since a decade, FELs based on this Self-Amplified-Spontaneous Emission (SASE) principle [4] are considered the most promising candidates for extremely brilliant, coherent light sources with wavelengths down to the Angström regime [5-7].

The TESLA Test Facility (TTF) was set up at DESY in 1993 to provide a testbed for the TESLA linear collider project, especially the superconducting niobium cavities for particle acceleration. In 1994, work began on the test accelerator to extend it into a 300-metre SASE FEL user facility for wavelengths down to 6 nm, comprising all the basic elements that will be needed in a future TESLA X-ray laser.

In a first phase (called TTF1 FEL) [8], now brought to laser saturation, the TTF was equipped with a 15m undulator, a bunch compressor (reducing the bunch length, thus increasing the bunch peak current) and a radiofrequency photocathode electron gun.

2. SASE results from TTF1 FEL

2.1 Demonstration of FEL Saturation

FEL action at the shortest wavelength achieved so far has been demonstrated at TTF1 FEL at DESY, Germany [9]. Details of the TTF1 FEL technical layout can be found in Refs. [10,11]. SASE FEL gain was observed up to saturation level in the range from 80 nm to 120 nm, and studied in great detail at wavelengths slightly below 100 nm. Figure 1 presents the measured average energy in the radiation pulse as a function of the active undulator length, defined as the distance over which the electron beam and the photon beam overlap [12]. The active length of the undulator can be varied over a large range by generating suitable orbit displacements of the electron beam, making use of the steering dipole magnets mounted inside the undulator. The radiation energy has been measured within a 10 mm aperture located 12 m behind the undulator by two kinds of detectors: a gold wire mesh scattering light into a microchannel-plate detector [13] and a thermopile [14]. Both agree within 50% in the measured pulse energy. Saturation sets in at the predicted pulse energy level of 30 to 100 μJ, depending on the accelerator tuning.

Figure 1 clearly exhibits the exponential growth of SASE power with the undulator length, yielding a power gain length of L_g=67±5 cm. The almost constant level of radiation energy observed for an active undulator length of less than 5 m does not imply that there is no FEL gain in this part of the undulator. In contrast, this is due to the fact that in the first few meters of the undulator, the FEL radiation stays below the energy of spontaneous radiation accumulated over the entire undulator. In fact, extrapolation of the exponential gain curve down to the beginning of the undulator results in a pulse energy of 0.3 pJ, in good agreement with the equivalent input power of the shot noise from spontaneous radiation, estimated for a random electron distribution [3]. The measured power growth is in agreement with the theoretical expectation indicated by the solid line in Fig. 1.

In the context of world-wide efforts towards proof-of-principle experiments on the SASE principle[16,17], the TTF1 FEL result plays a

particular role as it demonstrates the SASE FEL principle for the first time in a wavelength regime where it is clearly superior to classical lasers and to optical cavity FELs.
The peak brilliance of the TTF1 FEL photon beam exceeds that of any other source at this wavelength by several orders of magnitude. In particular, in comparison to the performance of state-of-the-art synchrotron radiation storage rings operating at this wavelength, the peak brilliance is larger by 8 orders of magnitude. The peak power is at the 1 GW level, corresponding to 2×10^{13} photons per pulse of 50 fs length (FWHM).

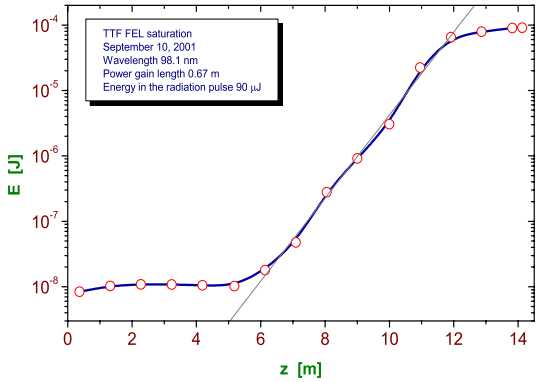

Figure 1: Demonstration of SASE exponential growth and saturation at the TTF1 FEL, DESY, Hamburg [12]. The undulator is approx. 15 m long. The solid line represents a numerical simulation with the code FAST [15].

As a consequence of this extraordinary photon beam quality, first scientific pilot experiments were performed already a few weeks after FEL saturation was demonstrated [18,19]. The operation statistics during one week of user operation is shown in Figure 2. The availability for users was some 65 % during this early week of "routine" operation.

2.2 Properties of SASE FEL radiation

In addition to the energy in each FEL pulse as discussed above, there are three more properties of the FEL radiation relevant to users:

- Transverse coherence
- Longitudinal coherence and/or pulse duration
- Fluctuation behaviour

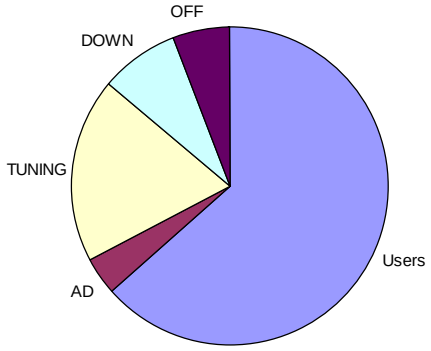

Figure 2: Reliability of TTF1 FEL during one week of operation for scientific users. The statistics was taken only short time after saturation was demonstrated for the first time.

According to FEL theory, one expects a large degree of transverse coherence close to saturation. Figure 3 shows a diffraction pattern of the TTF FEL radiation measured with a gated CCD camera viewing a Ce:YAG screen in a distance of 3 m behind a double slit [20]. The slits are located 12m behind the exit of the undulator. The remarkable high fringe visibility with a modulation depth of up to 70% is a proof of the high degree of transverse coherence. This interpretation has been corroborated by measurement of the opening angle of the radiation [12]. FEL theory expects the transverse coherence to drop significantly when entering the deep saturation regime [21]. This might be the reason for the modulation depth shown in Fig. 3 not being even higher.
Measurements of the spectral distribution are presented in Figure 4 [11]. Single-shot spectra were taken with a monochromator of 0.2 nm resolution equipped with an intensified CCD camera [14]. They show an ensemble of a few peaks which reflect the number M of longitudinal modes in the radiation pulse [22] as it is expected for SASE FEL radiation starting from shot noise.
The pulse duration is a very important parameter but not presently accessible to direct measurement in the time domain. The approximate pulse length τ_{rad} can however be calculated from the FWHM spectral width $\Delta\omega$ of each peak in the single shot

spectrum by $\tau_{rad} \approx 2\pi/\Delta\omega$. For the spectrum shown in the upper part of Figure 4 this results in $\tau_{rad} \approx 40$ fs. The lower plot in Figure 4 was taken with a bunch compressor setting for longer pulses. Consequently, the number of modes is larger (in average, M=6) and the spectral width $\Delta\omega$ of each spike is smaller, resulting in $\tau_{rad} \approx 100$ fs.

In addition to the fundamental wavelength, we have also observed the 2nd harmonics radiation. Figure 5 shows the 2nd harmonics spectrum, representing the shortest wavelength generated by a FEL so far. The intensity is a factor 100 to 1000 below that of the fundamental, the uncertainty being determined mainly by the uncertainty of the detector sensitivity at this wavelength.

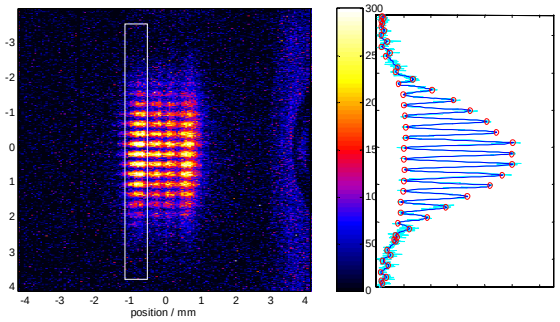

Figure 3, left: Diffraction pattern of a double-slit arrangement illustrating the transverse coherence of the radiation at TTF1 FEL [20]. Each slit is 2 mm wide × 200 μm high, the distance between the slits being 1 mm. Due to the size of the slits it is guaranteed that almost the entire FEL radiation takes part in the interference, thus indicating that the degree of transverse coherence is very high. Right: Intensity modulation within the white rectangle selected in the left.

2.3 Fluctuations of FEL pulse energy

Since SASE FEL radiation results from amplification of spontaneous undulator radiation, the pulse energy is subject to the same statistics. Thus, the spectra shown in Figure 4 will change from pulse to pulse, but they will always stay within the bandwidth of FEL amplification, and the average number of modes will remain unchanged for fixed bunch compressor setting. In addition to fluctuations of the single pulse spectra, there are also fluctuations of the pulse-to-pulse intensity. In the regime of exponential growth, the radiation pulse energy is expected to fluctuate according to a gamma distribution p(E) [22]:

$$p(E) = \frac{M^M}{\Gamma(M)} \left(\frac{E}{\langle E \rangle} \right)^{M-1} \frac{1}{\langle E \rangle} \exp\left(-M \frac{E}{\langle E \rangle} \right) \qquad (1)$$

where <E> is the mean energy, Γ(M) is the gamma function with argument M, and $M^{-1} = \langle (E - \langle E \rangle)^2 \rangle / \langle E \rangle^2$ is the normalized variance of E.

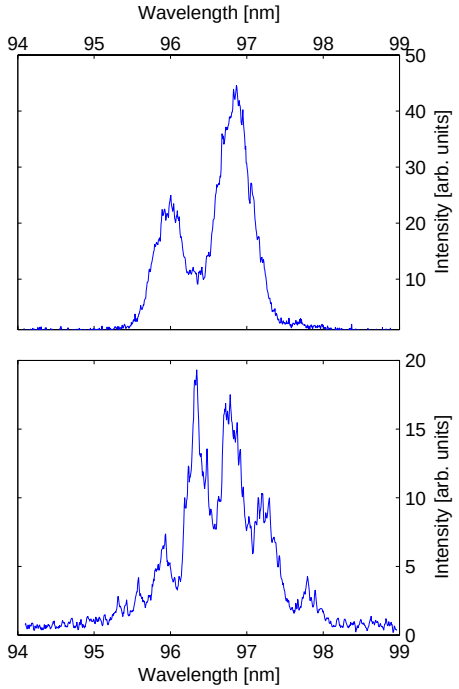

Figure 4: Spectra from short (top) and long (bottom) FEL pulses. It is seen that the number of longitudinal optical modes depends on electron bunch length which can be varied by tuning the bunch compressor settings. For short pulses (duration $\tau_{rad} \approx 40$ fs) there are, in average, 2.6 modes, while in the long bunch pulse setting ($\tau_{rad} \approx$ 100 fs, bottom) there are 6 modes in average.

M corresponds to the number of optical modes, which gives an intimate relationship between the number of modes (spikes) derived from single pulse spectra and the fluctuation (and distribution

function) of pulse energy. Figure 6 illustrates the pulse--to-pulse fluctuation of SASE pulse energy for different settings of the electron bunch length at TTF1 FEL at DESY [11]. The settings correspond to those used for Figure 4. For this radiation fluctuation analysis, all pulses with charge deviation more than 10 % from the mean bunch charge and all pulses with the electron position at the undulator entrance deviating by more than 50 μm from the mean value were rejected.

If one extracts the mode numbers 6 and 2.6, respectively, from the number of spikes in Figure 4, then there in no more free parameter in the determination of the probability distribution of pulse energies. As seen from Figure 6, the agreement between measurements and the expected distribution calculated from Eq. (1) (solid curves in the histograms) is very good.

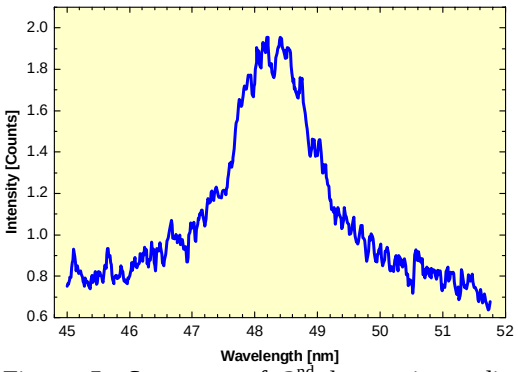

Figure 5: Spectrum of 2nd harmonics radiation from the TTF1 FEL, averaged over 3100 radiation pulses.

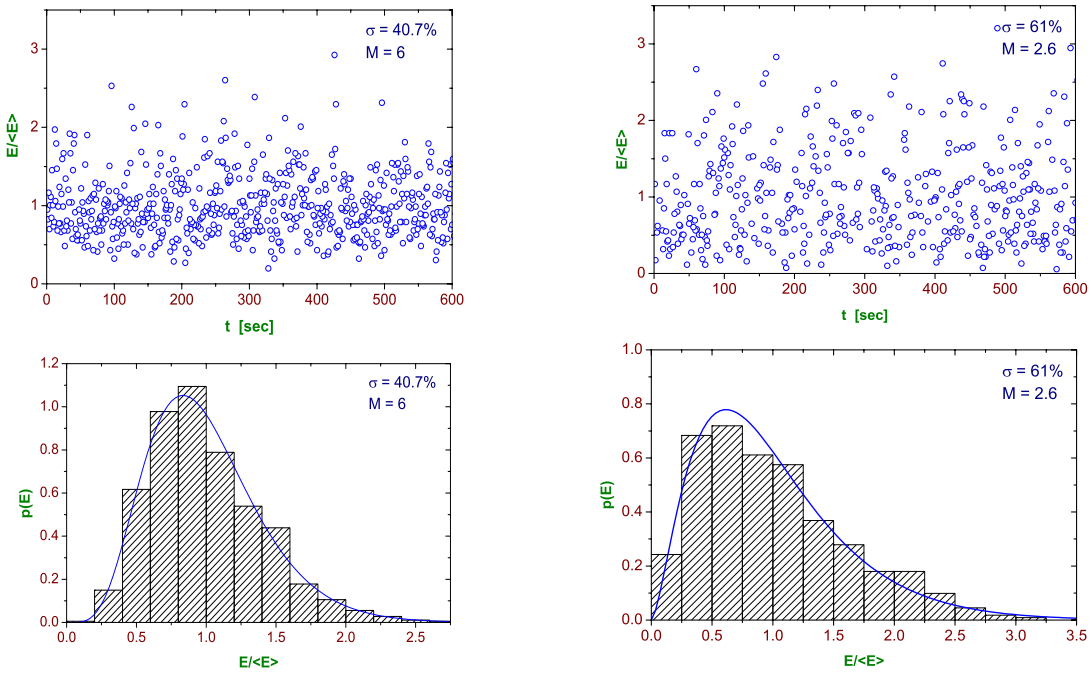

Figure 6: Pulse-to-pulse fluctuation of SASE pulse energy for different settings of electron bunch length at TTF FEL at DESY. Upper row: measured single pulse energy versus time; lower row: histogram of probability distribution extracted from the measurement. The SASE pulses are observed at high gain, but still in the exponential regime, not yet in saturation. The plots on the left hand side illustrate the long pulse case (M=6 modes), while on the right hand side the short pulse mode is shown (M=2.6).

3. Outlook

In the next phase of the TTF project, it will be extended into a 300-metre SASE FEL user facility for wavelengths down to 6 nm (TTF2 FEL). Figure 7 shows the linac tunnel (covered with sand for shielding) and the experimental hall for the TTF2 FEL at DESY.
For the TESLA X-ray FEL laboratory proposed as part of the TESLA project, it was originally planned to share the first part of the superconducting electron linac with the linear collider in an alternating rf pulse mode [7], mainly for cost saving reasons. Following a recommendation by the German Wissenschaftrat, this design has now been modified towards a solution where the XFEL has its own linac thus avoiding unwanted coupling between collider and XFEL operation, and to allow for more flexibility in the XFEL beam parameter space. It keeps all the other advantages of a joint project like savings in hardware, personnel and land, potential synergetic effects from various research communities on the same site, and it keeps the option of sharing part of the collider linac in a later stage.

Figure 7: Photography of TTF2 FEL at DESY. The hall in the background is housing TTF1, and in the foreground the experimental hall for scientific users of TTF2 FEL is seen.

4. References

[1] W.B. Colson, Nucl. Instr. Meth**. A 475**, 397 (2000)
[2] K.J. Kim, Phys. Rev. Lett. **57,** 1871 (1986)
[3] E.L. Saldin, E.A. Schneidmiller, M.V. Yurkov, *The Physics of Free-Electron Lasers* (Springer, 1999) and references therein
[4] A.M. Kondratenko, E.L. Saldin, Part. Accelerators **10**, 207 (1980)
[5] H. Winick et al., Proc. PAC, Washington and SLAC-PUB-6185 (1993)
[6] R. Brinkmann, et al., Nucl. Instr. Meth. **A 393**, 86 (1997)
[7] TESLA Technical Design Report, edited by F. Richard et al., DESY 2001-011 and http://tesla.desy.de
[8] W. Brefeld et al., Nucl. Instrum. Meth **A393**, 119 (1997)
[9] J. Andruszkow et al., Phys. Rev. Lett. **85**, 3825 (2000)
[10] H. Weise, this conference
[11] V. Ayvazyan, et al., Eur. Phys. J. D, 149 (2002)
[12] V. Ayvazyan et al., Phys. Rev. Lett. **88**, No.10 (2002)
[13] B. Faatz, et al., Nucl. Instr. Meth. **A483**, (2002)
[14] R. Treusch ,et al., Nucl. Instr. Meth. **A445**, 456 (2000)
[15] E. L.Saldin, E.A. Schneidmiller, M.V. Yurkov, Nucl. Instr. Meth. **A429**, 233 (1999)
[16] A. Murokh, et al., Proc. 2001 Part Acc. Conf. Chicago (2001)
[17] S. Milton et al, Science **292**, 2037 (2001)
[18] J. Schulz, et al., this conference
[19] J. Krzywinski et al., this conference
[20] for more details on transverse coherence, see R. Ischebeck, this conference
[21] E.L.Saldin, E.A. Schneidmiller, M.V. Yurkov, this conference
[22] E.L.Saldin, E.A. Schneidmiller, M.V. Yurkov, Opt. Commun. **148**, 383 (1998)

Statistical Properties of Radiation from SASE FEL Driven by Short Electron Bunches

E.L. Saldin[a], E.A. Schneidmiller[a], M.V. Yurkov[b]

[a]Deutsches Elektronen-Synchrotron (DESY), Notkestrasse 85, D-22607 Hamburg, Germany

[b]Joint Institute for Nuclear Research, Dubna, 141980 Moscow Region, Russia

We analyze statistical properties of the radiation from a SASE FEL driven by short electron bunches. In the linear regime the radiation from a SASE FEL is a Gaussian random process. When approaching saturation point, statistical properties of the radiation change drastically on a scale of one field gain length. Particular attention is devoted to the analysis of fluctuations of total energy in the radiation pulse and after a narrow-band monochromator. It was found that fluctuations at saturation are significantly suppressed when electron pulse length becomes comparable with cooperation length.

1. Introduction

Fluctuations of the electron beam current density can serve as the input signal in the FEL amplifier. These fluctuations always exist in the electron beam due to the effect of shot noise. An FEL amplifier which starts up from shot noise is frequently known as Self-Amplified Spontaneous Emission (SASE) FEL. It is accepted that one-dimensional theory describes in the clearest way the effects connected with longitudinal coherence. The results of the one-dimensional theory can be applied to the high-gain FEL amplifier when the transverse coherence of the radiation is settled. Some averaged output characteristics of SASE FEL in the framework of one-dimensional model have been obtained in [1,2]. An approach for 1-D time-dependent numerical simulations of SASE FEL have been developed in [3,4]. Realization of this approach allowed to obtain some statistical properties of radiation from a SASE FEL operating in linear and nonlinear regime [5,6].

At present there is significant progress in the description of the SASE FEL operation in terms of statistical optics (time and spectral correlation functions, time of coherence, interval of spectral coherence, probability density functions of the instantaneous radiation power and of the finite-time integrals of the instantaneous power, probability density function of the radiation energy after the monochromator installed at the exit of SASE FEL) [7]. Mostly these studies refer to the case of a long bunch, and up to now there is rather limited knowledge of short-pulse effects. Actually, there is only one study [4] where an asymptotic solution for average energy in the radiation pulse was found. Study of nonlinear mode of SASE FEL operation given in that paper is rather incomplete. In this paper we perform comprehensive study of SASE FEL driven by short electron bunches. Main emphasis is put on nonlinear mode of operation. It was found that slippage effects result in a set of novel features of the radiation. In particular, for very short pulses we found the effect of stabilization of fluctuations of energy in the radiation pulse and fluctuations of the energy after narrow-band monochromator. Suppression factor scales as a square root of pulse length.

2. Basic notations

The one-dimensional model describes the amplification of the plane electromagnetic wave by the electron beam in the undulator. When space charge and energy spread effect can be neglected, operation of FEL amplifier is described in terms of the gain parameter $\Gamma = \left[\pi j_0 K^2/(I_A \lambda_{\rm w} \gamma^3)\right]^{1/3}$, efficiency parameter $\rho = \lambda_{\rm w}\Gamma/(4\pi)$, and detuning parameter $\hat{C} = [2\pi/\lambda_{\rm w} - \omega(1+K^2)/(2c\gamma^2)]/\Gamma$ (see, e.g. [9,10]). Here $\lambda_{\rm w}$ is undulator period, $K = e\lambda_{\rm w} H_{\rm w}/2\pi mc^2$ is undulator parameter, γ is relativistic factor, $H_{\rm w}$ is undulator field, j_0 is the beam current density, $(-e)$ and m are charge and mass of electron, $I_A = mc^3/e \simeq 17$ kA, and ω is frequency of electromagnetic wave. When describing start-up from shot noise, one more

parameters of the theory appears – number of particles in coherence volume, $N_{\rm c} = I/(\rho\omega e)$, where I is beam current.

To be specific, we consider an electron beam with a Gaussian axial profile of the current density: $S(\hat{s}) = j(\hat{s})/j_{\max} = \exp\left[-\hat{s}^2/(2\hat{\sigma}_{\rm b}^2)\right]$, where $\hat{\sigma}_{\rm b} = \rho\omega_0\sigma_{\rm b}/c$ and $\sigma_{\rm b}$ is the rms bunch length. Here and below, the normalization is performed with respect to the maximal current density, $j_{\max}$. The rms bunch length is assumed to be large, $\omega_0\sigma_{\rm b}/c \gg 1$ or, in normalized form: $\hat{\sigma}_{\rm b} \gg \rho$. Under this assumption we can neglect the contribution of the coherent seed to the input signal of the FEL amplifier starting from the shot noise. Since ρ is always much less than unity, we can investigate short-pulse effects, when the bunch is comparable to (or even much shorter than) the typical slippage distance $c/(\rho\omega_0)$.

Shot noise in the electron beam is Gaussian random process [7]. FEL amplifier, operating in the linear regime, can be considered as a linear filter which does not change statistics. As a result, radiation is also Gaussian random process. In this case the probability distribution of the instantaneous radiation power should be the negative exponential distribution (the notion of instantaneous power refers to a certain moment of time and a certain $\hat{z}$ coordinate, and that the analysis must be performed over an ensemble of pulses). Also, the finite-time integrals of the instantaneous power and the integrated spectral density (measured after the monochromator) should fluctuate in accordance with the gamma distribution.

Nevertheless, a reasonable question arises what are the features of the radiation from SASE FEL operating in the nonlinear mode and, in particular, at saturation. This question can be answered only on the base of the results obtained with nonlinear simulation codes. Present study of amplification process in SASE FEL is performed with one-dimensional version of code FAST [7,8,10]. In this code the radiation pulse is simulated by discrete representation of the radiation field $E(z,t)$ with the step in longitudinal coordinate equal to radiation wavelength λ. Each simulation run starts from original statistical set of initial data and output results change from run to run. To obtain information about general properties of the output radiation one should use statistical methods [7,10].

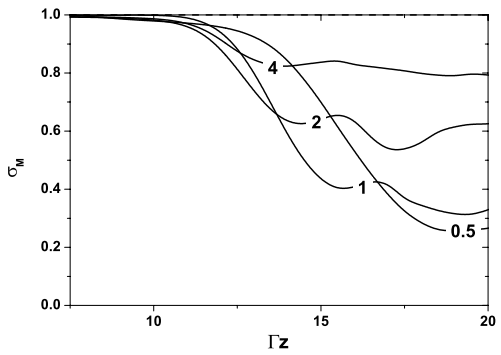

Figure 2. *Normalized rms deviation of energy after narrow-band monochromator versus undulator length. Length of the electron bunch changes in the limits* $\hat{\sigma}_{\rm b} = 0.5 - 4$. *Here* $N_{\rm c} = 10^8$

3. Average energy in the radiation pulse

Figure 1 shows evolution of the averaged efficiency $\langle\hat{\eta}\rangle = \langle E_{\rm rad}\rangle/(\rho\gamma m_{\rm e}c^2 N)$ along the undulator length. Here $E_{\rm rad}$ is energy in the radiation pulse, and N is number of electrons in the bunch. Dashed line in Fig. 1 represents averaged efficiency for the case of long electron bunch with rectangular profile. Amplification process passes three stages: start-up from shot noise, stage of exponential gain, and nonlinear stage. Let us define saturation point as the first maximum of the gain curve. At $\hat{\sigma}_{\rm b} \lesssim 2$ saturation length grows as $\hat{z}_{\rm sat} \propto 1/\sqrt{\hat{\sigma}_{\rm b}}$, and averaged saturation efficiency drops as $\langle\hat{\eta}_{\rm sat}\rangle \propto \sqrt{\hat{\sigma}_{\rm b}}$. At $\hat{\sigma}_{\rm b} \gtrsim 2$ saturation efficiency quickly approaches asymptotical value. Comparison with the case of a long electron pulse with rectangular profile shows that only 60% of electrons produce radiation. This is consequence of gradient profile of electron bunch.

4. Fluctuations of energy in the radiation pulse

Right plot in Fig. 1 shows normalized rms deviation of energy in the radiation pulse. Behaviour of the fluctuations in the linear regime has a straightforward explanation: number of longitudinal modes decreases with the pulse length and undulator length. Radia-

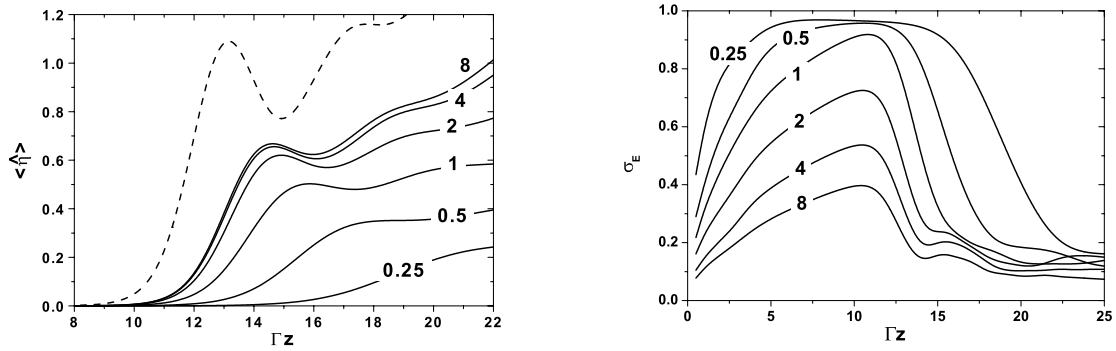

Figure 1. *Averaged efficiency of SASE FEL versus undulator length for different length of electron bunch* $\hat{\sigma}_{\rm b} = 0.25 - 8$ *(left plot). Right plot shows normalized rms deviation of energy in the radiation pulse. Here* $N_{\rm c} = 10^8$*. Dashed line represents the case of long electron pulse with rectangular profile*

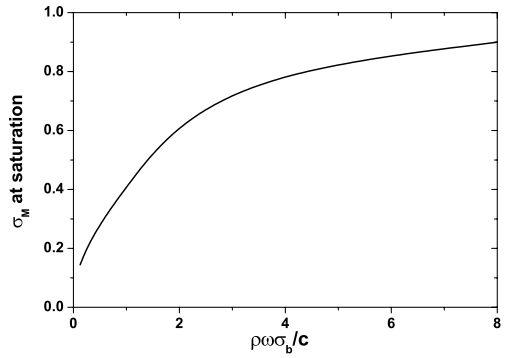

Figure 3. *Normalized rms deviation of energy after narrow-band monochromator versus length of electron bunch. SASE FEL operates at saturation*

tion of the SASE FEL operating in the linear regime is Gaussian random process, so probability distribution of the energy in the radiation pulse is gamma-distribution. Situation changes drastically when amplification process enters nonlinear stage. It is seen that deviation of energy drops quickly on a scale of a field gain length. In the case of a long pulse fluctuations at saturation are suppressed as $1/\sqrt{\hat{\sigma}_{\rm b}}$ which is a consequence of increasing the number of statistically independent spikes in the radiation pulse [4]. Physical picture becomes quite different for the bunch length $\hat{\sigma}_{\rm b} \lesssim 2$: deviation of energy in the radiation pulse at saturation starts to decrease with the bunch length as $\sqrt{\hat{\sigma}_{\rm b}}$. Nature of this phenomenon can be understood by analyzing structure of the radiation pulse. In the end of linear mode of operation SASE FEL driven by short electron bunch produces radiation pulses of nearly the same shape, but with amplitudes fluctuating nearly by negative exponential distribution. When amplification process enters nonlinear stage, radiation power is saturated, and pulses sleep forward. Further growth of the total energy occurs due to the radiation of bunched electron beam. Since maximal bunching of the electron beam is limited to the unity, this additional radiation is well stabilized, leading to the overall stability of the total energy in the radiation pulse.

Simulations show that statistics of the radiation also change drastically near the saturation point on a scale of one field gain length.

5. Fluctuations of energy after narrow-band monochromator

Let us study statistics of SASE FEL radiation filtered through narrow-band monochromator. The plots

of normalized rms deviation of energy after narrow-band monochromator versus undulator length are presented in Fig. 2. In the linear stage of SASE FEL operation the value of normalized energy deviation is equal to unity, and energy fluctuates in accordance with negative exponential distribution. This is consequence of the fact that in this case radiation is Gaussian random process. However, in the nonlinear mode of operation we obtain significant decrease of fluctuations when the pulse length goes down (see Fig. 3). This effect has simple physical explanation. When SASE FEL driven by short bunch operates in the linear regime, every time radiation pulses have similar shape, but amplitude fluctuates nearly by negative exponential distribution. When amplification process enters nonlinear stage, amplitudes of different pulses are equalized due saturation effects, while keeping close shape. Spectrum of the radiation pulse is given by Fourier transform of the radiation field, and at saturation we obtain nearly similar spectrum envelope for different pulses. As a result, we can expect that fluctuations of the radiation energy after narrow-band monochromator should follow fluctuations of the total energy in the radiation pulse. Comparison of Figs. 1 and 2 confirms this simple physical consideration. At saturation fluctuations of the energy after narrow-band monochromator drop as $\sigma_{\rm M} \simeq \sigma_{\rm E} \propto \sqrt{\hat{\sigma}_{\rm b}}$.

6. Conclusion

Study of amplification process in the SASE FEL driven by electron bunch of finite pulse duration allows us to make the following conclusions. For the bunch length $\hat{\sigma}_{\rm b} \gtrsim 4$ asymptotical results [7] for a long rectangular bunch are applicable. At $\hat{\sigma}_{\rm b} \lesssim 2$ SASE FEL exhibits quite different behaviour caused by strong influence of slippage effects. In addition to reduction of the FEL gain and efficiency [4], short-pulse effects strongly influence statistical properties of the radiation in the nonlinear regime. In particular, for very short pulses we found the effect of stabilization of fluctuations of energy in the radiation pulse and fluctuations of the energy after narrow-band monochromator. When SASE FEL operates at saturation, suppression factor scales as $\sqrt{\hat{\sigma}_{\rm b}}$ with electron bunch length.

REFERENCES

1. K.J. Kim, Nucl. Instrum. and Methods **A 250**(1986)396.
2. J.M. Wang and L.H. Yu, Nucl. Instrum. and Methods **A250**(1986)484.
3. W.B. Colson, Review in: W.B. Colson et al. (Eds), "Laser Handbook, Vol.6: Free Electron Laser" (North-Holland, Amsterdam, 1990), p. 115.
4. R. Bonifacio et al., Phys. Rev. Lett. **73**(1994)70.
5. P. Pierini and W. Fawley, Nucl. Instrum. and Methods **A375**(1996)332.
6. E.L. Saldin, E.A. Schneidmiller, and M.V. Yurkov, Nucl. Instrum. and Methods **A393**(1997)157.
7. E.L. Saldin, E.A. Schneidmiller, and M.V. Yurkov, Opt. Commun. **148**(1998)383.
8. E.L. Saldin, E.A. Schneidmiller, and M.V. Yurkov, Nucl. Instrum. and Methods **A429**(1999)233.
9. R. Bonifacio, C. Pellegrini and L. Narducci, Opt. Commun. **50**(1984)373.
10. E.L. Saldin, E.A. Schneidmiller, M.V. Yurkov, "The Physics of Free Electron Lasers" (Springer-Verlag, Berlin, 1999).

Coherence Properties of the Radiation from SASE FEL

E.L. Saldin[a], E.A. Schneidmiller[a], M.V. Yurkov[b]

[a]Deutsches Elektronen-Synchrotron (DESY), Notkestrasse 85, D-22607 Hamburg, Germany

[b]Joint Institute for Nuclear Research, Dubna, 141980 Moscow Region, Russia

We present a comprehensive analysis of coherence properties of radiation from SASE FEL. The effective transverse correlation function is calculated by means of numerical simulations with the code FAST. This allows us to calculate area and degree of transverse coherence. Evolution of these parameters is traced from the beginning of the undulator up to the deep nonlinear regime. It is shown that the degree of transverse coherence reaches maximum value at the saturation point. Then it drops drastically because of poor transverse coherence of the radiation produced in the nonlinear regime.

1. Introduction

The process of amplification in Self-Amplified Spontaneous Emission (SASE) FEL starts from shot noise in the electron beam. As a result, the radiation from SASE FEL has statistical nature. At the initial stage of amplification it has poor longitudinal and transverse coherence. Properties of the longitudinal coherence of SASE FEL radiation has been studied thoroughly [1–7]. It has been found that coherence time increases in the linear regime, reaches maximum value at the saturation point, and then drops drastically in the deep nonlinear regime [5,7]. Recent studies of transverse coherence of SASE FEL radiation were devoted to the linear stage of amplification. It has been found that the process of formation of transverse coherence is more complicated than that given by naive physical picture of transverse mode selection. It was found that even after finishing the transverse mode selection process the degree of transverse coherence of the radiation from SASE FEL visibly differs from unity [8]. This is consequence of the interdependence of the longitudinal and transverse coherence. The SASE FEL has poor longitudinal coherence which develops slowly with the undulator length thus preventing a full transverse coherence. In this paper we extend investigation of transverse coherence for general case of SASE FEL operation. Our study has shown that maximal degree of transverse coherence is achieved at saturation point. Further increase of the undulator length leads only to degradation of the properties of the radiation, despite output power continues to grow. Maximal brilliance of the radiation is achieved at saturation, too.

2. General description of transverse coherence

The transverse coherence properties of the radiation are described in terms of the transverse correlation functions. The first-order transverse correlation function is defined as

$$\gamma_1(\vec{r}_\perp,\vec{r}'_\perp,z,t)=\frac{\langle\tilde{E}(\vec{r}_\perp,z,t)\tilde{E}(\vec{r}'_\perp,z,t)\rangle}{\left[\langle|\tilde{E}(\vec{r}_\perp,z,t)|^2\rangle\langle|\tilde{E}(\vec{r}'_\perp,z,t)|^2\rangle\right]^{1/2}},$$

where $\tilde{E}$ is the slowly varying amplitude of the amplified wave:

$$E_y=\tilde{E}(\vec{r}_\perp,z,t)\,\mathrm{e}^{\mathrm{i}\omega_0(z/c-t)}+\mathrm{C.C.}\,. \qquad (1)$$

In the following we consider the model of a stationary process, thus assuming that γ_1 does not depend on time. The space analogue of a stationary statistical process is a model of a statistically homogeneous field. For such a field the correlation function (1) depends only on the remainder $\vec{\rho}=\vec{r}_\perp-\vec{r}'_\perp$, $\gamma_1(\vec{r}_\perp,\vec{r}'_\perp,z)=\gamma_1(\vec{\rho},z)$. Then we introduce notion of effective correlation function:

$$\gamma_1^{(\mathrm{eff})}(\vec{\rho},z)=\frac{\int\langle\tilde{E}(\vec{R}+\vec{\rho}/2,z)\tilde{E}^*(\vec{R}-\vec{\rho}/2,z)\rangle\,\mathrm{d}\,\vec{R}}{\int\langle|\tilde{E}(\vec{R},z)|^2\rangle\,\mathrm{d}\,\vec{R}}\,. \qquad (2)$$

The angular spectrum $h(\vec{k}_\perp,z)$ and the effective correlation function are connected by the Fourier trans-

form

$$h(\vec{k}_\perp, z) = \frac{1}{(2\pi)^2} \int \gamma_1^{(\mathrm{eff})}(\vec{\rho}, z) \exp\left(-\mathrm{i}\,\vec{k}_\perp \vec{\rho}\right) \mathrm{d}\,\vec{\rho}\,.$$

The angular spectrum $h(\vec{k}_\perp, z)$ is given by

$$h(\vec{k}_\perp, z) = \frac{\langle |A(\vec{k}_\perp, z)|^2 \rangle}{\int \langle |A(\vec{k}_\perp, z)|^2 \rangle \,\mathrm{d}\,\vec{k}_\perp}\,, \qquad (3)$$

where

$$A(\vec{k}_\perp, z, t) = \int \tilde{E}(\vec{r}_\perp, z, t) \exp(-\mathrm{i}\,\vec{k}_\perp \vec{r}_\perp)\,\mathrm{d}\,\vec{r}_\perp\,.$$

Thus, the averaged intensity distribution in the far zone $h(\vec{k}_\perp, z)$ is totally defined by the effective transverse correlation function, and vice versa. We consider SASE FEL driven by an axisymmetric electron beam. In this case the statistical process is isotropic: the effective correlation function depends on the modulus $\rho = |\vec{\rho}|$ and the angular spectrum depends on the modulus $k_\perp = |\vec{k}_\perp|$. Thus, we have a pair of transformations:

$$h(k_\perp, z) = \frac{1}{2\pi} \int_0^\infty J_0(k_\perp \rho) \gamma_1^{(\mathrm{eff})}(\rho, z) \rho \,\mathrm{d}\,\rho\,, \qquad (4)$$

$$\gamma_1^{(\mathrm{eff})}(\rho, z) = 2\pi \int_0^\infty J_0(\rho k_\perp) h(k_\perp, z) k_\perp \,\mathrm{d}\,k_\perp\,. \qquad (5)$$

The effective radius of coherence for an isotropic inhomogeneous field is:

$$r_\mathrm{c}(z) = \left[2 \int_0^\infty |\gamma_1^{(\mathrm{eff})}(\rho, z)|^2 \rho \,\mathrm{d}\,\rho \right]^{1/2}, \qquad (6)$$

and the area of transverse coherence is given by $S_\mathrm{c} = \pi r_\mathrm{c}^2$.

Number of transverse modes in the radiation beam can be defined as ratio of total power to the power inside the area of transverse coherence [10]:

$$M = \frac{W_\mathrm{tot}}{W_\mathrm{coh}} = \frac{\int_0^\infty |E^2(r)| r \,\mathrm{d}\,r}{\int_0^{r_\mathrm{c}} |E^2(r)| r \,\mathrm{d}\,r}\,, \qquad (7)$$

and the degree of transverse coherence is defined as

$$\zeta = \frac{1}{M} = \frac{W_\mathrm{coh}}{W_\mathrm{tot}} = \frac{\int_0^{r_\mathrm{c}} |E^2(r)| r \,\mathrm{d}\,r}{\int_0^\infty |E^2(r)| r \,\mathrm{d}\,r}\,. \qquad (8)$$

This is general definition valid for any radiation field.

3. Evolution of transverse coherence in SASE FEL

We consider an FEL amplifier with helical undulator and axisymmetric electron beam. H_w and λ_w are the amplitude of the magnetic field and the period of the undulator, respectively. The angle of the electron rotation in the undulator is equal to $\theta_\mathrm{s} = K/\gamma$, where $\gamma = \mathcal{E}_0/m_\mathrm{e}c^2$ is the relativistic factor of the electron with nominal energy $\mathcal{E}_0$, $K = eH_\mathrm{w}\lambda_\mathrm{w}/2\pi m_\mathrm{e}c^2$ is the undulator parameter, $(-e)$ and m_e are the charge and the mass of the electron, respectively, and c is the velocity of light (we use CGS units in this paper).

We assume the transverse phase space distribution of the particles in the beam to be Gaussian and the beam is matched to the magnetic focusing system of the undulator. The rms beam size is given by $\sigma_\mathrm{r} = \sqrt{\epsilon_\mathrm{n}\beta/\gamma}$, where β is the beta function and ϵ_n is the rms normalized emittance. When influence of space charge and energy spread is negligible, operation of SASE FEL is described in terms of the gain parameter $\Gamma = \left[I\omega^2\theta_\mathrm{s}^2/(I_\mathrm{A}c^2\gamma_\mathrm{z}^2\gamma)\right]^{1/2}$, diffraction parameter $B = 2\Gamma\sigma_\mathrm{r}^2\omega/c$, and the efficiency parameter $\rho = c\gamma_\mathrm{z}^2\Gamma/\omega$ [9,11]. Here $\lambda = 2\pi c/\omega$ is the radiation wavelength, I is the beam current, $I_A = mc^3/e \simeq 17$ kA is Alfven's current and $\gamma_\mathrm{z}^2 = \gamma^2/(1+K^2)$.

To be specific, we present numerical example for the value of diffraction parameter $B = 1$ and number of electrons in the coherence volume $N_\mathrm{c} = I/(\rho\omega e) = 7 \times 10^7$. These parameters are typical for SASE FEL of optical wavelength range. Calculations are performed with three-dimensional, time-dependent numerical simulation code FAST [12].

Figure 1 shows the evolution of averaged FEL efficiency versus undulator length. Averaged normalized efficiency is defined as $\langle\hat{\eta}\rangle = \langle W\rangle/(\rho P_\mathrm{beam})$, where $\langle W\rangle$ is averaged radiation power and $P_\mathrm{beam} = \gamma mc^2 I/e$. Amplification process starts from shot noise in the electron beam, passes the stage of exponential growth, and enters nonlinear stage. The first

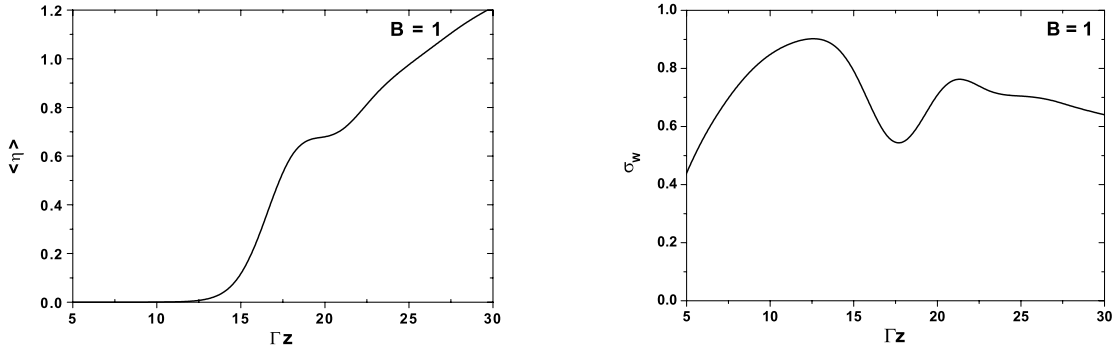

Figure 1. *Averaged efficiency of SASE FEL versus undulator length (upper plot). Right plot shows normalized rms deviation of instantaneous radiation power. Here* $B = 1$, $N_c = 7 \times 10^7$

maximum of the gain curve is usually defined as saturation point. After passing saturation point efficiency of the SASE FEL continues to increase due to the growth of sidebands.

Instantaneous power W of SASE FEL radiation is statistical variable and fluctuates in time. Right plot in Fig. 1 shows evolution along the undulator of normalized deviation of instantaneous radiation power. At the initial stage of amplification fluctuations of instantaneous power are strongly suppressed which is related to poor transverse coherence [8]. Note that in the deep nonlinear regime we also obtain strong suppression of fluctuations.

In the linear regime probability density distribution of the radiation power is gamma distribution. When amplification process enters nonlinear stage, probability density distribution deviates visibly form gamma distribution. If we trace evolution of the probability density distribution in the deep nonlinear regime, we obtain that it again approaches to gamma distribution. This is indirect indication that in the deep nonlinear regime properties of the radiation again correspond to properties of completely chaotic polarized radiation. Similar asymptote was obtained also in the framework of one-dimensional model [7].

Let us go over to quantitative description of the coherence properties of radiation. Calculation procedure proceeds as follows. Numerical simulation code produce array of field amplitudes in the near zone. Using these data, we calculate the field distribution in the far zone and find averaged intensity

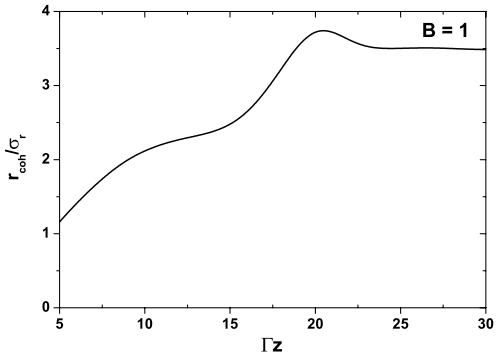

Figure 2. *Coherence radius of SASE FEL radiation versus undulator length. Here* $B = 1$, $N_c = 7 \times 10^7$

distribution. Then we calculate effective correlation function (5), and radius of transverse coherence (6) (see Fig. 2). Degree of transverse coherence is given by a fraction of the radiation power passing within area of transverse coherence (8). At this stage of algorithm actual distribution of the radiation intensity is used. Finally, using definition (7) and (8) we calculate evolution of the number of modes and degree of transverse coherence of the radiation along the undulator. It is seen that maximal degree of transverse coherence is achieved at the saturation point. In the

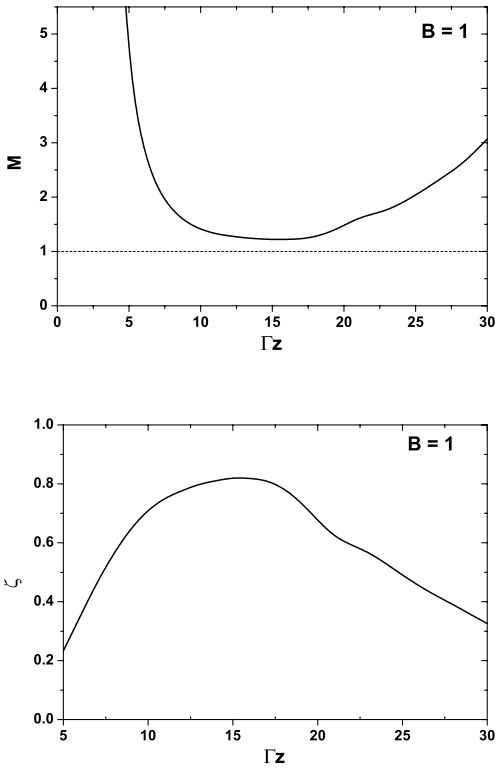

Figure 3. *Number of transverse mode (up) and degree of transverse coherence of the radiation from SASE FEL (down). Here* $B = 1$, $N_{\rm c} = 7 \times 10^7$

deep nonlinear regime it falls down rapidly. Comparison with the plot for averaged FEL efficiency (see Fig. 1 shows that in the deep nonlinear regime there is strict correlation between degradation of the degree of transverse coherence and increase of radiation power. This indicates that radiation produced in the nonlinear regime has poor transverse coherence. Actually, this is main message of our study. Namely, we conclude that the best quality of the radiation from SASE FEL is achieved at the saturation point. Further increase of the undulator length leads only to degradation of the properties of the radiation, despite output power continues to grow. Maximal brilliance of the radiation is achieved at saturation, too.

REFERENCES

1. K.J. Kim, Nucl. Instrum. and Methods **A 250**(1986)396.
2. J.M. Wang and L.H. Yu, Nucl. Instrum. and Methods **A 250**(1986)484.
3. W.B. Colson, Review in: W.B. Colson et al. (Eds), "Laser Handbook, Vol.6: Free Electron Laser" (North-Holland, Amsterdam, 1990), p. 115.
4. R. Bonifacio et al., Phys. Rev. Lett. **73**(1994)70.
5. P. Pierini and W. Fawley, Nucl. Instrum. and Methods **A 375**(1996)332.
6. E.L. Saldin, E.A. Schneidmiller, and M.V. Yurkov, Nucl. Instrum. and Methods **A 393**(1997)157.
7. E.L. Saldin, E.A. Schneidmiller, and M.V. Yurkov, Opt. Commun. **148**(1998)383.
8. E.L. Saldin, E.A. Schneidmiller, and M.V. Yurkov, Opt. Commun. **186**(2000)185.
9. E.L. Saldin, E.A. Schneidmiller, M.V. Yurkov, "The Physics of Free Electron Lasers" (Springer-Verlag, Berlin, 1999).
10. J. Goodman, Statistical Optics, (John Wiley and Sons, New York, 1985).
11. E.L. Saldin, E.A. Schneidmiller and M.V. Yurkov, Opt. Commun. **95**(1993)141.
12. E.L. Saldin, E.A. Schneidmiller, and M.V. Yurkov, Nucl. Instrum. and Methods **A 429**(1999)233.
13. E.L. Saldin, E.A. Schneidmiller and M.V. Yurkov, Opt. Commun. **97**(1993)272.

Scheme for Attophysics Experiments at a X-ray SASE FEL

E.L. Saldin[a], E.A. Schneidmiller[a], M.V. Yurkov[b]

[a]Deutsches Elektronen-Synchrotron (DESY), Notkestrasse 85, D-22607 Hamburg, Germany

[b]Joint Institute for Nuclear Research, Dubna, 141980 Moscow Region, Russia

We propose a concept for production of high power coherent attosecond pulses in X-ray range. An approach is based on generation of 8th harmonic of radiation in a multistage HGHG FEL (high gain high harmonic free electron laser) configuration starting from shot noise. Single-spike phenomena occurs when electron bunch is passed through the sequence of four relatively short undulators. The first stage is a conventional "long" wavelength (0.8 nm) SASE FEL which operates in the high-gain linear regime. The 0.1 nm wavelength range is reached by successive multiplication (0.8 nm $\rightarrow$ 0.4 nm $\rightarrow$ 0.2 nm $\rightarrow$ 0.1 nm) in a stage sequence. Our study shows that the statistical properties of the high-harmonic radiation from the SASE FEL, operating in linear regime, can be used for selection of radiation pulses with a single spike in time domain. The duration of the spikes is in the range of 400 – 600 attoseconds. Selection of single-spike high-harmonic pulses is achieved by using a special trigger in data acquisition system. The potential of X-ray SASE FEL at TESLA at DESY for generating attosecond pulses is demonstrated. The use of a 10 GW-level attosecond X-ray pulses at X-ray SASE FEL facility will enable us to track process inside atoms for the first time.

1. Introduction

A general objective in the development of synchrotron radiation sources is to produce radiation that is brighter than that from existing sources, or to produce radiation that comes in shorter pulses. Significant progress in both of these directions has been reported recently by the TESLA Collaboration [1], Argonne National Laboratory [2] and VISA Collaboration [3]. Impressive results have been obtained at the TESLA Test Facility (TTF) at DESY [1], using radiation pulses of 100 nm wavelength with sub-100 femtosecond pulse duration and peak power of approximately one GW. Comparing to present day synchrotron radiation sources its spectral brightness is more than a 100 million times higher, the radiation has full transverse coherence and pulse duration is reduced from the 100 picoseconds down to 100 femtoseconds in time domain. These demonstrations have been made possible by the technique of Self Amplified Spontaneous Emission Free Electron Laser (SASE FEL). Technical design studies were presented for XFEL laboratory [4] which should provide X-rays at wavelengths down to 0.1 nm in pulses of 100 fs duration. Peak spectral brightness would exceed those of synchrotron sources by over ten orders of magnitude.

The discussion in the scientific community over the past decade has produced many ideas for novel applications of the X-ray laser. Brilliance, coherence, and timing down to the femtosecond regime are the three properties which have the highest potential for new science to be explored with an XFEL. It is obvious that studies of time dependent phenomena can be tackled for the first time which relate the structural aspects with the transition states of those electrons which are responsible for the formation process of intra-molecular bonds, clusters, nanoparticles, liquids, solids and hot dense plasmas. Femtosecond-resolution experiments with X-rays can possibly show us directly how matter is formed out of atoms. In fact, X-ray pulse duration even shorter than femtosecond may be useful for many scientific applications.

Our studies have shown that this ultimate limit for pulse duration can be rached in a multistage, single-bunch HGHG FEL scheme [5] seeded by shot noise in the electron beam. The statistical properties of the high-harmonic radiation from the SASE FEL, operating in linear regime, can be used for selection of radiation pulses with a single spike in time domain [6].

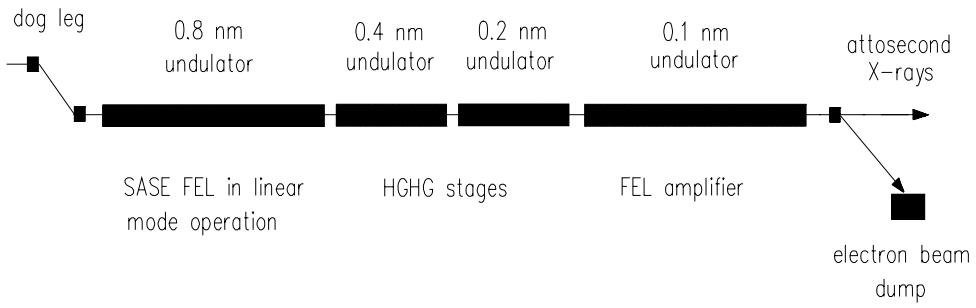

Figure 1. Concept of the attosecond X-ray facility. XFEL produces ultrafast X-ray pulses during a single pass of electron beam through a sequence of undulators which are resonant at different wavelengths. The amplification process develops from shot noise. The single-spike pulse selection can be achieved by using special trigger in data acquisition system

2. Main idea of the proposal

An attosecond laser requires a broadband gain medium. What ultimately limits the pulse duration? Since the temporal and spectral characteristics of the field are related to each other through Fourier transforms, the bandwidth of XFEL $\Delta\omega_{\rm FEL}$ and pulse duration $\tau_{\rm p}$ cannot vary independently of each other. There is a minimum duration-bandwidth product: $\Delta\omega_{\rm FEL}\tau_{\rm p} > 2\pi$. The larger the FEL bandwidth is, the shorter the minimal pulse duration than can be obtained. This simple physical consideration can lead directly to crude approximation for the minimum duration of the XFEL radiation pulses. We can expect that the width of the radiation spectrum at 0.1 nm wavelength should be of order of $\Delta\omega_{\rm FEL}/\omega \simeq 0.1\%$ [4]. Thus, the minimum duration should be $\tau_{\rm p} \simeq 300$ as.

SASE FEL produces radiation pulse consisting of independent wavepackets (spikes). For an X-ray FEL typical number of spikes is about a hundred which is defined by electron pulse length. Single-spike mode of operation can be possible, for example, when electron pulse length is comparable with the cooperation length. This is technically possible in the VUV range [1], but is not realistic for an X-ray FEL, since electron pulse length should be below a micrometer.

Our concept of attosecond X-ray facility is based on generation of the 8th harmonic of SASE radiation in the single-bunch, multistage HGHG configuration. Single-spike phenomena occurs when electron bunch is passed through the sequence of four relatively short undulators. The first stage is a conventional "long" wavelength (0.8 nm) SASE FEL operating in the high-gain linear regime. Figure 1 illustrates how the 0.1 nm wavelength range may be reached by successive multiplication in a stage sequence (0.8 nm $\rightarrow$ 0.4 nm $\rightarrow$ 0.2 nm $\rightarrow$ 0.1 nm).

The possibility of single-spike pulse production is demonstrated in a simple example. With reference to the left plot in Fig. 2 consider an intensity function I in the SASE FEL radiation pulse at fundamental frequency versus time t. Subjecting it, for example, to a 8th harmonic transformation, we obtain the "image" shown in the right plot in Fig. 2. An important distinction should be made between the sample fundamental instantaneous intensity function $I(t)$ and the transformed function $[I(t)]^8$. Due to the nonlinear generation mechanism, the temporal structure of the 8th-harmonic radiation is similar to the fundamental, but with more fluctuations from spike to spike. The fact that the 8th harmonic intensity is a single spike

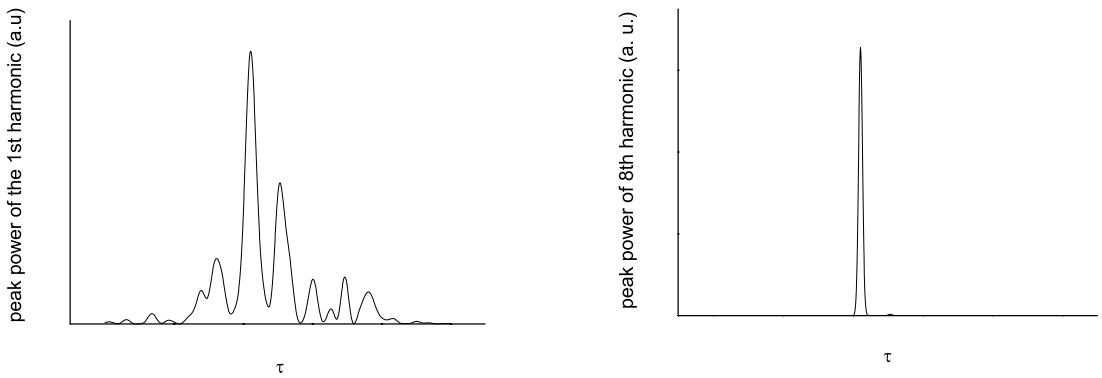

Figure 2. Illustration of the results of nonlinear transformation. Left: Sample function of fundamental harmonic instantaneous power for SASE FEL. Right: The nonlinear transform of plot at left representing the 8th harmonic instantaneous power

implies that the fluctuation of the fundamental intensity about the mean is rather pronounced. How likely are we to observe a practically single bright spike in the intensity of the 8th harmonic radiation? Clearly, a necessary condition for this event is that the energy $E_{(8)}$ in the 8th-harmonic radiation pulse is larger than the average energy $\langle E_{(8)} \rangle$. The results of numerical simulations for the case of the 8th-harmonic of the X-ray SASE FEL predict the probability of high-contrast single-spike pulses of about 1–10% only. For this method to be applicable, the electron pulse repetition rate should be larger than 100 pulses per second.

3. Statistical properties of SASE FEL high-harmonic radiation

The principle of operation of the proposed scheme is essentially based on the statistical properties of the SASE FEL harmonic radiation. SASE radiation is a stochastic object and at a given time it is impossible to predict the amount of energy which flows to a detector. The initial modulation of the electron beam is defined by the shot noise and has a white spectrum. The high-gain FEL amplifier cuts and amplifies only a narrow frequency band of the initial spectrum $\Delta\omega/\omega \ll 1$. In the time domain, the temporal structure of the fundamental harmonic radiation is chaotic with many random spikes, with a typical duration given by the inverse width of the spectrum envelope. For SASE FEL operating in the linear regime we deal with Gaussian statistics. As a result, the probability distribution of the instantaneous radiation intensity I is the negative exponential probability density distribution, and the energy in the radiation pulse E fluctuates in accordance with the gamma distribution.

The statistics of the high-harmonic radiation from the SASE FEL changes significantly with respect to the fundamental harmonic (e.g., with respect to Gaussian statistics). It is interesting in our case to be able to determine the probability density function of instantaneous intensity of SASE radiation after it has been subjected to nonlinear transformation. We know the probability density function $p(I) = \langle I \rangle^{-1} \exp(-I/\langle I \rangle)$ of the fundamental intensity I, and I is subjected to a transformation $z = (I)^n$. The problem is then to find the probability density function $p(z)$. It can be readily shown that $p(z) = (n\langle I \rangle)^{-1} z^{(1-n)/n} \exp(-z^{1/n}/\langle I \rangle)$. Using this distribution we get the expression for the mean value: $\langle z \rangle = n! \langle I \rangle^n$. Thus, the nth-harmonic radiation for the SASE FEL has an intensity level roughly $n!$ times larger than the corresponding steady-state case, but with more shot-to-shot fluctuations compared to the fundamental [7]. Nontrivial behavior of the intensity of the high harmonic reflects the complicated nonlinear transformation of the fundamental harmonic statistics. One can see that Gaussian statistics is no longer valid.

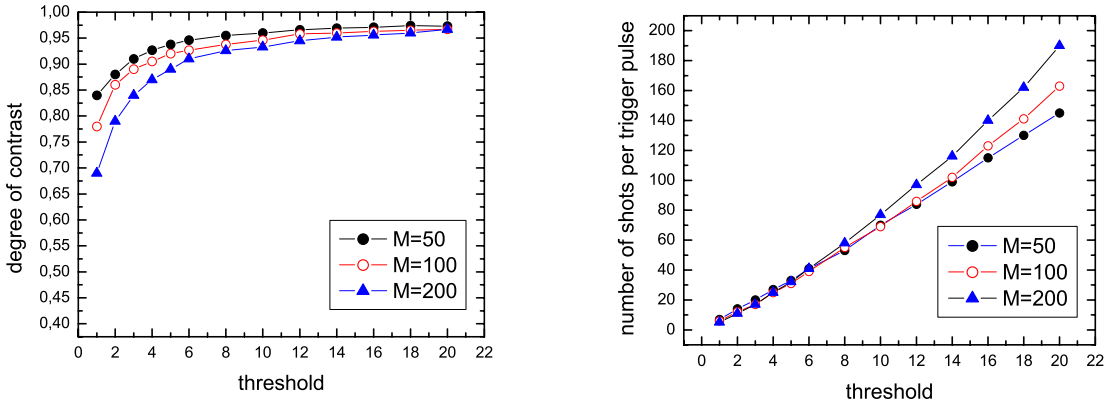

Figure 3. Left: Degree of contrast $\langle C\rangle$ versus energy threshold $E_{\rm th}/\langle E_{(8)}\rangle$. Right: Number of shots per trigger pulse $\langle N_{\rm sh}\rangle$ versus energy threshold $E_{\rm th}/\langle E_{(8)}\rangle$

Since amplification process starts from shot noise, properties of a single-spike selection should be dscribed in statistical terms. The statistics of concern are defined over an ensemble of radiation pulses. If we define the contrast C as the ratio of number of photons in the main spike to the total number of photons in the pulse, we find that $\langle C\rangle$ asymptotically approaches unity as the ratio $E_{\rm th}/\langle E_{(8)}\rangle$ increases, where $E_{\rm th}$ is the threshold level of the 8th harmonic energy pulse discriminator. Clearly, the larger the threshold level of discriminator $E_{\rm th}/\langle E_{(8)}\rangle$, the larger the number of shots per trigger pulse $N_{\rm sh}$. Note that the number of degrees of freedom M of the fundamental radiation pulse is a parameter of the functions $\langle C\rangle = F(M, E_{\rm th}/\langle E_{(8)}\rangle)$, $\langle N_{\rm sh}\rangle = f(M, E_{\rm th}/\langle E_{(8)}\rangle)$ as indeed we might have anticipated.

In Fig. 3 one can see the basic characteristics of the single-spike pulse selection process. The dependence of the degree of the contrast $\langle C\rangle$ on the value of the energy threshold $E_{\rm th}/\langle E_{(8)}\rangle$ is presented in the left plot in Fig. 3. It is seen that the contrast increases with an increase in the value of energy threshold, and it asymptotically approaches to unity. Simulations at different values of M show that the degree of contrast does not differ significantly when the number of modes is within the limits $50 < M < 200$. Right plot in Fig. 3 shows plots of the number of shots per trigger pulse $\langle N_{\rm sh}\rangle$ versus $E_{\rm th}/\langle E_{(8)}\rangle$ for several values of the parameter M. From Fig. 3 it is quite clear that the dependence of $\langle N_{\rm sh}\rangle$ on the number of modes M is not strong within the interval $M = 50 - 200$ and can be ignored.

4. Attosecond X-ray facility

Scheme of attosecond X-ray facility is shown in Fig. 1. It is based on a single-bunch, multistage High Gain Harmonic Generation (HGHG) FEL scheme [5]. In this technique the second harmonic in the nth stage becomes the fundamental in the $(n+1)$th stage. Each stage (except the first one) consists of radiator undulator, dispersion section (demodulator), FEL amplifier and end-stage dispersion section (modulator). The main difference with previous HGHG schemes [8–16] is that frequency multiplication is performed with a single electron bunch consecutively passing all HGHG stages. This is possible because the density modulation exiting each stage is relatively small. Hence, a small energy modulation is sufficient to create this microbunching in the dispersion section. In this case the growth of the energy spread due to HGHG process is much less than initial energy spread, and exponential growth rate in the main undulator is practically the same as without stage sequence. At chosen parameters for each stage the amplitude of the second harmonic of density modulation dominates significantly over the amplitude of shot noise harmonics, and the modulation of the beam

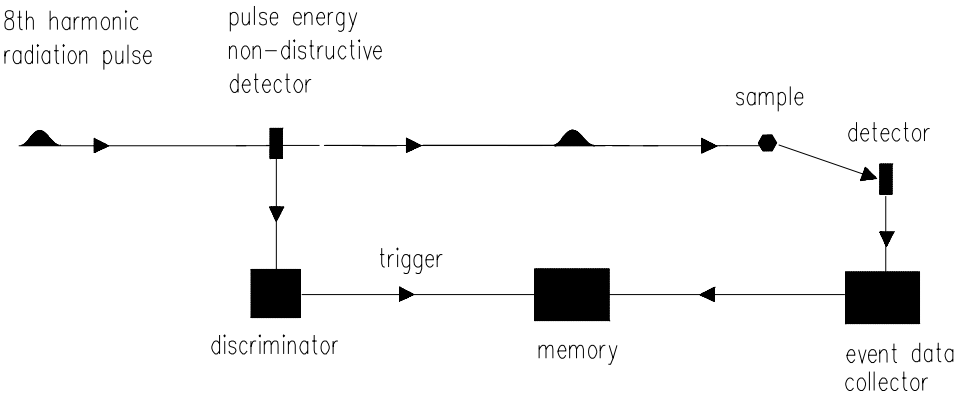

Figure 4. Experimental setup to obtain single spike pulse duration. Signals from a non-destructive 8th harmonic energy pulse detector are used to give trigger. The energy threshold is used to reject events with E smaller than $2\langle E_{(8)}\rangle$

density can be used as input signal for the next HGHG stage.

SASE radiation from the first stage serves as a seed signal for the next stages where it is subjected to nonlinear transformation. As result, the pulse of output radiation has much more pronouncing spikes. Average number of spikes is reduced so much that it becomes probable to generate pulses consisting of a single spike. The final steps involved in obtaining a single-spike pulses of the 8th-harmonic radiation are as follows. The energy in the high-harmonic radiation pulse must be measured by means of a nondestructive method. After each shot, the signal from the energy detector is sent to a discriminator having a threshold $E_{\rm th} \simeq 2\langle E_{(8)}\rangle$, where $\langle E_{(8)}\rangle$ is the mean energy of the 8th harmonic (averaged over the ensemble of pulses) After discrimination signal is used to give a trigger. A register is used to store information concerning the trigger and sample detector events. A schematic, illustrating these processes, is shown in Fig. 4.

To describe the single-spike selection, we should define the degree of contrast. A first question that arises is: what is the definition of the main spike? The question of when two closely spaced spikes are barely resolved is a complex one and lends itself to a variety of rather subjective answers. One possible definition can be made as follows. After analysis of smooth sample function $[I(t)]^8$ we find a time moment $t_{\rm m}$ when the intensity reaches its maximum value. Then we find the number of photons within the time interval $(t_{\rm m} - \tau_{\rm coh}, t_{\rm m} + \tau_{\rm coh})$, where $\tau_{\rm coh}$ is coherence time of the 8th harmonic radiation pulse. In fact, the ability to resolve two spikes depends fundamentally on the discriminator level associated with the selected 8th harmonic pulse, and for this reason for large ratio, $E_{\rm th}/\langle E_{(8)}\rangle$, this problem does not exist at all. It can be demonstrated that all reasonable definitions for the degree of contrast are consistent in the region $E_{\rm th}/\langle E_{(8)}\rangle \gg 1$.

Now we would like to discuss in more detail a single-spike contrast preservation during amplification process in the main undulator. The long main undulator can emit a SASE radiation pulse with duration of about 200 times longer than the seed ultrashort pulse. In view of this, the preservation of degree of single-spike pulse contrast is clearly of critical importance to the operation and scientific utility of the attosecond X-ray facility. The criteria that led to the selection of the third cascade and main undulator

parameters were established by first determining the minimum value of main undulator gain. The smaller the main undulator gain, the better the contrast of attosecond pulses and additionally the smaller the cost of undulator systems. For this reason, the best way to reduce the gain of main undulator is by generating maximum 8th harmonic in the spatial bunching at the third cascade exit. The optimum spatial bunching, keeping the linear mode operation, results in an amplitude of 8th harmonic of 10%. Optimized gain of the main undulator is equal to $G \simeq 10^2$. Calculation shows that in this case the ratio of the SASE pulse energy and attosecond pulse energy at the main undulator exit reaches a value of about per cent only. Thus, we find that effects of SASE radiation in the main undulator are not important in our case.

In conclusion let us estimate the repetition rate of the single-spike pulse production. In the case of TESLA X-ray FEL, the number of modes in the fundamental radiation pulse at a wavelength of 0.8 nm is about $M \simeq 50-100$. Suppose that we wish to achieve a contrast of 90%. The discriminator threshold required to achieve this contrast is about $E_{\rm th}/\langle E_{(8)}\rangle \simeq 2$. If the number of modes is close to $M \simeq 100$, plot in Fig. 3 shows that the number of shots per trigger pulse is about 10. Hence, the single-spike pulse repetition rate is still high (about a few thousands single-spike pulses per second). On the other hand, if the contrast of interest is 97% , the number of shots is about $\langle N_{\rm sh}\rangle \simeq 100$, and repetition rate of the single-spike pulse decreases up to a few hundreds per second.

Acknowledgments

We thank W. Brefeld, B. Faatz, J. Feldhaus, M. Körfer, J. Krzywinski, T. Möller, J. Pflüger, J. Rossbach, and S. Schreiber for many useful discussions. We thank J.R. Schneider and D. Trines for their interest in this work and support.

REFERENCES

1. V. Ayvazyan et al., Phys. Rev. Lett. 88(2002)104802
2. S. Milton et al., Science **292**(2001)2037.
3. A. Tremaine et al., Nucl. Instr. and Meth. **A483**(2002)24.
4. F. Richard et al. (eds), TESLA Technical Design Report, DESY2001-011
5. E. L. Saldin, E. A. Schneidmiller and M. V. Yurkov, Opt. Commun. 202(2002)169
6. W. Brefeld, et al., Preprint DESY 02-038, DESY Hamburg, 2002
7. Z. Huang and K.-J. Kim, Phys. Rev. E 62, 7295(2000)
8. I. Boscolo, V. Stagno, Nuovo Cimento B 58(1980)267
9. I. Schnitzer, A. Gover, Nucl. Instr. and Meth. **A237**(1985)124
10. R. Bonifacio, L. De Salvo, P. Pierini, Nucl. Instr. Meth. A 293(1990)627
11. L. H. Yu, Phys. Rev. A 44(1991)5178
12. I. Ben-Zvi et al., Nucl. Instr. and Meth. **A304**(1991)151
13. I. Ben-Zvi et al., Nucl. Instr. and Meth. **A393**(1997)II-10
14. L. H. Yu, I. Ben-Zvi et al., Nucl. Instr. and Meth. **A393**(1997)96
15. L. H. Yu et al., Nucl. Instr. and Meth. **A445**(2000)301
16. J. Wu, L. H. Yu Nucl. Instr. and Meth. **A475**(2001)104

Energy Absorption of Free Rare Gas Clusters Irradiated by Intense VUV Pulses of a Free Electron Laser

J. Schulz[a], H. Wabnitz[a], T. Laarmann[a], P. Gürtler[a], W. Laasch[a], A. Swiderski[a], A. R. B. de Castro[b], Th. Möller[a]

[a]Hamburger Synchrotronstrahlungslabor (HASYLAB) at Deutsches Elektronensynchrotron (DESY), Notkestr. 85, 22607 Hamburg, Germany

[b]LNLS 13084-971 Campinas SP, Brasil and IFGW-UNICAMP 13083-970 Campinas SP, Brasil

As one of the first experiments at the free electron laser of the TESLA Test Facility (TTF) the Coulomb explosion of Xenon clusters irradiated with high intensity pulses with 98 nm wavelength has been observed. Classical trajectory calculations have been performed in order to illuminate the energy absorption process. Comparison with typical parameters in the infrared regime shows that above barrier ionization is suppressed due to the fast oscillating field and thermionic ionization prevails.

1. Introduction

The vacuum ultraviolett (VUV) free electron laser (FEL) of the TESLA Test Facility (TTF) at DESY (Hamburg, Germany) [1] opens up new possibilities to study the interaction of strong laser fields with matter. Here we report on a study of rare gas clusters in the 97 nm radiation of the TTF FEL. While prior experiments have mainly used high intensity lasers in the IR and near UV spectral region [2], the FEL extends the available photon energy into the first ionization thresholds of the rare gases. In this energy region the absorption process that is dominated by inverse bremsstrahlung and tunnel ionization in the optical range [3,4] can be expected to be enhanced by single and multi photon ionization. On the other hand, the laser frequency is expected to get high in respect to the movement of the electrons and thus the frequently used quasi static approximation should break down for these wavelengths.

2. Experimental Setup

A xenon cluster beam has been produced by supersonic expansion of xenon gas through a 100 μm conical nozzle with an opening angle of 15° [5]. The beam passed a differential pumped skimmer to reduce the background pressure. The partial pressure of xenon clusters in the interaction zone could be estimated to 10^{-6} mbar. The FEL beam has been focused on the cluster target using an elliptical mirror. The spot size could be determined to 20 μm by measuring the focal spot on a fluorescent screen. The FEL produced pulses of 30-100 fs length with typical energies between 1.5 and 25 μJ. This results in power densities of up to $7 \cdot 10^{13}$ W/cm^2.

The produced ions have been detected by a time-of-flight (tof) mass spectrometer. The length of the spectrometer was 25 mm, short enough to ensure the detection of singly ionized Xe atoms in less than 1 μs – the time between two bunches in the 1 MHz operation mode of the FEL. The signal of the detector has been recorded by a digital sampling oscilloscope with sampling rates up to 8 billion samples per second (8 GS/s).

3. Results

Figure 1 shows a tof mass spectrum of Xe clusters comprising about 1500 atoms. The spectrum is taken with a sampling rate of 4 GS/s in a single bunch of the laser. It clearly demonstrates that the intensity of the laser is sufficient to take data within a single shot. This could be a valuable in-

formation for future experiments when more complicated probes that can vary from shot to shot will be examined [6].

The figure shows that the clusters are highly ionized by the laser pulse and completely fragment into atomic ions. Charge states up to Xe^{6+} are clearly visible and the Xe^{7+} and Xe^{8+} states seem to be hidden in the experimental noise. The very broad Xe^{+} peak is a clear evidence for high kinetic energies of the fragments. On average each atom absorbs up to 400 eV. This corresponds to a cross section of 10 Mbarn.

An important question is how the energy necessary for ionizing xenon atoms to the highly charged states can be absorbed by the cluster. The photon energy is sufficient to ionize each atom once via single photon ionization. After that initial ionization the electrons have to gain energy in the laser field in order to further ionize the atoms and overcome the Coulomb force to leave the cluster.

4. Classical trajectories calculation

To approach this question classical trajectories calculations have been performed. The calculations base on a model presented by Last and Jortner [7]. The electrons that are ionized by the first single photon processes can move freely inside the cluster. But due to the Coulomb force that is increasing with the charge state of the cluster only a few electrons can leave the cluster with their initial energy in the order of a few eV. Thus the classical simulations start with a spherical $(Xe^{Z+})_N$ cluster containing $N \cdot Z$ free electrons. These electrons are treated as classical point charges and move in the potential of the ions given by:

$$U_{\mathrm{Ion}} = -\frac{BZ}{r} + \frac{C}{r^6} \qquad (1)$$

The first term with the constant $B = 14.385$ eVÅ describes the attracting Coulomb potential. The second term simulates the elastic scattering of the electrons at the ion cores. The choice of the constant C has only minor influence on the results of the calculation. It has been set to $C = 410$ eVÅ^6 according to the choice of Last and Jortner [7] for $(Xe^{6+})_N$ clusters.

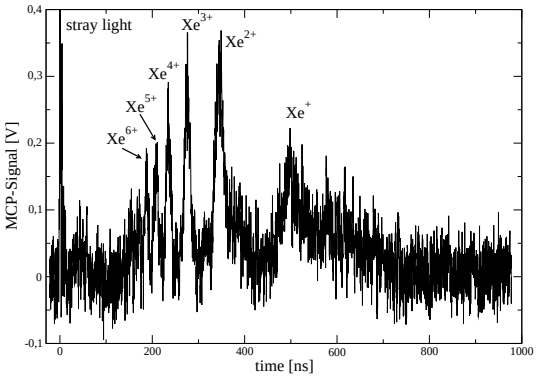

Figure 1. Time-of-flight mass spectrum of Xe clusters comprising 1500 atoms acquired within a single bunch of the TTF FEL.

In addition to the ionic potential the repelling Coulomb forces between the electrons have to be taken into acount:

$$U_{\mathrm{Elec}} = \frac{B}{\sqrt{r^2 + r_0^2}} \qquad (2)$$

where r is the distance between the electrons and $r_0 = 0.2$ Å is a parameter used to flatten the potential and thereby avoiding numerical instabilities.

Due to the limited computer performance the calculations have been limited to the electron dynamics of small Xe_{13} and Xe_{55} clusters where the central ion is surrounded by one or two spherical ion shells. For the positions of the ions a fcc-structure with atomic distances of 4.33 Å has been assumed. This simplification shouldn't influence the results significantly since the basic shell-like structure of the van-der-Waals cluster is not affected.

Figure 2 shows the temporal development of the total energy of the electron gas for a $(Xe^{6+})_{55}$ cluster with 330 freely moving electrons in laser fields with a power density of $5 \cdot 10^{13}$ W/cm^2 and different wavelengths. The solid line resembles the parameters that are realized in the presented experiment. Previous experiments have used lower frequencies so the simulations for 97 nm are

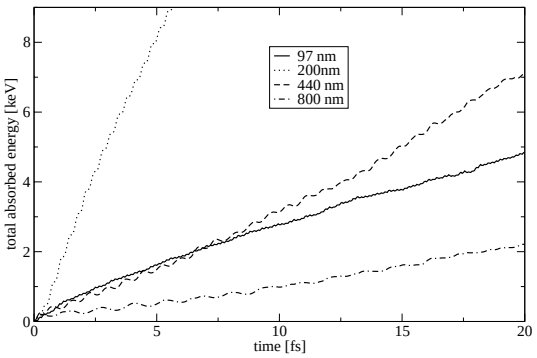

Figure 2. Energy absorption calculated by the clasical trajectory simulation for a Xe_{55} cluster containing 6 quasi free electrons per ion.

cluster	electr.	Absorp. $[\frac{\text{eV}}{100\text{fs atom}}]$	cross sec. [Mbarn]
$(Xe^{1+})_{13}$	13	16	0.5
$(Xe^{1+})_{55}$	55	33	1.0
$(Xe^{2+})_{55}$	110	86	2.8
$(Xe^{6+})_{55}$	330	472	15

Table 1
Simulated energy absorption and cross section for different cluster sizes and numbers of quasi free electrons.

compared with longer wavelength calculations in figure 2. It is obvious that the absorption is going through a maximum when the wavelength is changed from 97 nm to 800 nm. This resonant behaviour has also been seen in reference [7].

The fact that the used laser frequency lie on the high frequency side of the resonance is an indication for a qualitative difference to 800 nm radiation: While in the 800 nm laser field the electric field strength varies slowly compared with the electron movement, at 97 nm the field is changing with a frequency that is higher than the characteristic frequency of the electron gas.

The approximately linear increase in energy that can be observed for 97 nm in figure 2 shows that the absorption is hardly changing with the electron temperature. From the slope of this increase an absorption coefficient and thus a cross section for photon absorption can be obtained. Table 1 summarizes the results for different simulations. The cross section varies strongly with the density of free electrons. For one electron per atom in a $(Xe^{1+})_{55}$ cluster the absorption cross section is about 1 Mbarn. This value is increasing when more electrons are set free via inelastic electron ion collisions. The calculated cross sections do not reach the experimental value of 10 Mbarn unless a high density of quasi free electrons has been reached. This can be interpreted as a strong evidence for additional quantum mechanical effects that are increasing the energy absorption.

A different question that can be answered by the simulations is how the electrons leave the cluster. While under the quasi static approximation the electrons are emitted via tunnel ionization or above barrier ionization, the efficiency of these effects should decrease with increasing frequency. Both effects lead to an electron emission that is strongly aligned along the polarization direction of the laser field. Alternatively, the electrons could gain enough kinetic energy to leave the cluster and escape in random direction. This type of ionization is typical for thermionic emission.

Figure 3 shows electron positions for three different laser parameters. In the upper panel typical parameters for a high energy infrared experiment are used. The laser field has a wavelength of 800 nm with a power density of 10^{16} W/cm^2. The picture shows two snapshots of electron positions for two time steps after 10 and 20 fs respectively. A considerable fraction of electrons has been emitted via above barrier ionization in the direction of the electric field of the laser radiation.

To examine the influence of the wavelength, in the central panel the electron positions are plotted for 98 nm with the same power density. The electrons stay longer inside the cluster. The angular distribution is isotropical. This is a clear signature for the suppression of above barrier ionization at higher laser frequencies. The electrons are mainly leaving the cluster by thermionic emission.

In the presented experiment the power density has been more than two orders of magnitude

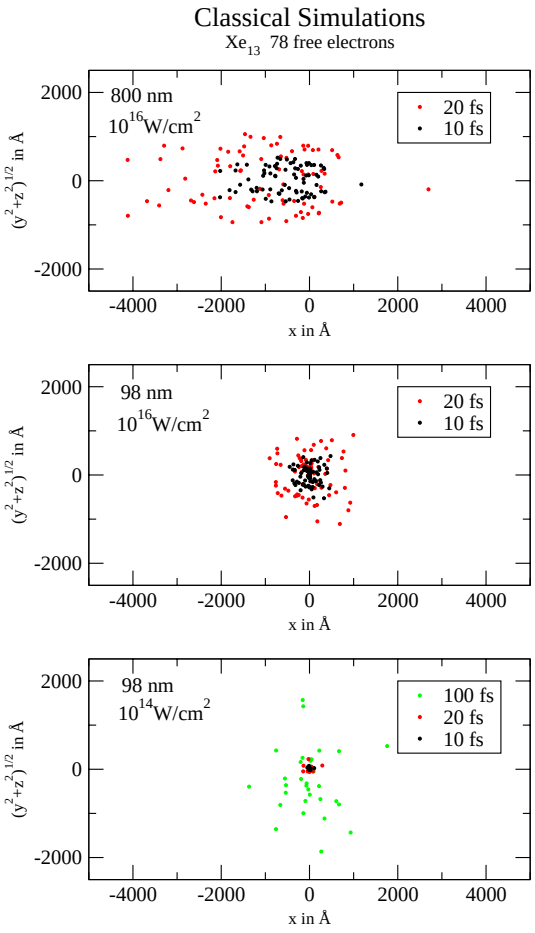

Figure 3. Electron emission calculated by the clasical trajectory simulation

lower compared with typical experiments using infrared lasers. To show that the electron emission still takes place at lower power densities, in the bottom panel of figure 3 the electron emission is shown for a power density of 10^{14} W/cm^2. The emission is strongly reduced and the electrons need more time to leave the cluster. To show that the simulation still predicts noticeable ionization a further timestep after 100 fs has been added.

5. Conclusions

The experimental results as well as the classical trajectories calculations could show that interesting physics can be done with a laser source in the wavelength regime under 100 nm. The absorption process showed to be very effective. The absorption rates derived from the classical simulations are still lower than the measured absorption. Thus quantum mechanical effects are considered to play a significant role in the absorption process. It can also be stated that field ionization effects play a negligible role using 97 nm radiation due to the fast oscillating field.

6. Acknowledgements

The authors thank the TTF team at DESY, especially P. Castro, M. Minty, D. Nölle, H. Schlarb, and S. Schneider for running the accellerator and B. Faatz, A. Fateev, J. Feldhaus, Ch. Gerth, U. Hahn, E. Saldin, E. Schneidmiller, K. Sytdev, K Tiedtke, R. Treusch ,and M. Yurkov for providing us with information on the laser properties and for many fruitfull discussions.

REFERENCES

1. J. Andruszkow, B. Aune, V. Ayvazyan, N. Baboi at al., *Phys. Rev. Lett.* **85**, 3825 (2000)
2. D. Batani, C. J. Joachain, S. Martellucci and A. N. Chester, *Atoms, solids, and plasmas in super-intense laser fields*, Kluwer Academic, New York (2001)
3. S. Aust, d. Strickland, D. D. Meyerhofer, S. L. Chin and J. H. Eberly, *Phys. Rev. Lett.* **63**, 2212 (1989)
4. T. Ditmire, T. Donnelly, A. M. Rubenchik, R. W. Falcone and M. D. Perry, *Phys. Rev. A* **53**, 3379 (1996)
5. R. Karnbach, M. Joppien, J. Stapelfeldt, J. Wörmer and T. Möller, *Rev. Sci. Instr.* **64**, 2838 (1993)
6. R. Neutze, R. Wouts, D. van der Spoel, E. Weckert and J. Hajdu, *Nature* **406**, 752 (2000)
7. I. Last and J. Jortner, *Phys. Rev. A* **60** 2215 (1999)

Structural changes at solid surfaces irradiated with femtosecond, intense XUV pulses generated by TTF-FEL

Ryszard Sobierajski[1], Jacek Krzywinski[2], Andrzej Andrejczuk[2,3], Bart Faatz[4], Frank Felten[5], Sandra Jacobi[6], Libor Juha[4,7], Marek Jurek[2], Anna Kauch[8], Dorota Klinger[2], Jerzy B. Pelka[2], Evgueni Saldin[4], Evgueni Schneidmiller[4], Marcin Sikora[9], Barbara Steeg[4], Mikhail Yurkov[10]

[1]*Warsaw University of Technology, Pl. Politechniki 1, PL-00-661 Warsaw, Poland*
[2]*Institute of Physics, Polish Academy of Sciences, Al. Lotników 32/46, PL-02-668 Warsaw, Poland*
[3]*Institute of Experimental Physics, University of Bialystok, Lipowa 41, PL-15-424 Bialystok, Poland*
[4]*Deutsches Elektronen-Synchrotron DESY, Notkestrasse 85, D-22603 Hamburg, Germany*
[5]*Technische Universität Hamburg, Denickestrasse 15, D- 21073 Hamburg, Germany*
[6]*GKSS Research Center, Max-Planck-Strasse 1, D- 21502 Geesthacht, Germany*
[7]*Institute of Physics, Czech Academy of Sciences, Na Slovance 2, 182 21 Prague 8, Czech Republic*
[8]*Warsaw University, Krakowskie Przedmiescie 26/28, PL-00-927 Warszawa, Poland*
[9]*Faculty of Physics, University of Mining and Metallurgy, Al. Mickiewicza 30, PL-30-059 Cracow, Poland*
[10]*Joint Institute for Nuclear Research JINR, 141980 Dubna ,Moscow Region,Russia*

Abstract

Interaction of ultrafast (~ 50 fs), high intensity (up to 10^{13} W/cm^2) XUV (λ ~ 85 nm) FEL beam with solids has been studied at the TTF-FEL facility. Damaged surfaces have been investigated using light, electron, and atomic force microscopy. Influence of the FEL radiation intensity on the structural changes at the surfaces has been investigated. Results obtained for different materials, i. e. metals (Au), semiconductors (Si), inorganic insulators (Ce:YAG, BaF_2, SiO_2), and organic polymers (polymethylmethacrylate - PMMA), are compared. Laser-induced periodic surface structures (LIPSS) were observed at amorphous carbon (a-C) layers.

1. Introduction

Before our experiments the shortest wavelengths at which laser ablation was investigated were 46.9 nm and 125 nm. The 46.9-nm radiation was emitted from a capillary-discharge Ne-like Ar XUV laser [1] and the 125-nm radiation was generated by a four-wave-sum-frequency mixing (FWSFM) of frequency-doubled Nd:YAG laser radiation in Hg vapour [2]. The pulse duration in both cases was in the nanosecond range. A few papers (for a review see [3]) reported ablation induced at even shorter wavelengths (i. e. in soft X-ray region) but the radiation used was not coherent. In the present study, not only the laser wavelength is short (< 100 nm) but also the pulse duration is very short (typically 50-100 fs [4]. The short wavelength and ultrafast coherent beam represent an unique combination. Ablation behaviour of a wide variety of materials has been investigated by us under these irradiation conditions.

2. Experimental

The samples were irradiated by SASE-FEL beam delivered from the Tesla Test Facility (TTF) operated at HASYLAB/DESY in Hamburg [4]. The wavelength was tuned between 85 and 98 nm. Spectral and energy characteristics of the laser beam were measured by the photon diagnostics described in details elsewhere [5]. The beam was focused by an elliptical mirror into the FELIS interaction chamber (FEL Interaction with Solids; for more details see [6]).

Morphological changes at the surface of the exposed samples were investigated by Nomarski, conventional optical, scanning electron, and atomic force microscopy. Raman spectra were made with a laser microbeam in the usual backscattering

geometry, which enables probing chosen places on the sample surface.

3. Results and discussion

3.1 Morphological changes following XUV ablation of various materials

Nomarski micrographs of Au, Si, Ce:YAG, BaF_2, SiO_2, and PMMA samples irradiated at a fluency of 0.5 J/cm^2 (well above a typical XUV-FEL ablation threshold [5]) show very similar global shape of a crater. It indicates that none of the materials exhibits very different ablation efficiency with respect to others. Investigation of the ablated surfaces with better spatial resolution leads to a conclusion that XUV-FEL ablation of inorganic (Ce:YAG, BaF_2, SiO_2) as well as organic (PMMA) insulators is very clean, i. e. the surfaces below the ablated layers remain very smooth. Contrary to this finding the semiconductor and metallic surface are strongly affected by the radiation. This is visible not only on surface morphology (numerous cones and cracks were created) but also in the Raman spectra where substantial changes were observed (for example amorphization of silicon).

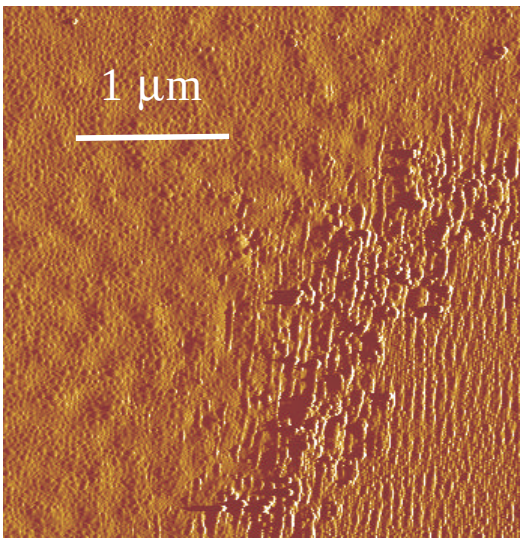

Fig. 1. AFM image of 39-nm a-C layer deposited on Si substrate and irradiated by focused 98-nm FEL radiation.

3.2 XUV-laser-induced periodic surface structures (XUV-LIPSS) at amorphous carbon (a-C)

Periodic ripples with a spatial period of 76(8) nm (Fig. 1) were indicated by AFM in the a-C sample area irradiated at lower FEL intensity, i.e. at a periphery of the FEL-created crater. The ripples (laser induced periodic surface structures - LIPSS) were formed here with the shortest-wavelength coherent radiation in almost forty years long history of this phenomenon's investigation (LIPSS were discovered by Birnbaum in sixties [7]; for a review see [8,9]). The ripple period reported above testifies to the ability of TTF-FEL to be used in nano-technology as a new tool for a production of nanostructures.

4. Conclusions

At higher intensities of FEL radiation the ablation efficiency depends only weakly on a kind of irradiated material. It was demonstrated by a comparison of Si, Au, Ce:YAG, and PMMA ablation behaviour. The FEL-induced ablation of Ce:YAG, BaF_2, SiO_2, and PMMA leads to a formation of very smooth surfaces below the removed material. It means that the ablation of these materials is very clean. This finding is encouraging for a prospective use of the FEL radiation in nanostructuring of such a material. Contrary to that, silicon surfaces were amorphized and their morphology changed dramatically. LIPSS with a spatial period slightly shorter than FEL wavelength were found at FEL-irradiated a-C surfaces.

5. References

[1] B. R. Benware et al., Opt. Lett. 24 (1999) 1714.
[2] D. Riedel, M. C. Castex, Appl. Phys. A69 (1999) 375.
[3] L. Juha et al., Surf. Rev. Lett. 9 (2002) 347.
[4] V. Ayvazyan et al., Eur. J. Phys. D20 (2002) 149.
[5] R. Treusch et al., Nucl. Instrum. Meth. Phys. Res. A467-8 (2001) 30.
[6] A. Andrejczuk, U. Hahn, M. Jurek, J. Krzywinski, J. Pelka, H. Reniewicz, E. A. Schneidmiller, W. Sobala, R. Sobierajski, M. Yurkov, TTF FEL team, HASYLAB Annu. Rep. (2001) 117.
[7] M. Birnbaum, J. Appl. Phys. 36 (1965) 3688.
[8] A. E. Siegman, P. M. Fauchet, IEEE J. Quant. Electron. QE-22 (1986) 1384.
[9] P. E. Dyer et al., Appl. Surf. Sci. 96-98 (1996) 537.

Total reflection mirrors for VUV Free Electron Lasers

B. Steeg[a], S. Jacobi[b], R. Sobierajski[a], C. Michaelsen[c], J. Feldhaus[a]

[a]HASYLAB at DESY, Notkestrasse 85, 22603 Hamburg, Germany

[b]GKSS Research Center, Max-Planck-Strasse 1, 21502 Geesthacht, Germany

[c]Incoatec GmbH, Max-Planck-Strasse 2, 21502 Geesthacht, Germany

1. INTRODUCTION

Advances in linear accelerators and undulators have recently boosted the development of short-wavelength free electron lasers (FELs). The FEL at the TESLA Test Facility (TTF) has demonstrated maximum light amplification in the range 80 nm to 120 nm wavelength with an output power in the GW range [1,2]. In the next development stage this FEL will provide intense, sub-picosecond radiation pulses with photon energies up to 200 eV for scientific applications. Very precise, ultra-smooth mirrors and gratings are required to transport, focus and disperse the radiation. Usually suitable thin film coatings on silicon or other subtrates are used in the vacuum ultraviolet (VUV) and x-ray spectral range. Coatings of light elements are preferred because of their superior reflectivity and, consequently, their low absorption at grazing angles of incidence. Carbon appears to be ideal for the TTF FEL since the K absorption edge at 284 eV is well above the photon energy range of the FEL. Therefore carbon coated mirrors have been developed in a joint project by GKSS and DESY.

2. EXPERIMENT

Single-layer amorphous carbon coatings have been produced on planar, well polished silicon substrates by magnetron sputtering [3] at GKSS. In order to optimize the deposition process, the coatings were routinely characterized with unpolarized Cu-Kα radiation using a conventional x-ray reflectometer [4]. The optical characterization of the coatings in the VUV and soft x-ray spectral region was done at HASYLAB/DESY using the soft x-ray reflectometer at beamline G1 [5]. For comparison carbon coatings produced by other deposition methods, i.e. plasma-enhanced chemical vapor deposition (PE-CVD) and pulsed laser deposition (PLD) were also investigated. Annealing experiments have been performed to test thermal stability [6].

The radiation stability of the carbon mirrors was investigated in the FELIS (Free Electron Laser - Interaction with Solids) [7] experiment at the TTF-FEL. The ablation of carbon was analyzed by a time-of-flight (TOF) spectrometer as a function of the radiation power density. All measurements were performed at room temperature under UHV conditions.

3. RESULTS AND DISCUSSION

Fig. 1 shows energy dependent reflectivity spectra of carbon coatings which were produced by three different methods. Characteristic properties of those coatings, such as thickness, roughness and layer density, were determined by fitting angle dependent reflectometry curves for a fixed photon energy [6]. The PE-CVD coating (dashed line) has the lowest reflectivity in the energy region of 50 - 200 eV. The low density of this coating can possibly be explained by the incorporation of hydrogen during the deposition process. The PLD film has high reflectivity and very high density, but also high roughness. The sputtered amorphous carbon coating has the highest reflectivity (95-96%). The density is about 2.2 g/cm^3 and the roughness is much lower than that of the PLD film. For the proposed application a reflectivity as high as possible in combination with high density and low roughness is required. The amorphous carbon coating produced by magnetron sputtering shows the best combination of properties.

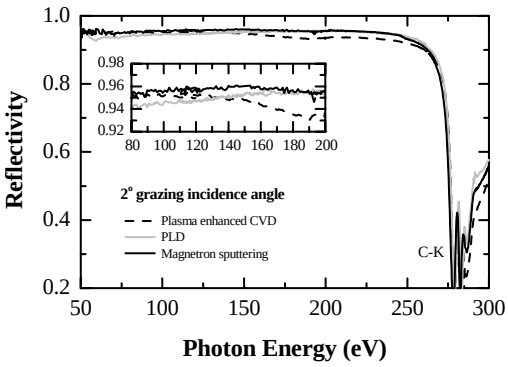

Figure 1. Energy dependent reflectivity spectra of different carbon coatings for a fixed grazing incidence angle of 2°.

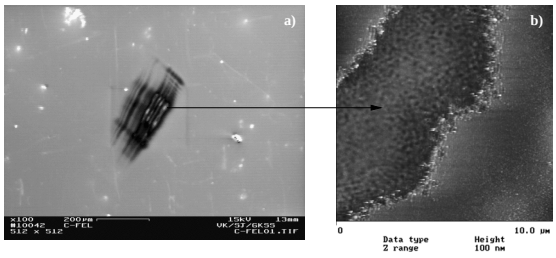

Figure 2. a) SEM image of a carbon mirror irradiated by the TTF-FEL beam (V. Küstner, GKSS). b) SFM topographic image of the irradiated area (F. Felten, TUUH).

Sputtered carbon coatings were investigated in the FELIS experiment at the TTF-FEL. The mirrors were irradiated perpendicular to the surface. The wavelength of the FEL was 98 nm (12.7 eV) with a pulse energy of 40 μJ and a pulse length of 100 fs. From TOF measurements at different FEL pulse energies the damage threshold for a 39 nm carbon film was estimated to 0.06 J/cm^2 [7]. Scanning Electron Microscopy (SEM) studies of irradiated carbon mirrors show clearly the spots where the FEL beam hit the surface (Fig. 2a). A stripe pattern arises from interference of the beam with a wire placed in the light path for beam diagnostics. The irradiated area shows, in most cases, two different regions of damage. One of strong damage is situated in the middle (small bright spots) surrounded by a second region of less damage (dark structure). Two different regions of damage could also be resolved with Scanning Force Microscopy (SFM). On the left of Fig. 2b, the area of strong damage is seen, which looks like melted material. On the right side, the region of less damage is visible.

Up to now it has not been possible to perform experiments with intense, sub-picosecond radiation pulses in the planned working energy range up to 200 eV. This energy range, however, is much less critical because the photoabsorption cross section of carbon is two to three orders of magnitude lower than in the VUV where the current studies have been made. In addition, the mirrors will be used at grazing angles of incidence in the regime of total reflection, reducing the absorbed power density to < 1 mJ/cm^2, i.e. two orders of magnitude below the damage threshold reported above. Therefore we are confident that the mirrors will not be damaged by the FEL radiation.

REFERENCES

1. V. Ayvazyan et al., Phys. Rev. Lett. **88**, 104802 (2002).
2. V. Ayvazyan et al., Eur. Phys. J. D **20** 149-156 (2002).
3. C. Michaelsen et al. Adv. X-ray Anal. **42**, 308 (2000).
4. S. Jacobi et al., in *Optics for Fourth-Generation X-Ray Sources* (San Diego, 2001), Vol. 4500 of *Proceedings of SPIE*, pp. 187 - 192.
5. http://www-hasylab.desy.de/facility/experimental_stations/stations/G1.htm
6. S. Jacobi et al., *Proceedings of SPIE 2002* (to be published).
7. A. Andrejczuk et al. *HASYLAB Annual Report*, pp. 117-120, 2001.

Commissioning of Multi-Segmented Undulators at the TESLA X-ray FEL

M. Tischer[a,*], P. Ilinski[b], U. Hahn[a], J. Pflüger[a], H. Schulte-Schrepping[a]

[a] *Hamburger Synchrotronstrahlungslabor HASYLAB, DESY, Notkestr. 85, D-22603 Hamburg, Germany*
[b] *Advanced Photon Source, Argonne National Laboratory, 9700 S. Cass Ave., Argonne, IL 60439, USA*

Abstract

Commissioning of the TESLA X-ray FEL undulator cells will start at low electron energy and long photon wavelength (~6nm) corresponding to the bottom end of TTF phase II operation. Electron and photon diagnostic schemes will be used to monitor the beam trajectory through the various undulator segments. Furthermore, photon diagnostics has to control all undulator gaps and prove the phase tuning of adjacent segments. Using higher harmonics of the spontaneous radiation of individual undulator segments, the photon diagnostic station can cover a wide spectral range and will be able to cope with the progression towards lower SASE wavelength (~1Å). The use of variable gap undulators allows to realize the photon diagnostic section in a single device located in the photon beamline downstream of the last undulator cell.

PACS codes: 41.60.Cr; 42.60.Jf; 07.85.Qe

Keywords: X-ray FEL; photon beam characterization; trajectory alignment; phase tuning

1. Introduction

X-ray FELs require very long undulators in order to achieve saturation at wavelength in the 1Å-range. The TESLA XFEL undulators will be made of up to ~50 short cells of 6.1 m length [1], i.e. a 5 m long undulator segment and a 1.1 m long intersection module containing items such as phase shifter, quadrupole, BPMs, and steering coils. The proposed X-ray diagnostics [2] is a tool for alignment and commissioning of the numerous undulator cells along an XFEL beamline. Photon diagnostics is also used successfully or foreseen in other SASE FELs as TTF [3,4], LEUTL [5] or LCLS [6].

In the commissioning phase of the TESLA XFEL operation will start at the TTF phase II lower limit (~6nm) and continuously progress towards shorter wavelengths. Here, diagnostic issues are discussed for undulator SASE3 (λ_U=45mm) which provides a 1st harmonic at 6.4 nm (193.5eV) for an electron energy of 2.5 GeV. The ρ-parameter corresponding to this wavelength is $\rho \sim 1 \cdot 10^{-3}$ which leads to considerably lower alignment requirements in the undulator section, namely a trajectory displacement within Δx=13µm, trajectory tilt $\Delta x'$=2.6µrad, gap adjustment Δg=6.5µm, and a phase tuning of a few degree.

The diagnostic station with a monochromator as a principal instrument is located about 100m downstream from the last undulator cell. The spatial distribution of the spontaneous radiation of individual or several consecutive undulator segments is imaged and analyzed in order to optimize angle and position of the electron beam trajectory, to verify the magnetic gap and to adjust the phase match between two undulator segments [7].

Wavefront calculations have been performed for the commissioning parameters of SASE3 in order to assess the feasibility of the proposed concept.

2. Trajectory alignment

The 1st harmonic at 193.5eV is not suited to monitor the electron trajectory in the undulator

* Corresponding author. fax: +49-40-8994-2923.
E-mail address: markus.tischer@desy.de

because its spatial distribution with a FWHM of 6.5mm is too broad. Observing the 5th harmonic results in a sufficiently narrow beam pattern which can resolve a trajectory misalignment in the range from 2.8µrad (observation precisely at 5th harm.) to about 1.8µrad for a detuning of the observation energy to slightly higher values (Fig.1). This will satisfy the required accuracy. The expected intensities are in the order of 10^5 and about twice as high as for the 1st harm.

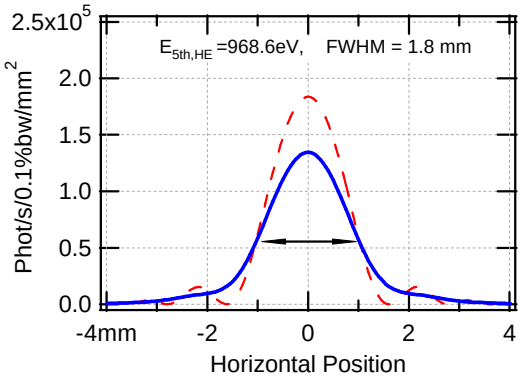

Fig. 1. Spatial distribution of the 5th harmonic (detuned to higher energies). Solid: incl. emittance effects; dashed: single electron

3. Gap adjustment

Measuring the beam intensity at fixed monochromator energy (5th harm.) as a function of the undulator gap will result in a sharp peak corresponding to related nominal gap. Assuming an intensity determination with only 20% accuracy results in a resolution of Δgap=3µm. A gap deviation of 6.5µm causes an intensity drop by a factor 2.4 .

4. Phase tuning

The phase of two successive undulator segments can be tuned by maximizing the intensity at either the 1st or 5th harmonic (fixed observation energy) as function of the electron beam delay (Fig.2). Though both ways allow to set the phase with an accuracy of several degrees, working at the 5th harm. gives higher contrast (~280), higher overall intensity (10^6) and higher sensitivity.

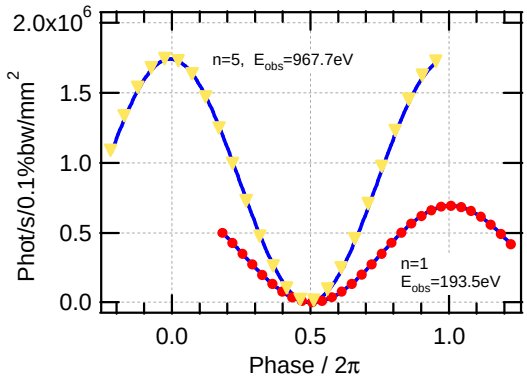

Fig. 2. Intensity variation at constant observation energy as function of the phase relation between two adjacent undulator segments.

5. Observation of high harmonics

A diagnostic station for the commissioning phase at 6.4nm requires a completely different hardware than the one for the final 1Å XFEL operation. The useful energy spectrum of SASE3 (spontaneous) at the initial settings ranges above 10keV. It could be attractive to work with this diagnostic scheme at E~6keV in order to use the same hardware setup as it will be needed at final stage and to accommodate smoothly to the progression towards shorter SASE wavelengths.

As known field errors and in particular the phase error degrade the performance of especially the high harmonics. Calculations for a non-ideal magnetic field with 0.5% rms Gaussian noise producing a 3° rms phase error result in a still symmetric spatial distribution at 6keV with FWHM=1.5mm which would be suited for trajectory and gap optimization. However, the actual applicability of high harmonics strongly depends on the attainable phase error.

References

[1] J. Pflüger et al., Nucl. Instr. Meth. A 483 (2002) 388
[2] M. Tischer et al., Nucl. Instr. Meth. A 483 (2002) 418
[3] R. Treusch et al., Nucl. Instr. Meth. A 445 (2000) 456
[4] K. Tiedtke et al., "Photon Beam Diagnostics for the FEL in the Second Phase of the TESLA Test Facility", this conference
[5] E. Gluskin et al., Nucl. Instr. Meth. A 429 (1999) 358
[6] E. Gluskin et al., LCLS TN-00-13, SLAC, (2000)

Electron Beam Diagnostics for TTF II

M. Wendt[a] for the TESLA collaboration *

[a] Deutsches Elektronen Synchrotron DESY
Notkestr. 85, D-22607 Hamburg, Germany

This paper presents an overview of the electron beam diagnostics for the upgrade of the TELSA Test Facility (TTF II). Beside of a program for testing components, especially superconducting accelerating structures, for the linear collider project TESLA, TTF II will serve as SASE FEL 4th generation synchrotron radiation user facility.

1. INTRODUCTION

In phase II of the TESLA Test Facility (TTF II) the electron beam energy will be increased – by use of 6 TESLA cryo-modules – from 250 GeV/c (TTF I) up to 1 GeV/c (Fig. 1.).

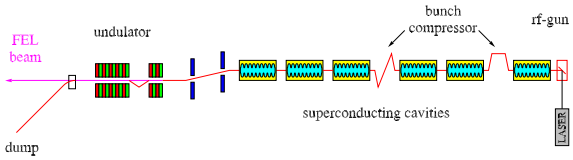

Figure 1: Schematic overview of TTF II.

Table 1
Parameters of the TTF II electron beam.

max. beam energy	=	1 GeV
max. rep. rate f_{rep}	=	10 Hz
macro pulse length t_{pulse}	=	800 μs
bunch spacing $\Delta\, t_b$	=	110 ns or 1 μs
N_e per bunch	=	0.1...4 nC
bunch length σ_z	=	50 μm
norm. emmittance ϵ_{norm}	=	2 mm mrad

* This work is carried out in the framework of the TESLA collaboration and therefore represents also the contribution of many coworkers within the collaboration, who cannot be mentioned here.

While still acting as test accelerator for the development of the superconducting L-band (1.3 GHz) cavity technology for the TESLA linear collider [1], emphasis is now put on driving the 30 m long SASE FEL to wavelength as short as 6 nm. In order to act as SASE-based 4th generation synchrotron radiation user facility [2],[3] a set of new reliable, precise instruments are required to ensure the required quality, stability and control of electron and photon beams [4]. Table 1 gives an overview of the electron beam parameters.

In order to control orbit and charge stability required for stable and reproducible FEL operation, the "basic" beam instrumentation – *charge* and *position* of the electron beam – needs single bunch resolution, i.e. each of the up 7200 electron bunches within the macropulse has to be measured individually to control drifts or slopes within the macropulse, originating from sources like beam loading or wake fields. This yields an integration or measurement time of < 110 ns.

Also the measurements of the *beam profiles* (transverse and longitudinal) are challenging. Low emittance and strong bunch compression require a resolution < 20 μm for the transverse profile and subpicosecond techniques to measure bunch-lengths on the order of 100 fs.

2. LINAC INSTRUMENTATION

2.1. Bunch Charge

Apart of **Faraday cups** in the gun region, the single bunch charge measurements in TTF II rely on broadband **toroids** (bandwidth: 10 kHz...$>$ 50 MHz). In

contrast to most current transformers, the ferrite core of this type, developed at DESY, is made out of two half rings, allowing to complete the assembly after the vacuum parts including the ceramic gap are already mounted.
A prototype toroid, already tested in TTF I, has demonstrated the single bunch capability for 9 MHz bunch rep. rate. The toroid signals are not only used for bunch charge monitoring, but also in connection with the realtime protection system.

2.2. Beam Position

Different types of BPM pickup's are used throughout the TTF II linac [5]:

Cavity BPM's A *re-entrant* cavity BPM will be tested as alternative to the 1.5 GHz *dipole mode* cavity monitors, used so far inside all the cryomodules. Recent studies show high cryogenic losses for using the dipole mode BPM in the TESLA linear collider. The strong damping by external loads in case of the re-entrant BPM minimizes this effect and it's broadband characteristic offers an improved single bunch capability.

Stripline BPM's are foreseen in most of the "warm" parts of TTF II. They will be located inside the quadrupole magnets, not only to save space, but also for alignment purposes. Using an automatic procedure on a wire test bench, the magnetic axis of the quadrupole can be aligned to the electric axis of the stripline pickup to an absolute error $< 20\ \mu$m [6].

Button BPM's equipped with commercial feedthrough electrodes are considered at space critical locations, like the injector and the bunch compressors. To cover the whole aperture of the wide, flat vacuum chamber in the dispersive section of the bunch compressor, an array of 4+4 button electrodes will be installed.

In order to simplify operation and maintenance an updated version of the TTF I undulator BPM *read-out electronics* will be used for most pickup stations, i.e. all stripline and button type BPM's. The signal processing is based on the *AM/PM principle*, which delivers a bunch charge independent beam position analog signal for every passing bunch [7].

The cavity BPM's (re-entrant, as well as dipole mode) require special treatment with dedicated read-out techniques.

2.3. Beam Emittance and Energy Spread

The *transverse beam profile* will be measured with *OTR screens* and *wire-scanners*. The *beam emittance* is deduced by either quadrupole scanning methods or beam size measurements at four consecutive locations along the FODO lattice.

OTR screens TTF II will be equipped with approximately 25 screen monitors, which are distributed along the accelerator. Most of them uses a 300 μm thick silicon wafer OTR target (without coating). For machine commissioning, i.e. low intensity beams some dedicated stations will be equipped with YAG crystals. The imaging system consists out of single achromatic lenses. Different image scales and variable attenuation will be handled by sliding lenses and filters remote controlled into the optical path. A resolution of 20 μm is expected for these systems.

Wire-scanners A modified version of the CERN-LEP wire-scanner [8] will also be used for transverse beam profile monitoring. Mounted under 45^0 with respect to the horizontal plane and using a V-like wire schema allows x and y profile measurements with a single scanner.

2.4. Bunch Length

In order to operate the SASE FEL successfully high current densities in the electron bunches are mandatory. Therefore the bunches have to be compressed down to a length of 50 μm or below ($\equiv$ 160 fs). Monitoring the *bunch length* with conventional methods, i.e. observing radiation produced by the beam bunches with a streak camera, is only possible at the early stages of compression. Several methods have been developed to monitor the ultimate bunch length at TTF II:

Longitudinal phase space tomography is based on phase scans in the accelerating structures in combination with transverse beam images in dispersive sections to reconstruct the longitudinal phase space [9].

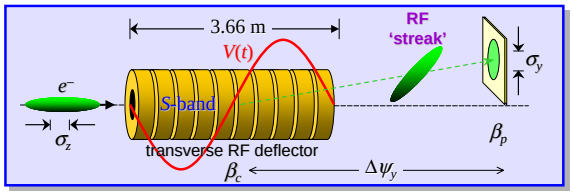

Figure 2: Deflecting S-band cavity for bunch length measurements (courtesy of P. Emma).

Interferometric methods uses coherent far infrared (FIR) transition or diffraction radiation with an interferometer. The coherent FIR radiation, produced by the sub-picosecond bunches, is accessed by using a screen, an aperture or just at a discontinuity of the vacuum chamber. In the following interferometer this radiation is used to measure the autocorrelation signal [10],[11].

Electro optical sampling (EOS) measure directly the electromagnetic field of the bunch by changing the optical properties of a crystal. The changes are probed by means of ultrashort laser pulses. The electron bunch is sampled by scanning the delay of the laser pulses with respect to the bunch, which results in a longitudinal image of the bunch [12].

Transverse mode cavity The bunches are deflected ("streak") directly in the transverse rf-fields of a S-band dipole mode cavity structure (similar to the streak camera principle, see Fig. 2). In this way the longitudinal plane is transformed into a transverse image, which can be detected with a screen downstream the cavity [13].

2.5. Beam Phase

In order to achieve stable SASE operation, the stability of beam energy and longitudinal beam profile have to be accomplished. Phase "jumps" in the accelerating structures yield both, an energy variation and due to the use of magnetic bunching to a change in the longitudinal beam profile.

A set of **phase monitors** will be installed behind the gun and between each of the accelerating sections. The pickup consists out of an impedance matched ring electrode, supplying a differentiated broadband pulse signal when passed by an electron bunch. A *beam phase signal* can be derived by I/Q mixing a filtered 1.3 GHz component with signal of the 1.3 GHz master oscillator. *Time-of-flight (TOF)* measurements can be realized by precise measurement of the time difference of the signals from two phase monitors.

3. UNDULATOR DIAGNOSTICS

3.1. Diagnostic Block

The undulator of TTF II [14] is divided in six 4.5 m long sections. The position and transverse profile of the electron beam are monitored in seven *diagnostic blocks* (see Fig. 3), which are located between these sections:

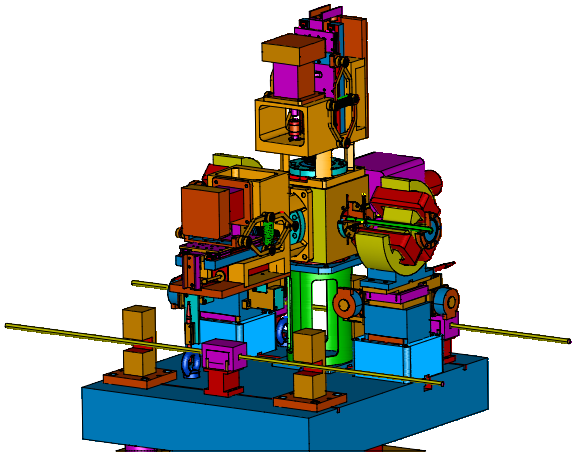

Figure 3: The diagnostic block keeps two wire-scanners and a beam position monitor.

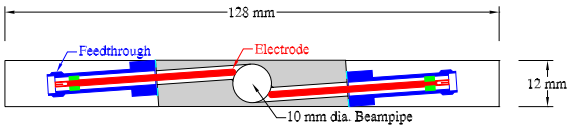

Figure 4: Cross-section of the BPM pickup eletrodes mounted inside the undulator.

Wire-scanner For the transverse beam profile a new type of *wire-scanner* with an unidirectional drive unit has been developed. Individual units of this new type are foreseen for scanning horizontal and vertical plane.

Beam position monitor (BPM) A removable unit holds 4 symmetric arranged *electrostatic electrodes*, which are similar to the well-known "button"-BPM's. These BPM electrodes are the same as those inside the undulator, but here they can be arranged in the horizontal and vertical plane.

3.2. Undulator BPM's

In contrast to TTF I, the undulator will be operated without internal strong focussing, relaxing the need for BPM's inside the undulator. Only two additional electrostatic "button" BPM's will be integrated in the vacuum chamber of each undulator section. These BPM's (Fig. 4) are identical to those used successfully in TTF I [15],[16].

4. ACKNOWLEDGEMENT

The author is indebted to all members of the TESLA collaboration [1] to their contributions to TTF, particular thanks to INFN Frascati and CEA Saclay. Further thanks to SLAC, for their help in setting up the transverse mode cavity.

REFERENCES

1. TESLA Collaboration, "TESLA Design Report", TESLA Report 2001-011 (2001)
2. M. Körfer, et. al., "The TTF-FEL Status and its Future as a Soft X-ray User Facility", Proc. of the 23rd FEL Conf., Darmstadt (2001), Germany, to be publ.
3. B. Faatz, et. al., "The SASE FEL at the TESLA Test Facility as User Facility", these procedings
4. D. Nölle, "The Diagnostic System of TTF II", Proc. of the EPAC 2002, Paris (2002), France, pp.242-44
5. C. Magne, M. Wendt, "Beam Position Monitors for the TESLA Accelerator Complex", TESLA Report 2000-41 (2000)
6. F. Brinker, et. al., "Precision Alignment of BPM's with Quadrupole Magnets", Proc. of the 18th Int. Linac Conf. LINAC 96, Geneva (1996), Switzerland, pp.502-4
7. M. Wendt, "BPM Read-Out Electronics based on the Broadband AM/PM Normalization Schema", Proc. of the DIPAC 2001, Grenoble (2001), France, pp.63-65
8. J. Camas, et. al., "High Resolution Measurements of the Lepton Beam Transverse Distribution Proc. of the PAC 93, Washington D.C. (1993), U.S.A., pp.2504-6
9. M. Hüning, "Investigation of the Longitudinal Charge Distribution in Very Short Electron Bunches", Proc. of the DIPAC 2001, Grenoble (2001), France, pp.56-60
10. M. Geitz, "Investigation of the Transverse and Longitudinal Beam Parameters at the TESLA Test Facility Linac", DESY Thesis 1999-033 (1999)
11. J. Menzel, et. al., "Experimental Investigations on Coherent Diffraction, Synchrotron and Transition Radiation", these procedings
12. M. Brunken, et. al., "Electro-Optic Experiments at the TESLA Test Facility", Proc. of the 23rd FEL Conf., Darmstadt (2001), Germany, to be publ.
13. R. Akre, et. al., "A Transverse RF Deflecting Structure for Bunch Length and Phase Space Proc. of the PAC 01, New York (2001), U.S.A., pp.2353-55
14. B. Faatz, et. al., "Undulator System for the VUV-FEL at the TESLA Test Facility – Phase 2", these procedings
15. R. Lorenz, et. al., "Beam Position Monitors inside the TESLA Test Facility Linac", Proc. of the Particle Accelerator Conf. PAC 97, Vancouver (1997), Canada, pp.2134-36
16. P. Castro, et. al., "Orbit Analysis at the TTF Linac using Model Independent Methods", Proc. of the EPAC 2002, Paris (2002), France, pp.2134-36